SECURITY CLASSIFICATION OF THIS PAGE *(When Data Entered)*

REPORT DOCUMENTATION PAGE		READ INSTRUCTIONS BEFORE COMPLETING FORM
1. REPORT NUMBER AFFDL-TR-79-3060	2. GOVT ACCESSION NO.	3. RECIPIENT'S CATALOG NUMBER
4. TITLE *(and Subtitle)* A METHOD FOR ASSESSING THE IMPACT OF WAKE VORTICES ON USAF OPERATIONS		5. TYPE OF REPORT & PERIOD COVERED FINAL REPORT 15 Dec 1978 - 5 Apr 1979 6. PERFORMING ORG. REPORT NUMBER
7. AUTHOR(s) George Kurylowich		8. CONTRACT OR GRANT NUMBER(s)
9. PERFORMING ORGANIZATION NAME AND ADDRESS Control Dynamics Branch, Flight Control Division Air Force Flight Dynamics Laboratory (AFFDL/FGC) Wright-Patterson Air Force Base, Ohio 45433		10. PROGRAM ELEMENT, PROJECT, TASK AREA & WORK UNIT NUMBERS Program Element 62201F Project 2403 Task 05 Work Unit 24030507
11. CONTROLLING OFFICE NAME AND ADDRESS Control Dynamics Branch, Flight Control Division Air Force Flight Dynamics Laboratory (AFFDL/FGC) Wright-Patterson Air Force Base, Ohio 45433		12. REPORT DATE July 1979 13. NUMBER OF PAGES 100
14. MONITORING AGENCY NAME & ADDRESS*(if different from Controlling Office)*		15. SECURITY CLASS. *(of this report)* Unclassified 15a. DECLASSIFICATION/DOWNGRADING SCHEDULE

16. DISTRIBUTION STATEMENT *(of this Report)*

Approved for public release; distribution unlimited.

17. DISTRIBUTION STATEMENT *(of the abstract entered in Block 20, if different from Report)*

18. SUPPLEMENTARY NOTES

19. KEY WORDS *(Continue on reverse side if necessary and identify by block number)*

Airplanes	Terminal Area Separation
Helicopters	Formation Flight
Wake Turbulence	Trainers
Vortical Wakes	Simulators
Operational Hazard	Wake Simulation

20. ABSTRACT *(Continue on reverse side if necessary and identify by block number)*

Experience as a consultant to the Safety Office at Norton AFB led to compiling the engineering tools presented so that this report can be used by engineering personnel to investigate future incidents/accidents and existing USAF operations that are impacted by the vortical wake hazard. The approach presented is amenable to easy hand computations. Mixed airplane/helicopter operations can be assessed, since the engineering tools to determine the location and strength of the rotor downwash field behind a helicopter are presented. Finally, a simplified mathematical model is given to represent this hazard for use in USAF

DD FORM 1 JAN 73 1473 EDITION OF 1 NOV 65 IS OBSOLETE

SECURITY CLASSIFICATION OF THIS PAGE *(When Data Entered)*

simulators, to make pilots aware of the problems associated with operating in wake-contaminated airspace.

FOREWORD

This report describes an in-house effort conducted by the author of the Control Dynamics Branch (FGC), Flight Control Division (FG), Air Force Flight Dynamics Laboratory, Air Force Wright Aeronautical Laboratories, Wright-Patterson Air Force Base, Ohio, under Project 2403, "Stability and Control for Aerospace Vehicles", Work Unit 24030507, "Stability and Control Prediction Methods."

The work reported herein used methodology developed as part of a Wake Turbulence program conducted during the period January 1972 to June 1976, under the direction of the author, Dr. George Kurylowich (AFFDL/FGC), principal investigator. The helicopter analysis reported herein was performed during the period 15 December 1978 and 5 January 1979. The report was submitted by the author in April 1979.

The author wishes to extend sincere thanks to Tammy S. Ferrell, typist for the Design Predictions Group within the Control Dynamics Branch. Even though overburdened with other work, she worked diligently, conscientiously, and accurately in preparing this report; her cheerful attitude was truely appreciated. Special thanks are also extended to R. J. Woodcock, Handling Qualities Group, for his careful review of the draft and valuable suggestions that improved the quality of the final report.

TABLE OF CONTENTS

LIST OF ILLUSTRATIONS

LIST OF ILLUSTRATIONS (CONCL'D)

LIST OF TABLES

LIST OF SYMBOLS

A_o	Rotor disk area (ft^2)
ÆR	Wing aspect ratio
b	Wing span (ft)
b'	Separation distance between vortices trailed behind an aircraft at altitude (ft)
C_L	Lift coefficient $\sim L/ \frac{1}{2} \rho V^2 S$
C_{L_α}	Lift coefficient derivative w.r.t. angle of attack (rad^{-1})
C_ℓ	Vortical-wake induced roll moment $L/\frac{1}{2} V^2 Sb$
$C_{\ell\,AERO}$	Roll moment due to conventional aerodynamic contributions
g	The constant for gravity ($ft\text{-}secs^{-2}$)
H	Wing or rotor disk plane altitude above ground (ft)
H_{INV}	Temperature-inversion layer above ground (ft)
H_{V_R}	Altitude of the right wing or rotor-right side vortex above ground as seen by the pilot (ft)
H_{V_L}	Altitude of the left wing or rotor-left side vortex above ground as seen by the pilot (ft)
I_{XX}	Aircraft inertia about the X axis of the body-fixed axis system where X points out of the nose of the aircraft (slugs - ft^2)
I_{XY}	Aircraft cross-inertia between the X-Y body-fixed axes where the X axis points out of the nose while the Y axis is directed out the right wing relative to the pilot (slugs - ft^2)
I_{YY}	Aircraft inertia about the y axis of the body-fixed axes where the y axis is directed out the right wind relative to the pilot (slugs - ft^2)
I_{ZZ}	Aircraft inertia about the Z axis of the body-fixed axes of the vehicle where the origin is at the center-of-gravity of the aircraft and the Z axis is directed down below the pilot (slugs - ft^2)
K	Vortical decay factor
K_1	Function relating $C_{L_{\alpha_{3\text{-}D}}}$ to the encountering aircraft
K_2	Function relating spanwise distance to encounter time
K_3	Vortical wake attenuation factor

LIST OF SYMBOLS (CONT'D)

L	Aircraft lift (lbs)
n	Normal load factor, g's positive up
P	Roll rate about the X axis of the body-fixed axes of the aircraft, positive right wing down (deg - sec^{-1})
Q	Pitch rate about the Y axis of the body-fixed axes of the aircraft, positive nose up (deg - sec^{-1})
R	Yaw rate about the Z axis of the body-fixed axes of the aircraft, positive nose right (deg - sec^{-1})
R	Helicopter rotor radius when referred to vortical-wake location and not vehicle dynamics (ft)
R_D	Equivalent duct radius (ft)
r	Radial distance as measured from the core of a viscous vortex (ft)
r_c	That core radius where the swirl velocity V_Θ is maximum, i.e. $V_{\Theta_{MAX}}$ (ft)
S	Wing planform area (ft^2)
t	Time (secs)
t_G	Time from vortex formation until it reaches a height b'/2 above the ground or inversion layer (sec)
V	Encountering aircraft flight speed (ft - sec^{-1})
V_d	Downward velocity of vortical pair below an aircraft (ft - sec^{-1})
V_F	Generating aircraft flight speed (ft - sec^{-1})
V_J	Equivalent-jet exhaust velocity (ft - sec^{-1})
V_o	Downwash velocity through the rotor-disk plane (ft - sec^{-1})
V_s	Atmospheric crosswind component as shown in Figure 3, to the right relative to the pilot (ft - sec^{-1})
V_s	Aircraft stall speed at 1-g flight when referred to Table 1 (ft - sec^{-1})
V_T	Rotor blade tip velocity (ft - sec^{-1})
V_W	Atmospheric tailwind component (head wind is negative) (ft - sec^{-1})
V_Θ	Vortex-induced swirl velocity (ft - sec^{-1})

LIST OF SYMBOLS (CONCLUDED)

W	Aircraft or helicopter weight (lbs)
X	Downstream distance of vortical wake from generating aircraft (ft)
Y	Lateral distance of the vortical wake (ft)
$\bar{y}$	Vortex center location relative to the mid-span of the wing (ft)
Z	Downward distance of vortical wake from generating aircraft (ft)
α	Wing angle of attack, positive nose up; rotor angle of attack positive tilt-path plane up (rad^{-1})
$\alpha(y)$	Local wing angle of attack at station y on the wing to the right of the pilot (rad^{-1})
Γ_o	Circulation strength of the trailed vortices (ft^2 - sec^{-1})
λ	Wing quarter chord sweep angle when related to aircraft geometry (deg)
$\mathcal{L}$	Roll moment induced about the X axis of the aircraft body-fixed axis system, right wing down (ft - lbs)
Θ	Angle of airflow through the rotor (deg)
ρ	Density of air (slugs - ft^{-3})
ν	Kinematic voscosity of air (ft^2 - sec^{-1}) (0.00015757 at sea level standard)

All other nomenclature is defined at the point of use

SECTION I

INTRODUCTION

The hazard associated with a pilot's conception of wake turbulence behind an aircraft is due to the persistence of a strong trailing vortex system. Another aircraft flying into this vortex system can experience large perturbations in flight path leading to possible loss of control (see Figure 1). The hazards associated with flying into this wake generated behind another aircraft have been documented (see References 1 through 5). The severity of this hazard is best indicated by describing the following encounters reported in Reference 2. A Beechcraft Bonanza initiated ground run shortly after a Douglas DC-7 had lifted off at Atlanta's Municipal Airport in November 1961. The Beechcraft became airborne at approximately the DC-7 lift-off point on the runway. The Beechcraft presumably encountering this vortical wake performed violent longitudinal motions, rolled, and then crashed. Also, a Twin Otter crashed on takeoff at Kennedy International Airport in June 1969. This aircraft flew into the wake of a Boeing 707-30 that had taken off on an intersecting runway. Just after the intersection point, the Otter rolled left and crashed.

The persistence of the wake vortex system far behind the generating aircraft is illustrated in Reference 2. McCormick indicates that vortices behind a jumbo jet are still very strong 14 nautical miles behind the vehicle. At 9.5 nautical miles, McCormick suggests that an F-104 can be inverted in less than one second when encountering this wake. In addition, a "Convair 990 can experience 25 degrees of bank and full sideslip ball deflection when encountering the wake of a jumbo jet at some 5 nautical miles behind the generating aircraft."

The slipstream of a propeller, "prop wash", and the efflux from a jet engine, "jet wash", serve to alter the structure of the trailing vortex system discussed above. For example, vortices trailed and shed from the propeller blades interfere with the wing trailed vortices. In addition, the slipstream of a propeller or the efflux from the jet engine may be entrained partially into the wing vortex cores. The axial flow in these vortices may be sufficiently affected by this entrainment that the vortex system behind an aircraft with outboard engines may be significantly different from that behind a vehicle with engines nested close to the fuselage. Despite these alterations, the prime contributor to the potential hazard associated with the far wake behind the generating aircraft is still the wing vortex system.

The problems encountered by the pilot because of this wake are best illustrated by examining three ways of flight into or through the trailing vortex system generated by another aircraft. These ways are indicated in Figure 1.

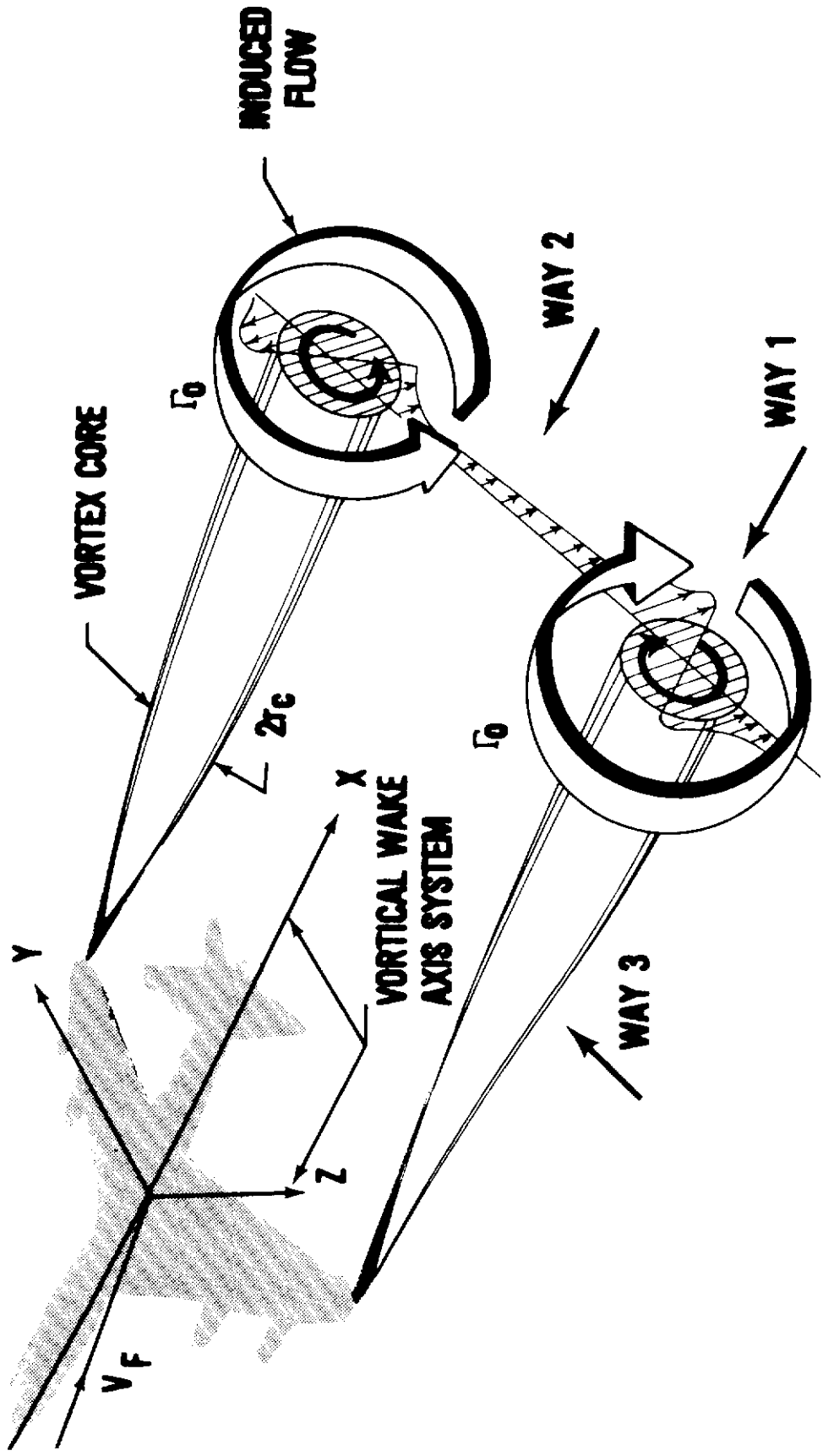

Figure 1. The Vortical Wake Behind an Aircraft

The first entry is along the axis of a vortex. The rotational flow of fluid within the vortex core and the upwash and downwash flow field just outside the core induce the vehicle to roll. The pilot may be caught unaware, or sufficient capability may not be available to counter the rolling so that the aircraft will roll and fall out of the vortex core. If this encounter occurs during takeoff or climbout, sufficient altitude may not be available for recovery; such an encounter may have occurred in the Beechcraft crash discussed above. This form of penetration could occur during an approach to mid-air refueling, where sufficient altitude is available for recovery. Here, the danger lies in a collision with another aircraft when flying in formation. The second form of encounter, or way (2), results in a sudden loss in lift upon entering the more-or-less symmetric downwash field between the vortex cores of the aircraft ahead. The affected aircraft experiences a decrease in climb rate following takeoff or an increased descent rate during landing, and the pilot may not be able to maintain a safe flight path. The third way of penetrating the wake is across the vortices (see Fig. 1). The aircraft is subjected to reversals in normal acceleration due to induced changes in angle of attack; this may lead to loss of control if the pilot aggravates the vehicle motion as a consequence of the encounter. Finally, all of the above responses may be combined in the terminal area where aircraft are following a variety of traffic patterns and the encountering aircraft penetrates the vortical wake system at some oblique angle.

1. The David and Goliath Syndrome

Because of this problem, there is emphasis within the Air Force that the appropriate separation be maintained behind large jets such as the KC-135, C-141, and C-5 during terminal operations. The FAA and NASA (Vortical) Wake (Turbulence) Programs have been concentrating upon operations where a heavy jet may takeoff ahead of small and lighter aircraft. All of this has resulted in a David and Goliath syndrome, fostered further by the FAA and USAF-produced educational films and pamphlets which show that heavy jet aircraft (Goliath) can generate a dangerous vortical wake that can flip a light aircraft like the Cherokee (David). As a result, many pilots are not fully aware that "David can slay David". For example, the vortical wake behind a fighter is a potential hazard to another fighter where both aircraft are of the same weight.

More specifically, air combat experience has shown certain transonic flight conditions where an F-104 may inadvertently exceed its design load limits. Several cases have been reported where structural deformations or failures have occurred while pilots were performing high-g maneuvers. The flight conditions for these failures were strikingly similar. At least two cases have been documented where an F-104 experiences excessive g-loadings while chasing another F-104; the flight Mach numbers varied from 1.1 to 1.2 at altitudes from 13,000 to 15,000 feet. The conditions under which these failures have occurred tend to suggest that the excessive loading is caused by flying through the trailing-vortex wake of the lead airplane. This has been verified by a pilot's report in at least

one case. On 18 October 1968, a Royal Danish Air Force F-104 was flying a mock aerial combat mission in pursuit of another F-104. The pilot of the pursuing airplane reported that he could feel an increase in g-loading as he traversed the wake of the lead airplane; this increase in loading caused wrinkles at the wing root and several other locations on the airplane. On March 25, 1971, the chase airplane in a formation of two RCAF F-104's suffered structural failure in circumstances that suggest the possibility of a wake encounter. The important point here is that a 20,000 pound fighter pulling 6 g's trails a vortical wake equivalent to that of another aircraft that weighs six times 20,000 pounds - a wake as strong as that behind a 120,000-pound C-130.

A similar incident occurred in USAF operations in early 1975. While on mission, one F-104 flew through the vortical wake immediately behind another F-104. Upon encountering the hazard, the affected aircraft rolled left and pitched down in a 90 degree dive. The pilot heard a loud bang when he initiated a recovery which was completed at an altitude of 200 feet. Upon landing it was found that the leading-edge flaps had separated from the aircraft, and that both trailing-edge flap actuators were damaged beyond repair. In addition, the main wing structure and ventral fin had been significantly damaged.

It is true that this damage was sustained during the power dive and recovery. It is also possible that the power dive would not have occurred if the F-104 had not passed through the vorticity field behind the other F-104. Clearly, the David and Goliath syndrome must be dispelled as soon as possible; especially during pullup maneuvers when a fighter can trail a wake as strong as that behind large transports.

2. Similarity of Wake Structure Behind Helicopters

In the 1962-1965 time span, the Seventh Air Force Headquarters reported a number of mishaps involving flight of aircraft behind helicopters. Of interest was the fact that the wake or rotor wash behind the helicopter may have caused these accidents (see Reference 6). Of interest here is the fact that the wake behind the helicopter in forward flight bears a strong resemblance to the vortical wake trailed behind a conventional aircraft. Therefore, other aircraft flying into this wake are subjected to a large roll moment if flight occurs up the vortex as shown in Figure 2. As before, the following aircraft is subjected to a downwash field if flight occurs between the vorticies, and the aircraft is subjected to reversals in normal load if flight occurs across the trailed vortices.

Now, vortices are trailed from the rotor blades in the conventional manner to form the vortex sheath shown in Figure 2. Except for hover and transition from hover to forward flight, this vortex sheath distorts and forms two vortex cores approximately 1.5 rotor diameters below and back of the rotor disk. It is these vortices which are formed from the distorted sheath that probably caused most of these mishaps[6]. Of specific interest here is that the same analyses developed for investigating wake accidents attributed to aircraft, including the establishment of safe terminal area operations, can be applied to operations involving helicopters.

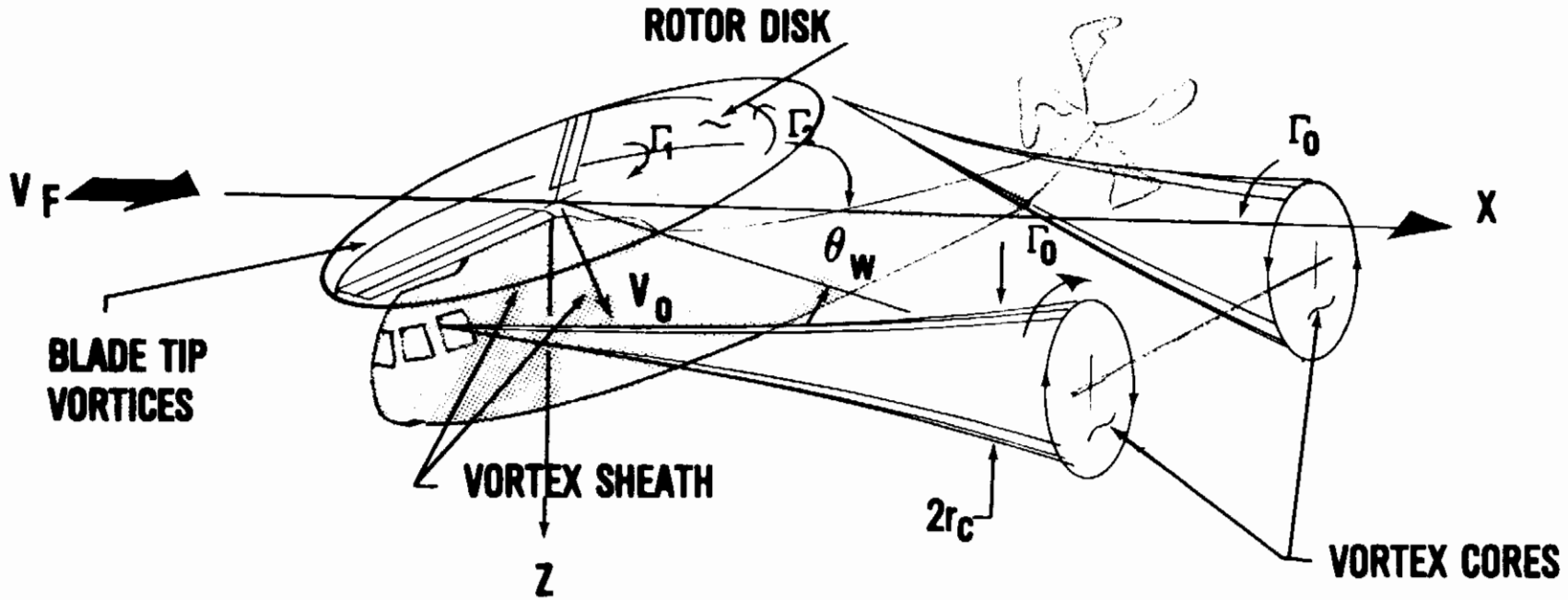

Figure 2. The Vortical Wake Behind a Helicopter

An example of such operations is at Nellis AFB, where a mix of A-10 aircraft and HH-53 helicopters operate in close proximity from the same field.

Again, the emphasis upon appropriate separations between "heavy" aircraft and light aircraft can lead to the David and Goliath Syndrome. At 38,000 pounds, the HH-53 helicopter is not a "heavy" configuration according to the separation criteria as specified by the FAA. Yet at the lower speed as we shall see, more vorticity is needed to generate a given amount of lift. Also, a rotor seems to generate more vorticity than a wing for the same lift because a helicopter performs a landing at speeds significantly below that of an aircraft. The vortical wake strength trailed behind a HH-53 flying at 60 knots is similar to to that trailed behind a KC-135 or Boeing 707 in landing approach. Obviously, an effort is necessary to insure that all USAF pilots involved in mixed aircraft-helicopter operations are well aware of the hazards associated with helicopter wake turbulence.

3. Purpose of this Effort

From 1972 through 1976, the Flight Control Division (FGC) of the Flight Dynamics Laboratory (AFFDL) at Wright-Patterson AFB was involved in an effort to significantly reduce wake associated accidents in USAF operations (see Reference 7). This program included: (1) a hard look at existing technology for developing engineering diagnostic tools[8]; (2) definition[9,10] of separation distances between aircraft, and of altitude definition for both take-offs and approach from which safe recovery can be made if an encounter occurs; and (3) educational summaries including training films to familiarize the pilots with the hazard (see for example Military Air Command (MAC) movie film S-99 titled "Vortical Wake Upset"). Since then the author has occasionally advised the Safety Office at Norton AFB on wake turbulence or more appropriately - vortical wake-related accidents.

As a result of this experience, this technical report summarizes simplified analyses which can be used as diagnostics for Air Force operational problems[11] impacted by vortical wakes. The report has been expanded to include mixed operations involving helicopters such as the HH-53. Additionally, the report presents a simplified mathematical model developed for equipping appropriate USAF trainers and simulators with the capability of simulating wake encounters. It is felt that this move is imperative because many pilots are not fully aware of the dangers involved when encountering these vortices; this is especially so if the generating aircraft is not a heavy transport, defined by the FAA as being an aircraft weighing approximately 300,000 pounds.

Section II of this report presents analyses that can be used to estimate the location of the vortical wake field behind generating airplanes and helicopters. The impact of vortex decay and atmospheric disturbances upon the vortical wake is presented. Section III of this report presents the simplified mathematics for equipping appropriate USAF trainers and simulators with the capability of simulating these encounters. Representative cases are analysed and discussed in Section 4. A synopsis of these

analyses for "quick-turn-around" investigations by Accident Boards involved in vortical-wake incidents and accidents is given in Section 5; concluding remarks and recommendations are given in Section 6.

SECTION II

VORTICAL WAKE TRACKING BEHIND AIRPLANES AND HELICOPTERS

The development of an all-inclusive model for the vortical wake structure and its descent behind an airplane can lead to a complicated formulation for vortex-induced and atmospheric effects. It was felt that such a model was not amenable to rapid hand computations; a simple representation is used here. The results have provided fair agreement with test data.

1. Airplane Vortical Wake Location

In aerodynamic theory, circulation strength Γ_o is the basis for lift. The spanwise circulation distribution on the wing influences all properties of the vorticity field. It is assumed that only one pair of vortices persist several wingspans behind an aircraft[12]; the pair move in their induced field causing the vortices to convect with a velocity proportional to the airplane weight and inversely proportional to air density, wing span, and forward speed. Using the elliptic lift approximation[13], the circulation strength of each trailed vortex is:

$$\Gamma_o = \frac{4\ L}{\pi\rho V_F b} \tag{1a}$$

where ρ is air density, V_F is airspeed, b is wingspan, and L is lift, or nW where n is normal load factor (g's) and W is the airplane weight. Additionally, the airplane is in the "clean" configuration with landing gear up and flaps retracted. Equation (1a) is modified to become:

$$\Gamma_o = \frac{4\ L}{\pi\rho V_F b}\ ,\ \frac{\mathbf{X}\ C_L}{b\ \mathbf{A}R} \leq 9.58 \tag{1b}$$

$$\Gamma_o = 9.58\left[\frac{4\ L}{\pi\rho V_F b}\right]\left[\frac{\mathbf{X}\ C_L}{b\ \mathbf{A}R}\right]^{-1}\ ,\ \frac{\mathbf{X}\ C_L}{b\ \mathbf{A}R} > 9.58$$

for landing approach or when the landing gear and flaps are fully extended. This modification is based on FAA wake measurements made of approximately 50,000 landing approaches and is discussed further in Section 2.3 in relation to the data presented in Figures 8 and 9.

The distance separating these vortices is given by:

$$b' = \frac{\pi b}{4} \tag{2}$$

Based upon the Biot-Savart Law[14], the descent velocity of the pair is:

$$V_d = \frac{\Gamma_o}{2\pi b'} \tag{3}$$

The sideways drift of these vortices is just equal to the crosswind velocity V_s across a runway; reference is made to Figure 3.

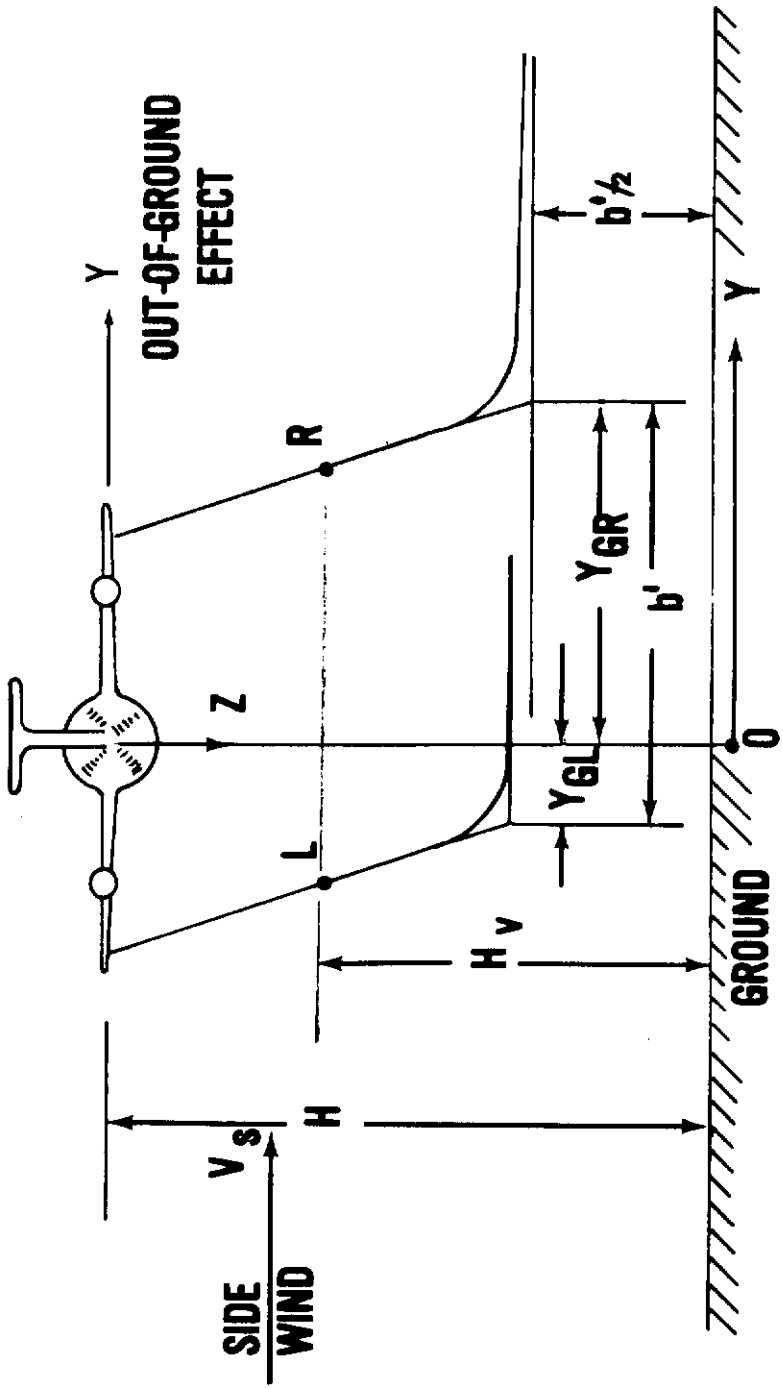

Figure 3. Aircraft Vortical Wake Tracking

Integration of these velocities relative to the coordinate system given in Figures 1 and 3 yields, for height and lateral location of the right and left vortices:

$$\begin{aligned} H_V &= H - \Gamma_o t/(2\pi b') \\ Y_L &= -b'/2 + V_s t \\ Y_R &= b'/2 + V_s t \\ X_V &= (V_F + V_W)t \end{aligned} \tag{4}$$

where H_V is the height of the left and right trailed vortices above the ground, Y_R and Y_L are their lateral distance from the airplane centerline; and V_s is the sidewind, the crosswind component normal to the path, and V_W the tailwind component.

Equations (4) provide the "out-of-ground-effect" location of the vortices during landing approach which are trailed from the wing tips following t = 0. These vortices slow down in their approach towards ground until they level-off at an altitude of b'/2. Now, potential flow theory involving the use of "mirror imaging" can be used to formulate the slowing-down and spreading-apart process as the vortices are affected by ground. An engineering approximation that can be used for evaluating military operations is:

$$\begin{aligned} H_V &= b'/2 \\ Y_L &= Y_{G_L} + (V_s - \Gamma_o/2\pi b')(t - t_G) \\ Y_R &= Y_{G_R} + (V_s + \Gamma_o/2\pi b')(t - t_G) \\ X_V &= (V_F + V_W)t \end{aligned} \tag{5}$$

in ground effect; the quantities Y_{G_L} and Y_{G_R} are shown in Figure 3. The quantity t_G is the time needed for the trailed vortices to reach the altitude b'/2 above ground according to Equation (2).

This type of analysis was used by FAA personnel during the initial phases of the program reported in Reference 12. In the absence of large wind shears and gusts, good correlation with flight test[12] was obtained (Figure 4). These results were obtained from a series of flight tests conducted at the National Aviation Facilities Experimental Center (NAFEC) at Atlantic City, New Jersey. The motion of the vortices was made visible by means of smoke, and the attendant meteorological conditions were recorded. The test series made use of commercial B-747, B-707, and DC-6 aircraft; USAF airplanes were not used during any of the program reported in Reference 12. As is evident, the vortices convect parallel to the ground at an altitude of approximately b'/2.

Wind shear can have an effect upon the locations of the trailed vortices. The concept of wind shear is included here to explain trends

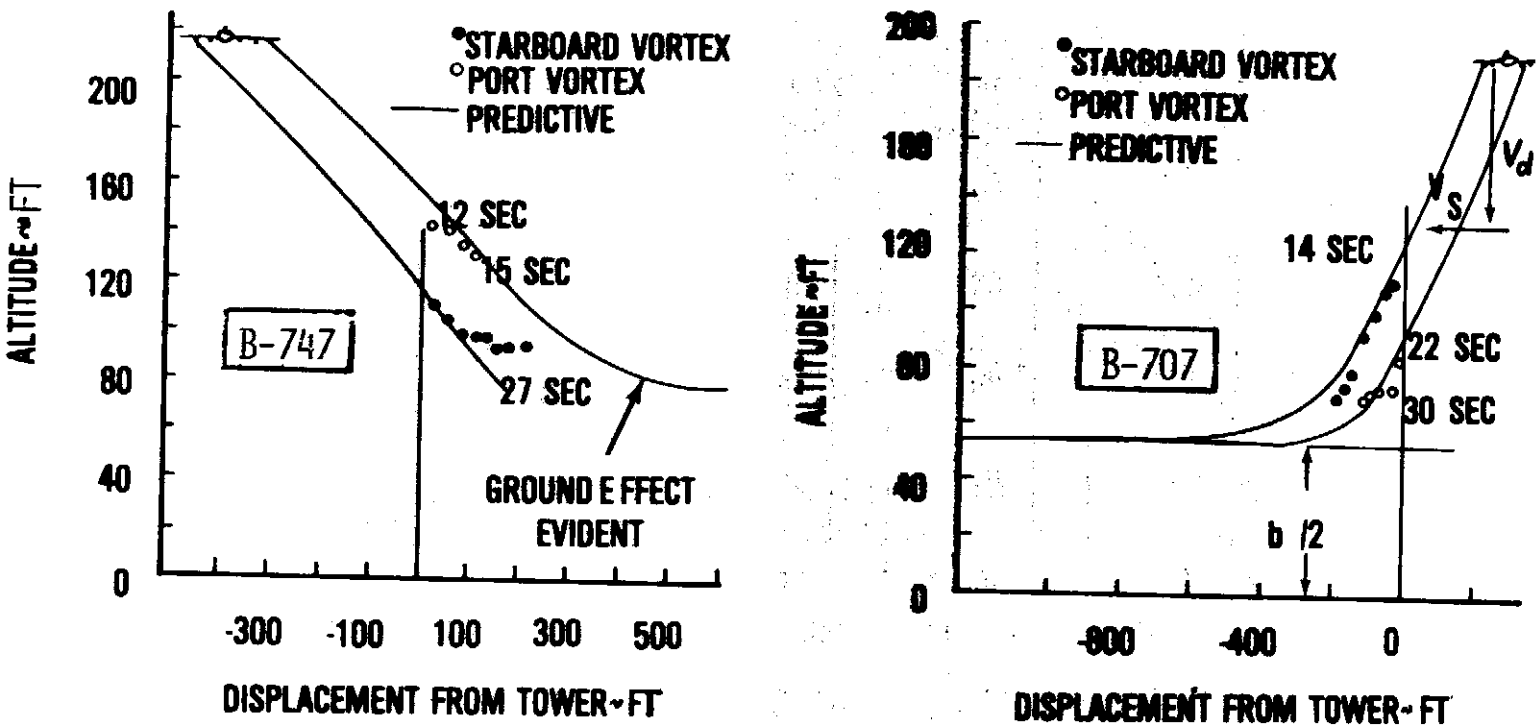

Figure 4. Correlation of Analysis with Experiment (A/C Wake Transport)

known to exist from qualitative experiment. The downwind vortex often rises while the upwind vortex sinks below the predicted altitude; the line through the two vortices can rotate, as X increases, to an angle that is large relative to the surface of the earth. This effect has not been predicted by any analysis. For the purpose of this effort, the relative displacement is assumed to be within the error band discussed below; research is necessary in this area to understand this phenomenon more fully.

Under atmospheric vagaries, there are indications that buoyancy of the air may have a significant effect on the transport of the vortices. This force is a result of differences in air density created by the descent of the vortex pair through a relatively-unknown atmospheric medium. The density of air within the vortex may be different from that of the atmosphere because of engine exhaust entrainment or increases in atmospheric density as the vortices descend. This density difference produces a buoyant force that can significantly affect the vertical momentum of the vortex pair.

Tombach[15], Scorer and Davenport[16] have theoretically investigated the effect of buoyancy upon the transport of vortices. The results indicate that the neglect of the buoyancy effect (i.e., no engine exhaust entrainment) may cause errors in predicted vortex location of up to 15% during the first minute of vorticity life. It seems that the effects of buoyancy could be ignored in predicting the track of the vortices; but the error analysis given below defines the region of uncertainty in vortex location. Again, research is needed in this area to understand this phenomenon more fully.

Brashears[12] suggests that velocity fluctuations and other atmospheric vagaries during the time of vortex transport can lead to a deviation in transport velocity of 25%. When this error was applied to all of the data gathered during the FAA program[12], Brashears found that the differences between predicted and observed data lay within the 25% error band. That is:

$$\Delta V_d = \pm V_d/4 \qquad (6)$$

$$\Delta V_S = \pm V_S/4$$

with V_d and V_S calculated from Equations (3) and (4).

Integration of Equation (6) with respect to time gives:

$$\Delta H_v = \pm V_d \cdot t/4 \qquad (7)$$

$$\Delta Y = \pm V_S \cdot t/4$$

where ΔH_v is the possible error in predicted altitude and ΔY is the possible error in predicted lateral displacement of the trailed vortices.

A temperature inversion layer influences the motion of vortical wakes. It has been only observed that the effect of the layer is similar in nature to the effect of the ground; that is, the vortices sense the temperature inversion layer and start spreading apart as if the inversion layer altitude were the ground[4]. No theory exists that can predict this vortical behavior; further research is required. For engineering purposes, it may be assumed that the inversion layer acts approximately as ground effect. Equations (4) and (5) are then modified to become, with H_{INV} the height of the inversion layer above ground level:

$$H_V = H - H_{INV} - \Gamma_o t/2\pi b' \tag{8}$$

$$Y_L = -b'/2 + V_S t$$

$$Y_R = b'/2 + V_S t$$

for vortical location out of the effect of the temperature inversion layer and, with Y_{INV_L} and Y_{INV_R} the equivalents of Y_{G_L} and Y_{G_R} (Eq. 5) for the inversion layer:

$$H_V = H_{INV} + b'/2$$

$$Y_L = Y_{INV_L} + (V_s - \frac{\Gamma_o}{2\pi b'})(t - t_G) \tag{9}$$

$$Y_R = Y_{INV_R} + (V_s + \frac{\Gamma_o}{2\pi b'})(t - t_G)$$

in the vicinity of the temperature inversion layer.

2. Airplane Vortical Wake Decay

There are many analyses that have reflected the viscous or turbulent decay of vortices in quiescent air; these are described in Reference 8. Many of the analyses are complex, requiring the use of a digital computer for a solution; such analyses are beyond the scope of this effort. An analysis amenable to hand computation, that has provided reasonable correlation with experiment, was developed by the author[8]. This analysis is summarized here.

It is assumed in the analysis that each vortex trailing from the vicinity of the wing tips is axisymmetric. This assumption is not valid in the near wake behind the wing, where the vorticity sheet is in the process of rollup. The assumption is reasonable, however, at distances of approximately 4 wing spans behind the airplane where the rollup is complete; in addition, it is consistent with the assumptions made in formulating Equations (1) through (9).

Details of the author's analysis can be found in Reference 8. The results relevant to this effort are as follows. The swirl velocity induced by the vortex is given by:

$$V_\theta = \frac{\Gamma_o}{2\pi r}\left(1 - e^{-1.26(\frac{r}{r_c})^2}\right) \tag{10}$$

where r is the radial distance from a vortex center and r_c is the vortex core radius where the swirl velocity is a maximum; r_c is given by:

$$r_c = 36.2\sqrt{\frac{\nu X}{V_F \cos^2\lambda}} \qquad (11)$$

where $X = V_F t$, ν is the air viscosity, and λ is the sweep back angle of the wing quarter-chord. The variation of V_θ with r is shown in Figure 5. The quantity r_c was determined in Reference 8 by correlating with experimental measurements made behind full-scale CV990, CV880, and the British Handley-Page aircraft (HP115).

The results shown in Figure 5 are of interest in the sense that the viscous effects associated with vortical flows need to be considered only in the immediate vicinity of a vortex; that is, when the quantity r/r_c is less than or equal to $\frac{r_c}{r} = 2.0$. The more familiar Biot-Savart solution[14] or $V_\theta = \Gamma_0/2\pi r$ can be applied wherever $r/r_c \geq 2.0$. Equation (10) is not needed in forming Equation (3). Here, the vortices are separated by at least quantity b', which generally exceeds $2r_c$.

3. Aircraft Wake Breakup by Atmospheric Means

The wing tip vortices from an aircraft are generated into an environment that is rarely quiescent. Thermals, temperature inversions, and winds which include updrafts and downdrafts cause decay and eventual transition into a form of clear-air turbulence. In many instances the atmosphere has caused the wing tip vortices to burst. Bursting produces some combination of a marked increase in the size of the vortex core, an increase in turbulence level, and an instability and significant restructuring of the wake vorticity behind an aircraft[17]. By hastening the interplay between the vortical wake and the atmosphere, bursting may significantly reduce the wake hazard during the landing approach. Discussion of this interplay will help establish which atmospheric conditions cause vortices to persist and which do not. This would help determine when separation distance during landing approach should be based upon the wake hazard.

In many instances[17], atmospheric conditions have caused the two tip-trailed vortices to oscillate behind the aircraft (see Figure 6); the altitude of the B-47 in this Figure is not known. The sinusoidal interaction between the trailed vortices increases with time until the vortices touch. Upon contact, vortex rings are formed which diffuse with time and the influence of the wind until the wake reduces to a form of clear-air turbulence. For an aircraft in ground effect, the trailing vortices can interact with the earth to break apart and form a series of semi-circles with ends perpendicular to the ground. Crow[18] developed a theory that applied to this phenomenon. It is seen in Figure 6 that sufficient breakup of the vortices has occurred approximately 90 seconds behind the B-47, so that the vorticity field may not be a severe hazard to a aircraft following FAA separation of 3 nautical miles.

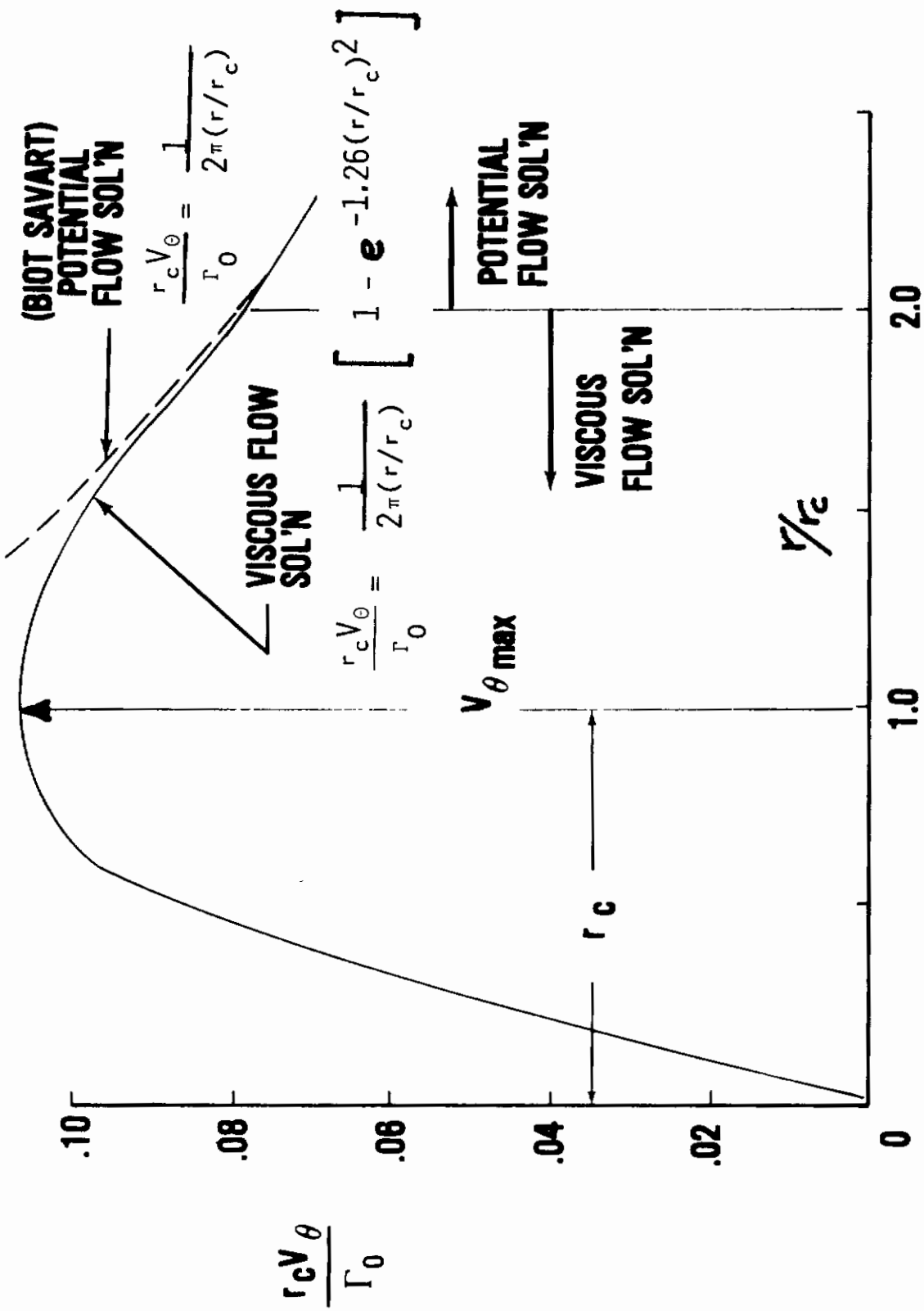

Figure 5. The Effect of r/r_c on Swirl Velocity

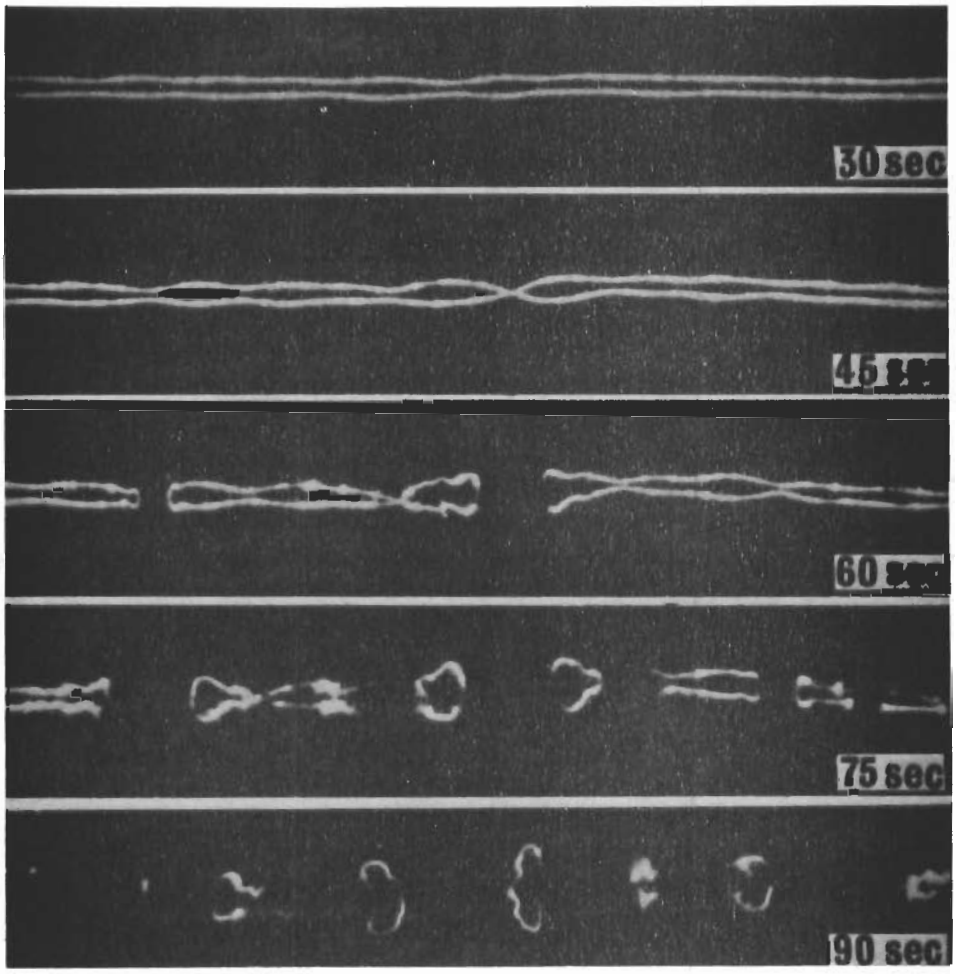

Figure 6. B-47 Vortical Wake Instability

Tombach[15], in a field investigation on the motion and decay of trailing vortices generated by a Cessna 170 high-wing aircraft, obtained some interesting results. The site selected was near El Mirage Dry Lake in California, so that the vortices could be photographed from below and also from the side, up level with the flight path of the aircraft. The vortices were made visible by means of colored smoke generated by grenades mounted at the wing tips. Atmospheric interplay with the vortices caused the sinusoidal instability described above; the vortices were observed to burst in approximately 18 seconds following their generation. Similar interplays could occur with the vortices behind USAF aircraft during landing approach. Another interesting form of observed instability is shown in Figure 7. During this flight, the vortices linked together and burst at their juncture point. Within a short time no smoke residue was left outside the vortex cores at the point of contact. Of interest in the above is that the observations in vortical-wake interplay could not be repeated from day to day even though the atmospheric conditions seemed to be the same for each flight. Research is needed to further our understanding of these fluid-interaction phenomena.

During this test program, Tombach found that the interpretation of results from photographs was made difficult because the vortex wake had a tendency to roll on its side. In some instances Tombach observed that in about 80 seconds after generation, the pair of vortices appeared to be perpendicular to the ground. The symmetrically loaded aircraft performed this series of flights at about 450 feet above the earth. As a result, Tombach suggested that the wake may have been affected by the atmospheric boundary layer in the El Mirage Dry Lake area of California. During one flight, one of the wing tip vortices was abated by a bursting instability at an age of 65 seconds. The other vortex subsequently became fixed in space and persisted with no apparent decay for over two minutes. MacCready[19] indicated a similar situation where one Boeing 747 vortex remained unchanged near the ground for just over three minutes. The possibility of the existence of such a long-term vortex has serious ramifications on the vortical wake hazard in the terminal area.

The bursting observed by Tombach[10] is described as a sudden increase in core diameter and the formation of ring vortices near the point of burst. Furthermore, Tombach observed that this "core bursting is independent of the sinuous instability, since bursting was observed at all points along the vortex and it did not seem to have any relation to the curvature of the vortex filaments or to their local separation." In addition, "the core bursting instability was observed at all levels of turbulence and atmospheric stability."

The FAA has had a program for safely increasing the air traffic rate into airports. A part of this program is a wake investigation that was conducted at the National Aviation Facilities Experimental Center (NAFEC) in New Jersey. The facility has a 140-foot tower to the side of a runway; the tower is equipped with colored smoke grenades which are actuated prior to an aircraft fly-by so that the vortices are made visible. Hot film anemometers, capable of measuring vortical flow characteristics, are located at four-foot intervals up the tower to probe the vortices after

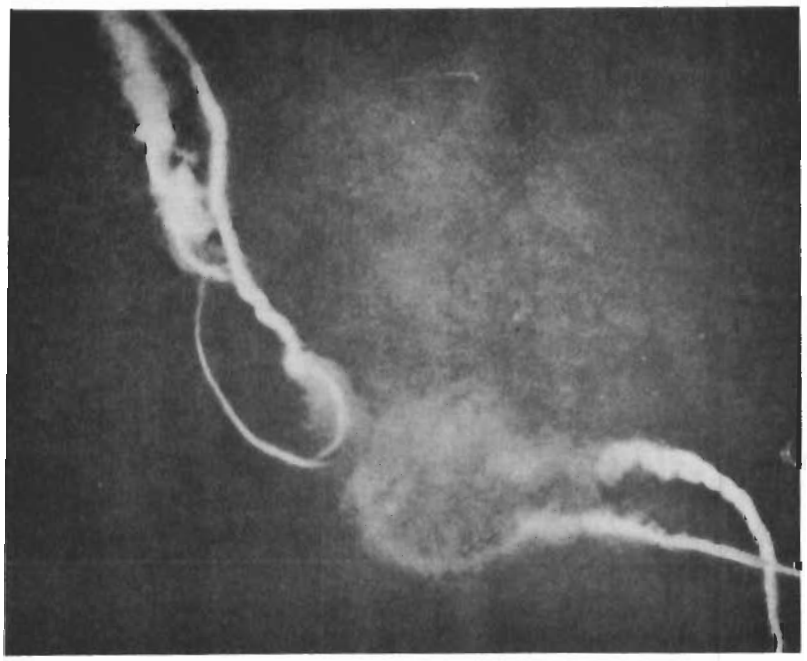

Figure 7. Vortex Bursting Behind a Cessna 170 (Ref. 15)

the test aircraft had flown past the tower; results are reported in References 20 through 22. The hot film anemometers on the towers could not detect the presence of well-organized vortices behind the DC-7, and Boeings 707 and 727 when the aircraft had flown past the towers within about 2 minutes when the vortices may have drifted past the tower.

A flight test investigation of the vortex characteristics behind a Boeing 727 was conducted in a joint FAA/NASA program to assess conventional and two-segmented ILS approaches[23]. The Boeing 727 was equipped with smoke generators for making the vortices visible, and a Lear Jet model 23 (LR-23) and a Piper Twin Comanche (PA-30) were intentionally flown into a vortex to record aircraft perturbations during and following the encounter.

Comments summarized during the program by the pilots of the LR-23 were as follows (these comments are taken directly from Reference 23):

"1. Calm air and a 'flaps-up' configuration of the generating airplane presented the worst case to the trailing airplane. With the passage of time, even in calm air, wake vortices dissipate. The characteristic breakup occurs as a longitudinal gathering of the vortex, followed by a radial expansion appearing as a large doughnut, and within approximately five or so minutes after that, dissipation is complete."

"From the pilot point of view, safe separation must be based on this worst case until other effects can be adequately measured and taken into account. The above described breakup and dissipation consistently happens between a minute, and a minute and a half, in the case of the B-727. A separation of two minutes should therefore provide safety as well as an adequate margin. With a typical approach speed of 130 knots for the generating airplane, a separation distance of 4.5 nautical miles would assure vortex dissipation even in the worst case for the trailing airplane."

"2. Generating airplane flap-deflection was observed very clearly to provide secondary vortices which tended to mingle with and speed the destruction of the primary wing tip vortices in proportion to the amount of flap deflection. Penetration of the trailing vortices produced significantly less disturbance with 30° or more flap deflection compared to the flaps-up configuration at equal vortex ages. Therefore, separation could be safely reduced somewhat (i.e., less than two minutes or 4.5 n.m.) if the generating B-727 were known to have at least 30° of flaps extended. However, where decelerating approaches are made at lesser flap deflection until the last two or three miles prior to touchdown, the reduced separation could not be considered appropriate."

The Transportation System Center (TSC) of The Department of Transportation (DOT) developed a system for tracking vortices and their persistence in the approach alley (see References 24 and 25). The approach alley is the volume of air just prior to touchdown which lies up to 150 feet on either side of the runway centerline, from ground level up to an altitude of approximately 300 feet, and from the middle marker on into touchdown.

The purpose behind the program was to develop a Vortex Advisory System (VAS) to be used in the terminal area to detect, track, or predict the presence of vortices. Algorithms were also developed for evaluating the persistence of the hazard; appropriate information would then be transmitted to the aircraft in the landing pattern. Of interest were those atmospheric conditions which caused rapid vortex breakup. Under these conditions, the terminal approach spacing could be decreased, thus increasing airport capabity.

By 1979, the vortices behind over 50,000 commercial airliners (Boeing, 747, 707 and 727; McDonnell Douglas DC-10, etc) had been tracked in the approach alley[24,25] from vortex measurement systems installed at John F. Kennedy, Denver, Heathrow, and Toronto Airports. Additionally, the use of the algorithm was tested in a program conducted at Chicago O'Hare Airport. The results are shown in Figures 8 and 9.

The probability that a vortex persists longer than anytime in the approach alley is given in Figure 8 as a function of cross wind. Most of the vortices either break up or drift out of the approach alley in less than two minutes. It is noted again that the volume of air of interest is approximately 150 feet on either side of the runway centerline, from the middle marker on into touchdown, and at an altitude below approximately 300 ft. The data shown in Figure 8 is a composite of all aircraft that were tracked at Heathrow International Airport. Now, eighty seconds represents an aircraft spacing of less than 3 nautical miles for the approach speeds of most modern airplanes. It is reasonable, then, to predict that wake vortices are not a hazard at Heathrow when there are crosswinds greater than 10 knots.

In 1973 and as a result of the vortical wake hazard, the FAA increased the separation standards behind heavy jets (take-off weight of 300,000 pounds or more) to 4 nautical miles for a following heavy aircraft; the separation distance for a following non-heavy aircraft was set at 5 nautical miles. The standard was revised in 1975 by setting the separation for following light aircraft (take-off weight less than 12,500 pounds) at 6 nautical miles. So, the algorithm presented in Figure 9a, taken from Reference 25, was of particular interest to the FAA. The algorithm consists of two concentric ellipses with the major axes aligned in the direction of the runway.

Now, the algorithm is as follows. The 3/4/5/6-nautical-mile separations are to be used when the averaged wind vector is on or inside the inner ellipse. The uniform 3-nautical-mile separation regardless of aircraft size is to be used when the averaged wind vector is on or outside the outer ellipse; that is, the approach alley is clear of persisting vortices for incoming airplanes. Additionally, the averaged wind vector must increase from on or inside the inner ellipse until it reaches the outer ellipse prior to instituting the 3 nautical mile separation criteria. Conversely, the averaged wind vector that is on or outside the outer ellipse must decrease so as to be on the inner ellipse before the 3/4/5/6 criteria is applied.

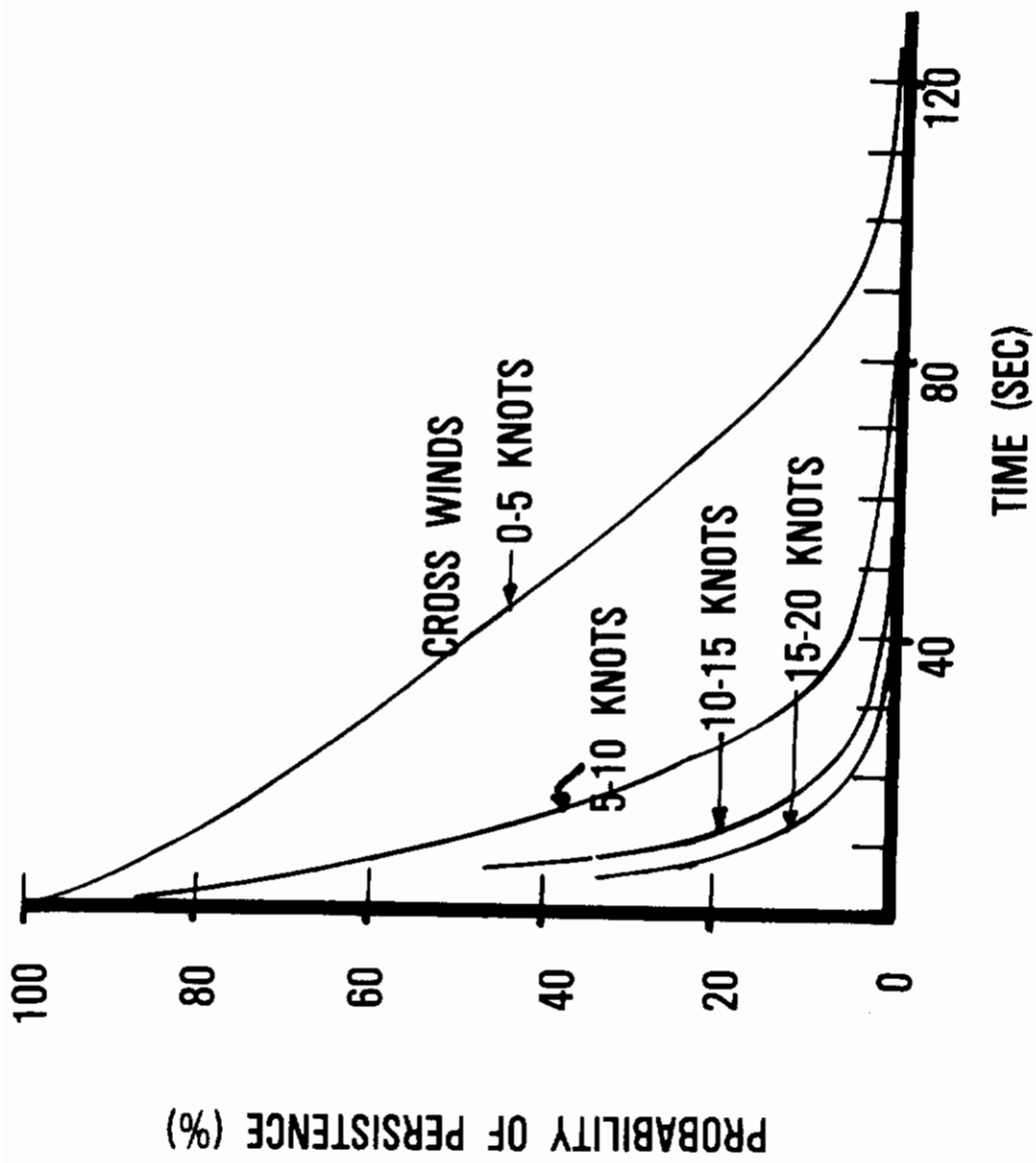

Figure 8. Probability of Vortex Persistence In Approach Alley (Ref. 24 & 25)

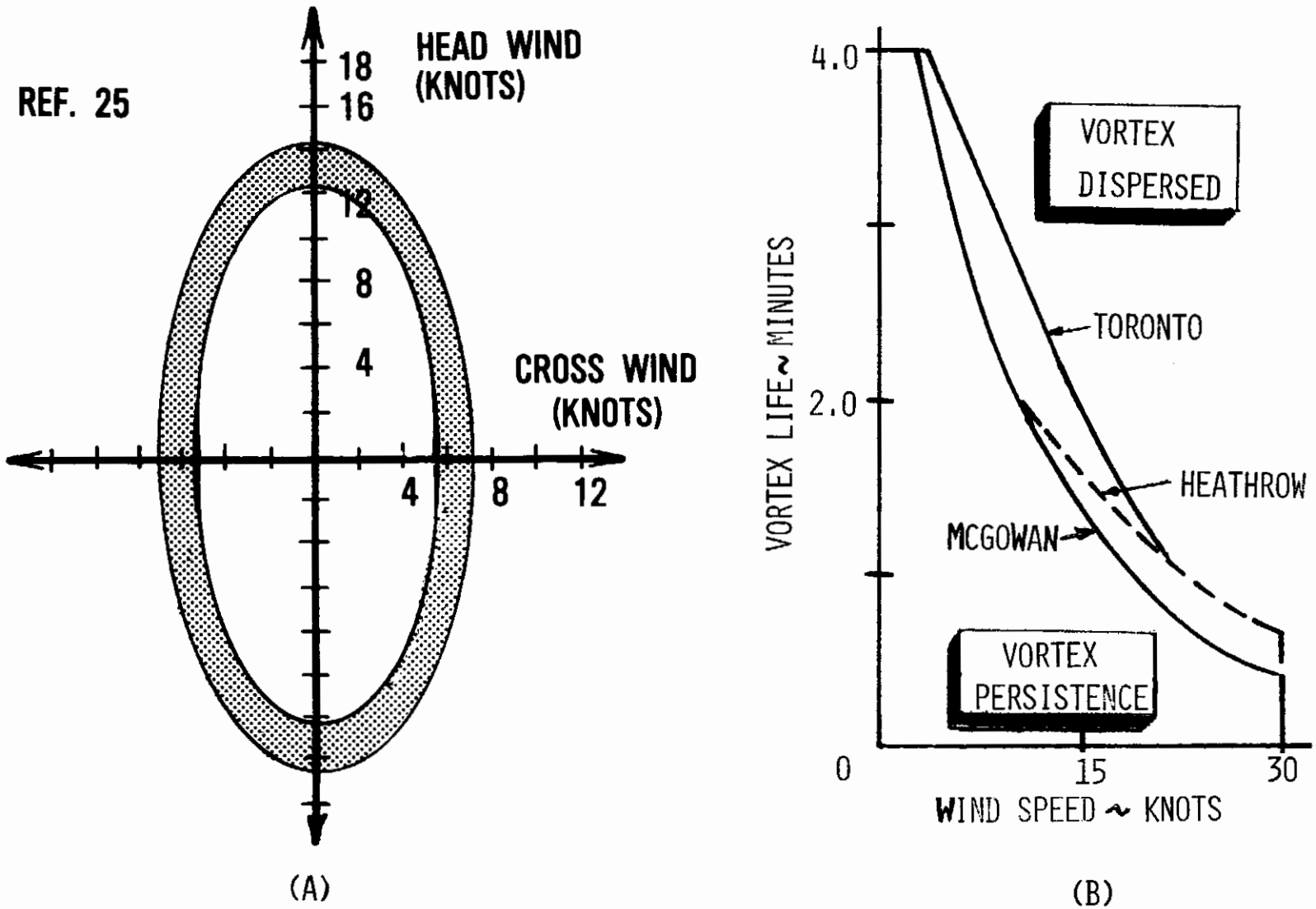

Figure 9. Wind Vector Criteria

According to Hallock[24,25], for safety purposes the algorithm was developed to be conservative; it is primarily based upon the persistence of strong vortices behind jumbo jets. Hallock contends that the algorithm is ultra-conservative when applied behind aircraft in the 100,000 to 300,000 pound class or to fighter aircraft. However, this contention remains to be examined further.

The vortices can still persist for a long time after they have cleared from the approach alley as given by the above algorithm; Reference is made to Figure 9b. These results represent the lifetime of vortices trailed behind airplanes as a function of wind magnitude. McGowan devised the original curve by fairing it to all known vortex-lifetime data in 1970 such that all of the data were included within the curve. McGowan's curve was updated to include all of the measurements obtained as part of the VAS program[25]. It is seen that a vortex can persist for up to 4 minutes when the total wind is less than 6 knots in magnitude. Thus a vortex that has cleared from an approach alley can pose a problem for aircraft landing on an adjacent runway.

Reference is now made to Equation (1b) or:

$$\Gamma_o = \frac{4\ L}{\pi\rho V_F b}\ ,\ \frac{\chi\ C_L}{b\ AR} \leq 9.58 \qquad (1b)$$

$$\Gamma_o = 9.58\left(\frac{4\ L}{\pi\rho V_F b}\right)\left(\frac{\chi\ C_L}{b\ AR}\right)^{-1},\ \frac{\chi\ C_L}{b\ AR} > 9.58$$

The decrease in circulation strength, Γ_o, once $\chi\ C_L/b\ AR$ exceeds 9.58 behind an aircraft in landing approach (flaps fully deployed) was deduced from ground-based measurements taken by TSC at Kennedy Airport, NASA/FAA flight test measurements using probe aircraft, and NASA towing tank results (see Reference 25). This decrease in Γ_o is attributed to the interference effect occurring when flaps and wingtip vortices interact. The interaction causes the circular symmetry of the vortices to be destroyed resulting in an increase in diffusion and in an increase in vorticity spreading. Additionally, atmospheric disturbances cause shearing, sinuous instabilities, vortex linking, and vortex bursting. All of the above eventually cause a significant restructuring of the vortical flow field into a form of clear-air turbulence.

4. Helicopter Wake Location

The rotor wake of a helicopter is depicted in Figures 2 and 10. The vortices from the rotor blades trail in the conventional manner from the blade-tips to form a sheath. Except for hover and transition to or from forward flight, this vortex sheath begins to distort, forming 2 vorticies starting at and trailing aft from approximately 1.5

* McGowan, W. A., Aircraft Wake Turbulence Avoidance, 12th Anglo-American Aeronautical Conference, Paper 72/6, Calgary, SK, Canada, July 1971

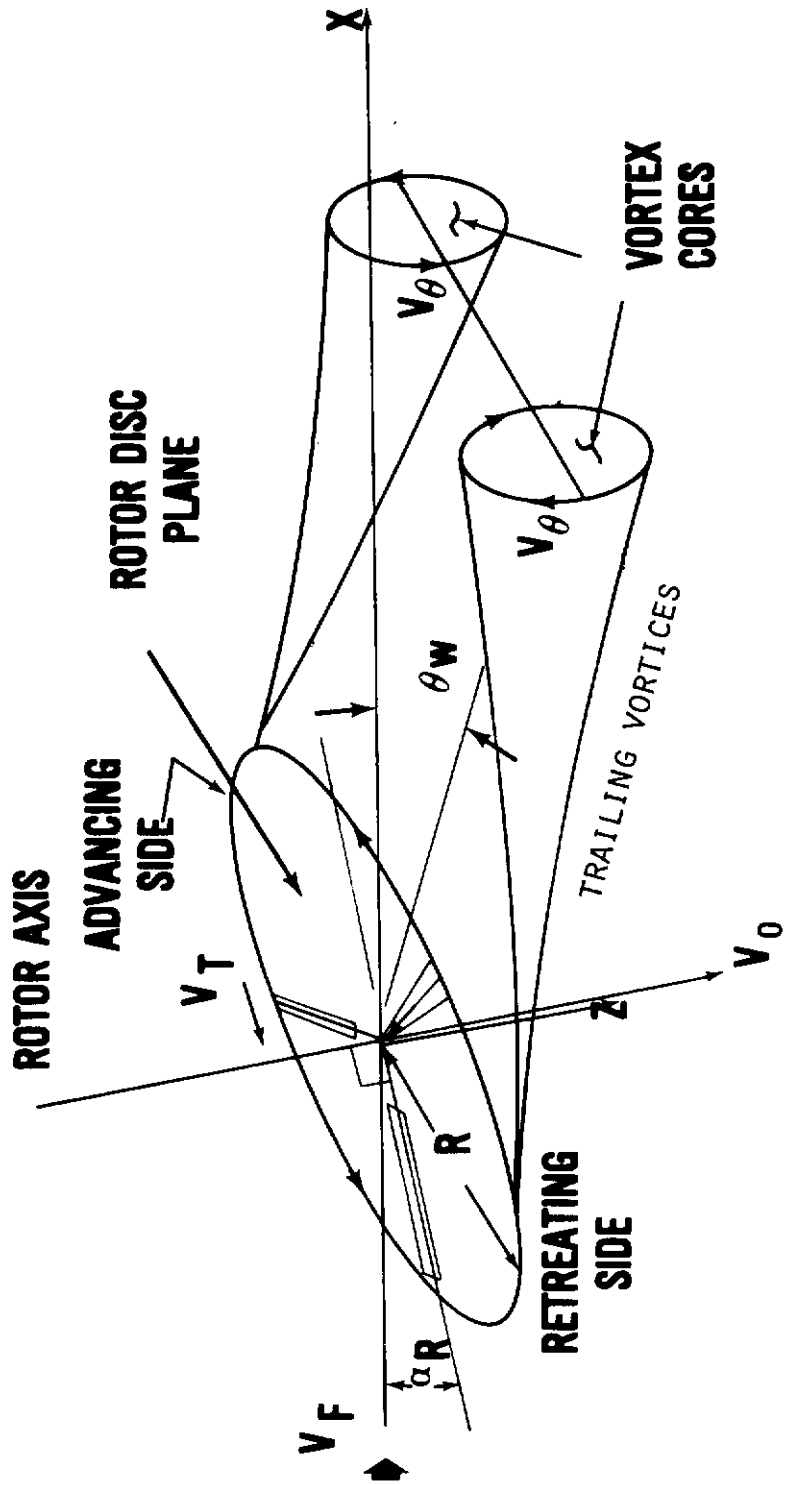

Figure 10. Helicopter Rotor Wash

radii behind the rotor disk plane. It is these vortices which are formed from the distorted sheath that can persist for a long time, causing severe wake encounters in the terminal area.

Now, the development of an all-inclusive mathematical representation for the rotor wake including blade tip vortices and the distortion of the sheath into trailing vortices in the far wake is far beyond the scope of this effort. In fact it is doubtful that any of the helicopter-producing companies have a digital computer code that accurately predicts the distorting sheath in the far downstream, simply because they have never had a need for it. The emphasis in company-generated predictive methods is on rotor performance and efficiency, so a representation for the vortices trailed in the wash from the rotor blades is needed for computation of the angle of attack induced back at the rotor blades. The velocity induced by a blade-tip vortex in the rotor wake far downstream contributes very little to the induced velocity at the rotor blade. Consequently, helicopter companies concentrate their efforts on accurately locating the rotor-blade-tip vortices in the immediate vicinity of the rotor blades and up to approximately two rotor diameters aft of or below the disk plane (depending on whether the prediction is for a rotor in forward flight or in hover).

The alternative course taken here was to take advantage of existing experimental data in locating the rotor wake. NASA Langley data was used in determining the rotor wash angle Θ_w shown in Figure 10. This angle together with the downwash velocity V_o through the rotor disk plane was related to formulations for an equivalent circular jet representation of flow through the rotor disk, in a wind. This type of system was tested intensively in the 1960 time period in relation to V/STOL's (see Reference 26). A correlation of results from the formulations developed in this way was then made with helicopter flight test data to assess method relevance and accuracy.

Now, the downwash velocity V_o that is shown in Figure 10 is given in Reference 27 as:

$$V_o = \frac{1}{2} C_T V_T \Big/ \sqrt{\lambda^2 + \mu^2} \qquad (12)$$

where V_T is the rotor tip speed, and where the thrust coefficient C_T for level flight, the advance ratio μ, and the induced-velocity ratio λ are defined as:

$$\begin{aligned} C_T &= W/\rho\pi R^2 V_T^2 \\ \mu &= V_F \cos\alpha / V_T \\ \lambda &= (V_F \sin\alpha - V_o)/V_T \end{aligned} \qquad (13)$$

Substituting Equations (13) into (12) yields:

$$V_o = \frac{1}{2V_F} \cdot \frac{C_T V_T^2}{\sqrt{1 + \left(\frac{V_o}{V_F}\right)^2 - 2\left(\frac{V_o}{V_F}\right)\sin\alpha}} \qquad (14)$$

Assuming that $(\frac{V_o}{V_F})^2$ and $2(\frac{V_o}{V_F})$ sin α are far less than unity produces:

$$V_o = W/2\rho\pi R^2 V_F \qquad (15)$$

The assumptions made in this analysis limit the use of this equation to helicopters in level forward flight speed V_F with advance ratios equal to or greater than $\mu = .1$.

Heyson[28,29] at NASA-Langley was heavily involved in rotor and V/STOL development in the late 1950's and in the 1960's. With the results of many experimental test programs and an analytical effort[29], Heyson developed the relationship shown in Figure 11: the initial wake efflux angle Θ_w is given as a function of level forward flight speed V_F and helicopter weight W. This relationship is used here in establishing the initial jet efflux angle Θ_w for the equivalent circular jet in a cross wind as mentioned above. The equivalent subsonic jet, initially at an angle to the wind, is shown in Figure 12. The coordinate axes x and z and the jet efflux angle Θ_w are directed as in Figure 10. As the jet exhausts at an angle Θ_w to the relative wind, it is deflected into the wind direction by viscous entrainment of the crossflow by the jet, and also by the effect of induced pressure forces on the jet boundary layer. Additionally, the initial circular cross section of the jet distorts into a kidney shape, which distorts further to form two contra-rotating vortices much like the wing-tip vortices trailed behind an aircraft (reference is made to Figure 12). These vortices then trail into the far wake, separated from one another by a distance of approximately the diameter of the duct (see Reference 26). In fact, the distortion of the jet efflux is equivalent in nature to the distortion of the vortex sheath below the helicopter rotor disk plane. It was felt, then, that empirical formulations developed during the 1960's for predicting the jet duct centerline could be appropriately modified to provide an estimate of the rotor wake centerline relative to the helicopter; the coordinate systems of both are indicated in Figures 10 and 12.

A review[26] of the literature of the 1960 time period was made for appropriate empirical formulations which gave centerline location as a function of Θ_w and V_J, and which was relatable to the co-ordinate system shown in Figure 12. The empiricisms selected for evaluation were as follows:

Margason[30]

$$\frac{X}{2R_D} = \frac{(V_F/V_J)^2}{4 \sin^2 \Theta_w} \left(\frac{Z}{2R_D}\right)^3 + \left(\frac{Z}{2R_D}\right) \cos \Theta_w \qquad (16)$$

Heyson[31]

$$\frac{X}{2R_D} = \frac{(V_F/V_J)^2}{4 \sin \Theta_w} \left(\frac{Z}{2R_D}\right)^3 + \left(\frac{Z}{2R_D}\right) \cos \Theta_w \qquad (17)$$

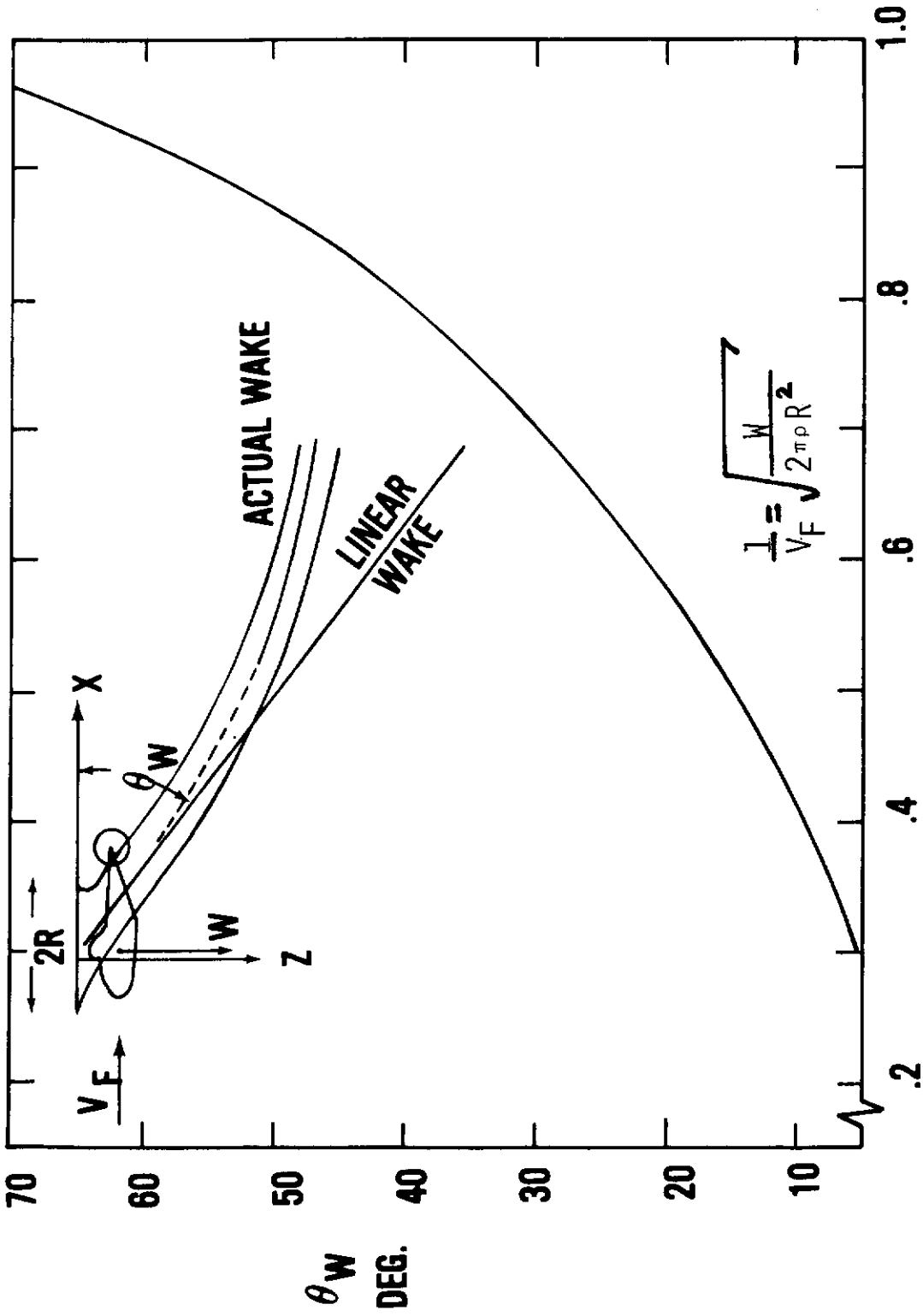

Figure 11. Rotor Wash Tilt Angle Θ_W

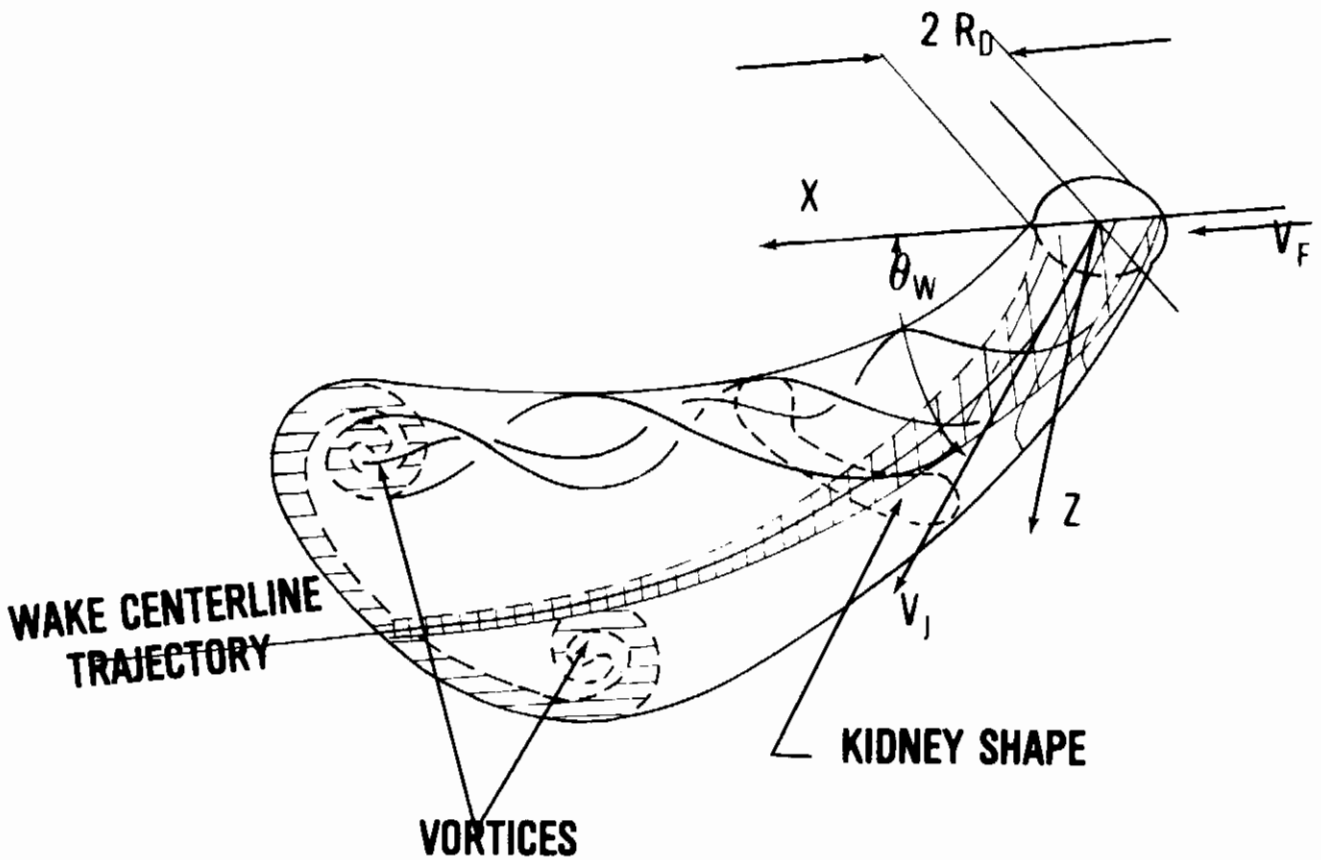

Figure 12. Subsonic Jet Initially at Angle θ_W to the Wind

Abramovitch[32]

$$\frac{X}{2R_D} = \left(\frac{V_F}{V_J}\right)^{2.6} \left(\frac{Z}{2R_D}\right)^3 + \left(\frac{Z}{2R_D}\right) \cot \Theta_w \qquad (18)$$

A comparison of the results from these formulations with the experimental data of Keffer and Baines[33], and Jordinson[34] is shown in Figure 13 for Θ_w = 90 degrees. It is seen that Margason and Heyson's empiricisms given in Equations (16) and (17) become equivalent when the jet exhausts perpendicular to the wind. The comparisons among Equations (16) through (18) and the experimental data also indicate that Abramovitch's empiricism provides better agreement with experiment than Margason's and Heyson's.

Figure 14 provides correlation of the same empirical formulations with the experimental data of Braun and McAllister[35] for a jet efflux angle of 60.9 degrees relative to the wind. Again, the Abramovitch empiricism provides better correlation with the experimental data than either Heyson's or Margason's. It is also seen from both Figures 13 and 14 that all of the empiricisms selected for evaluation under-predict the amount of curvature incurred. As a result of only these correlations, the Abramovitch empiricism, Equation (18), was selected for modification in estimating the centerline location of the rotor wake.

The final step in developing this method for predicting the wake behind a rotor is to relate the jet equivalent duct radius, R_D, and equivalent exhaust velocity, V_J, to the rotor diameter, R, and inflow velocity, V_O. The diameter of the jet of air from a round orifice remains fairly constant in circular cross-section until the jet-air boundary distorts as shown in Figure 12. For that matter, this diameter may even increase if significant entrainment occurs before the wake distortion takes place. The rotor wake, on the other hand, contracts immediately below the rotor disk as shown in Figure 15, causing a corresponding increase in the velocity of the air in the vorticity stream tube. Slipstream contraction just aft of the rotor disk plane occurs not only in hover but also at the advance ratios μ of interest to this effort.

The classical approximation to the axial variation of slipstream velocity for a hovering propeller is a tubular vortex sheet of constant circulation strength per unit length, γ (see sketch 2 in Figure 15). From Davenport[36], this results in an axial variation in velocity of:

$$V(Z) = V_O\left[1 + Z/R\Big/\sqrt{1 + Z/R\Big/\sqrt{1 + \left(\frac{Z}{R}\right)^2}}\right] \qquad (19)$$

The principle of continuity as applied to incompressible flow in a stream tube leads to the result that the product of velocity and area is constant; that is:

$$V_O A_O = V(Z)A(Z) \qquad (20)$$

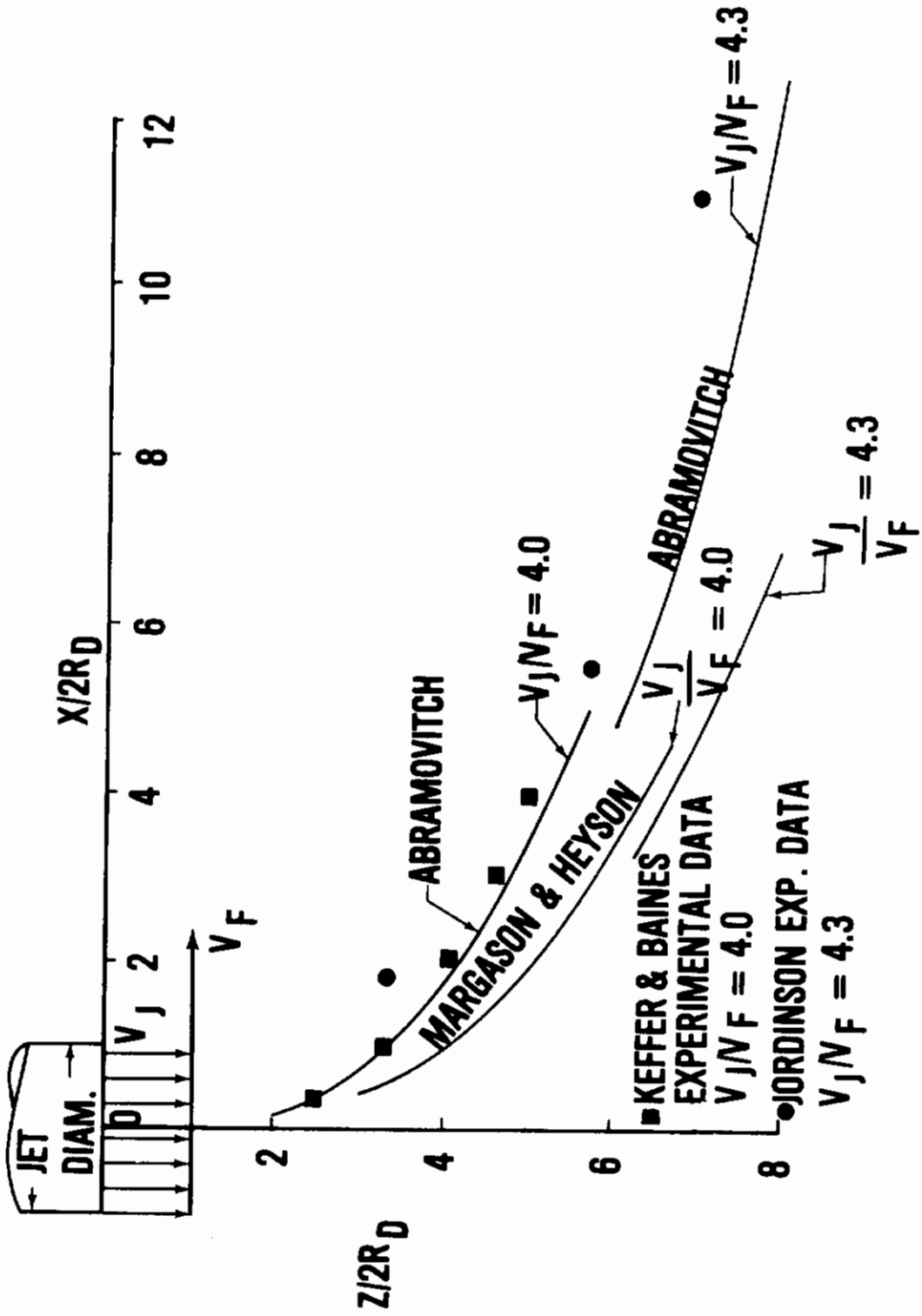

Figure 13. Correlation of Jet Centerline Theories with Experiment ($\Theta_W = 90°$)

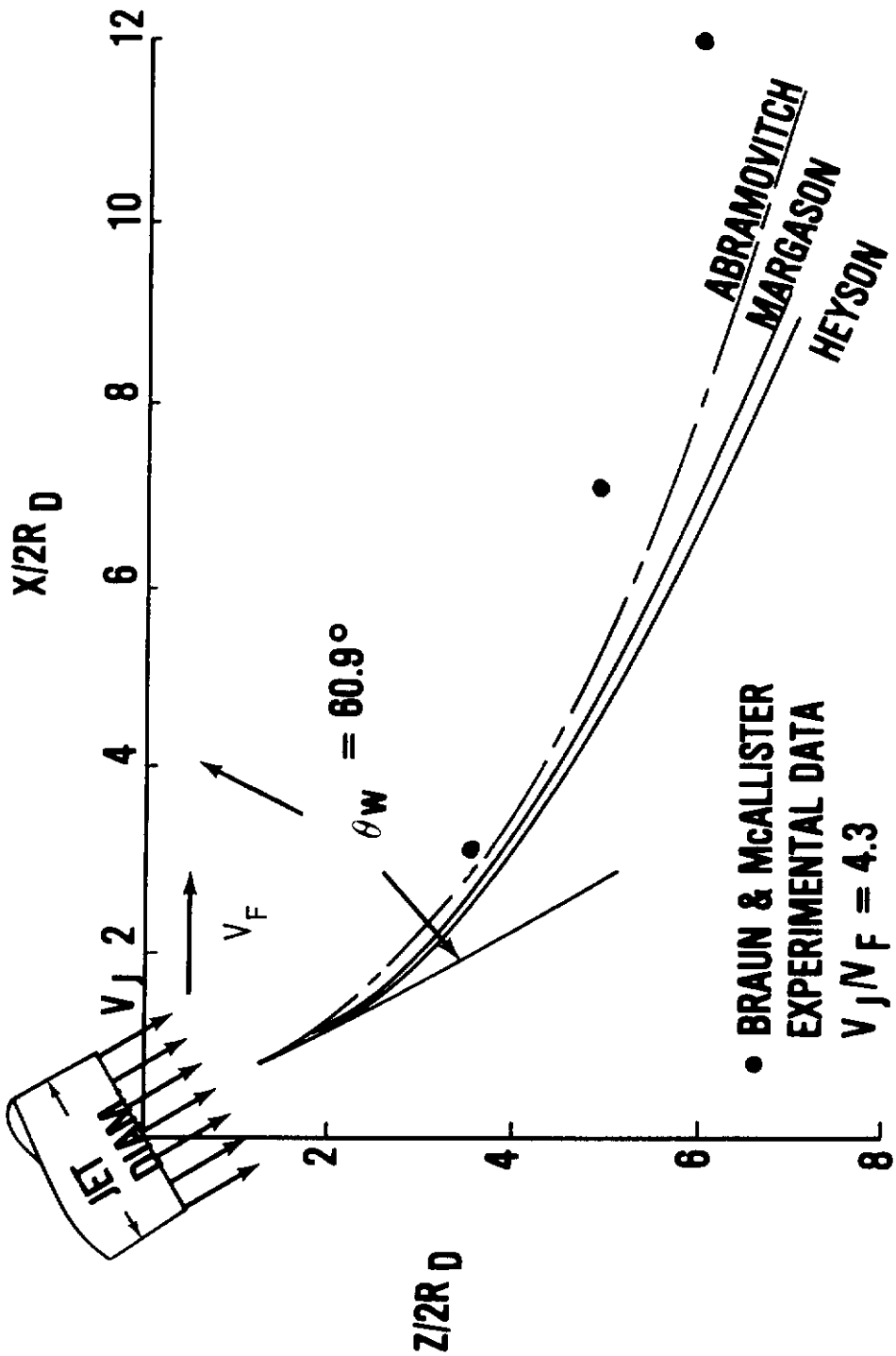

Figure 14. Correlation of Jet Centerline Theories with Experiment (θ_W = 60.9°)

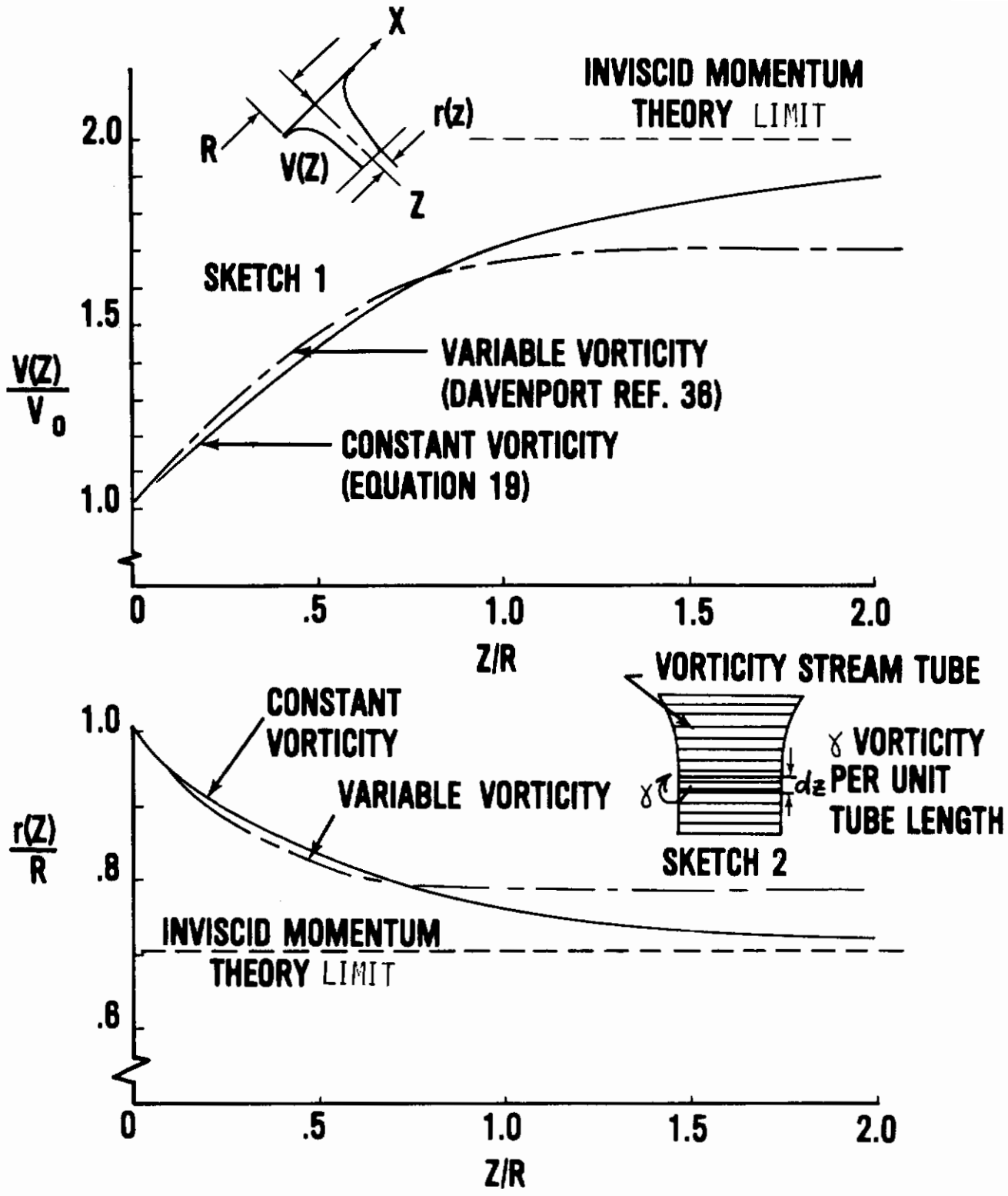

Figure 15. Rotor Wake Contraction in Hover

so that:

$$\frac{r(z)}{R} = V_o^{\frac{1}{2}} V(Z)^{-\frac{1}{2}} \qquad (21)$$

Equations (19) and (21) are plotted in Figure 15 as functions of Z/R. It is seen that the classical far-downstream inviscid momentum results are approached: the velocity in the stream tube far down stream is twice that at the rotor disk plane, and the stream tube radius far downstream is .707R.

Hovering rotor performance calculations using vortex structure based on these assumptions gave results for rotor efficiency which were clearly optimistic in comparison to test data. Davenport[36] improved the correlation between prediction and test data by using a variable-vorticity model for the vorticity stream tube; these results for V(Z) and r(z) are also shown in Figure 15. Davenport's results were used here in relating the equivalent duct radius, R_D, and equivalent jet exhaust velocity, V_J, of Equation (18) to the rotor diameter, R, and rotor inflow velocity, V_o.

Using our engineering judgement and Davenport's results, we assumed that the rotor wash in forward flight could be represented by the duct exhaust as shown in Figure 16. The relationships used to form this transformation are:

$$R_D = .8R$$
$$V_J = 1.6\ V_o \qquad (22)$$

Substituting Equations (22) into Equation (18) then gives:

$$\frac{X}{R} = .11\left(\frac{V_F}{V_o}\right)^{2.6} \left(\frac{Z}{R}\right)^3 + \frac{Z}{R} \cot \Theta_w \qquad (23)$$

This expression, illustrated in Figure 16, can now be used to estimate the wake location relative to the rotor disk. Its use is as follows: (1) the quantity V_o is determined from Equation (15) where W, R, ρ, and V_F are known from the operating conditions of the helicopter; (2) the wake efflux angle Θ_w is determined from Figure 11 where, again, W, R, ρ, and V_F are known parameters; and (3) Equation (23) is then used to determine the X location of the rotor wake for a range of Z/R as the input parameter into this equation.

The first right-hand part of Equation (23) is the effect of entrainment and cross-flow drag effects upon the rotor wake below the disk plane. It is this term that causes the curvature in the rotor wake. The second term or Z/R cot Θ_w, often called the linear wake solution, provides the location of the rotor wake if entrainment and viscous effects were ignored.

5. Helicopter Vortical Wake Decay

The circulation strength, Γ_o, for helicopters in 1-g flight is obtained from Equation (1b) by relating the aircraft span, b, to the rotor diameter, D. The result of this modification is:

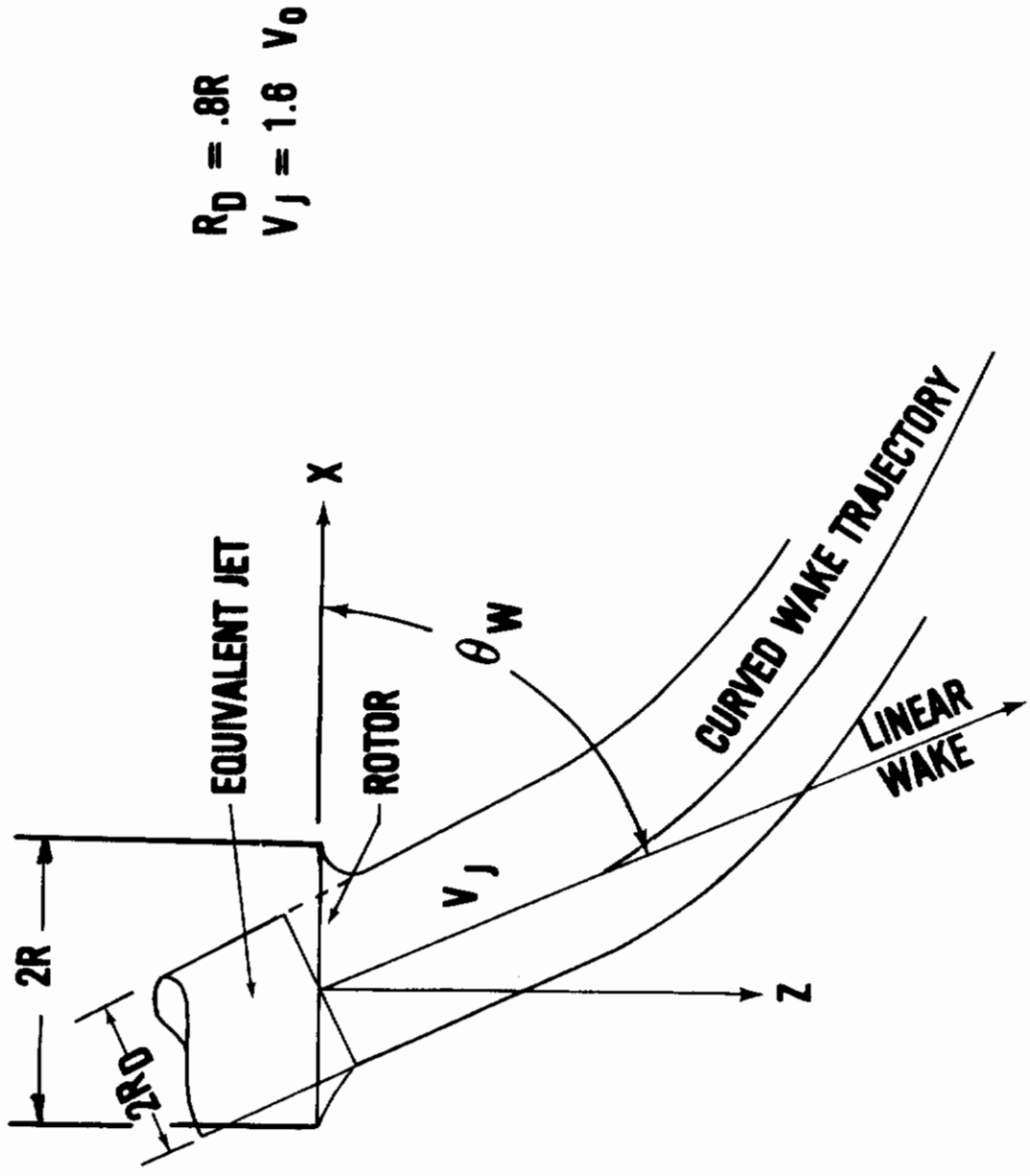

Figure 16. Curved Wake Trajectory Schematic

$$\Gamma_o = \frac{2W}{\pi\rho V_F R}, \quad \frac{XW}{4\rho V_F^2 R^3} \leq 9.58$$

$$\Gamma_o = 9.56 \left(\frac{2W}{\pi\rho V_F R}\right)\left(\frac{XW}{4\rho V_F^2 R^3}\right)^{-1}, \quad \frac{XW}{4\rho V_F^2 R^3} > 9.58 \tag{24}$$

The reason for not using Equation (1a) is pursued further following Equation (26). The question now is whether Equation (10), which was developed for aircraft use, can be applied to the analysis of operations involving helicopters.

In Equations (10) and (11), the variation of r_c with time t followed a $t^{-\frac{1}{2}}$ power law; that is, $X = V_F t$:

$$r_c = K\sqrt{t} \tag{25}$$

When this power law was compared with the vortex decay determined from helicopter flight test summarized by Flinn[6] (see Figure 17), the agreement proved favorable. Therefore, Equation (10) was used in applying vortical decay formulations to helicopters. The flight test data given in Reference 27 was used in obtaining an empirical fit for r_c which becomes:

$$r_c = 244\sqrt{\frac{\nu X}{V_F}} \tag{26}$$

It is noted that the vortex core size as given by Equation (26) is approximately 7 times larger than that given in Equation (11) for airplanes even with flaps fully extended; this result was expected. Now, the results given in Reference 8 indicate that an increase in turbulence level within a vortex causes an increase in core radius r_c. Qualitatively, we would expect that the turbulence level in the rotor wash of a helicopter would be higher than that in the wake behind a wing even with flaps extended. Consequently, the turbulence level in the vortices trailed behind a rotor, as shown in Figure (2), should be larger than that in the vortices trailed behind airplanes even in the landing approach configuration. This leads to the use of the flaps-down definition for Γ_o given in Equation (1b). Further research in this area is required.

Collecting the helicopter wake equations for 1-g flight yields:

$$\Gamma_o = \frac{2W}{\pi\rho V_F R}, \quad \frac{XW}{4\rho V_F^2 R^3} \leq 9.58$$

$$\Gamma_o = 9.58\,(2W/\pi\rho V_F R)\left[\frac{XW}{4\rho V_F^2 R^3}\right]^{-1}, \quad \frac{XW}{4\rho V_F^2 R^3} > 9.58 \tag{27}$$

$$V_\theta = \frac{\Gamma_o}{2r}\left(1 - e^{-1.26/(r/r_c)2}\right)$$

$$r_c = 244\sqrt{\frac{\nu X}{V_F}}$$

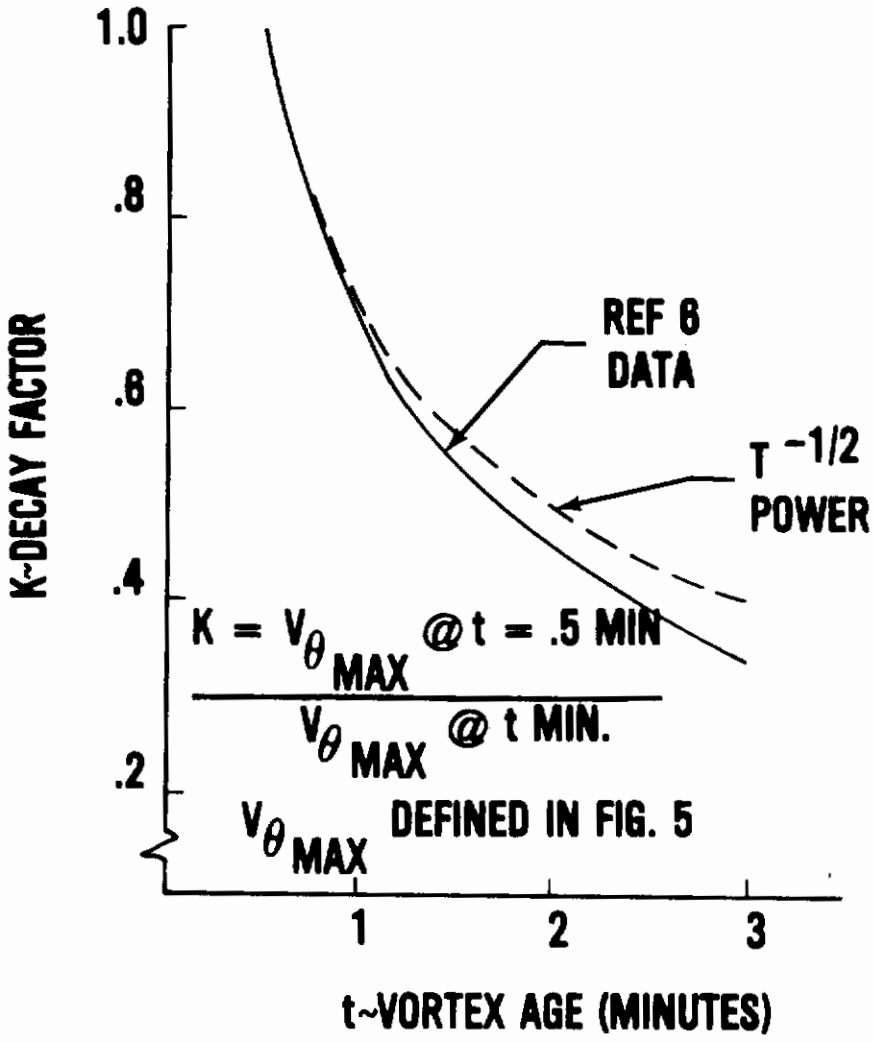

Figure 17. Effect of Time on Helicopter Vortex Decay

6. Helicopter Method Assessment & Other Comments

The method developed above is based upon an equivalent-jet analogy, with empirical equations developed from experimental data on jets exhausting into a freestream; the V_J/V_F ratio tested was of the order of 4.0. Yet, it is known that the V_o/V_F ratio for helicopters with advance ratios of interest here is closer to $.1 \leq V_o/V_F \leq .3$. Therefore, a correlation was needed of the above method with actual helicopter flight test data to assess applicability; the data used was obtained from Reference 37.

The single-rotor helicopter shown in Figure 18 was used to generate the wake and a North American T-28 was used to penetrate the wake in the NASA Langley flight test program described in Reference 37. Colored smoke was streamed into the wake behind the helicopter as an identification device. Recording instruments installed in the airplane were an accelerometer to measure normal acceleration at the center of gravity of the airplane, and a roll control position transmitter to measure pilot control inputs. All other in-flight variables such as airspeed, altitude, heading, and bank angle were indicated on the normal instrument display of the airplane. No recording instruments were installed in the helicopter.

The airplane with 10° flaps penetrated the wake while the helicopter flew at 40 to 60 knots, with a constant heading and altitude (4,000 feet). The wake penetrations consisted of: (1) converging penetrations where the airplane gradually crossed through the helicopter wake from a course nearly parallel to that of the helicopter; (2) descent through the wake on the same heading as the helicopter; and (3) intersecting penetrations from a course 90° to the helicopter heading.

A velocity contour of the wake behind the helicopter is given in Figure 19. This contour was estimated by the probe T-28 aircraft at approximately 3 radii behind the helicopter. Also indicated in this figure is the prediction for the centerline of the helicopter wake; the correlation indicates good agreement between prediction and test data.

As indicated earlier, the equivalent duct radius is .8R, where R is the rotor radius (see Equation (22)). The separation distance b' between the trailed vortices behind the disk plane at 3 radii behind the helicopter is then twice R_D:

$$b' = 1.6R \tag{28}$$

The swirl velocity, V_Θ, through the cross-section of the curved rotor wake is then obtained as follows: (1) use Equation (27) starting at $y = -b'/2$ and determine $V_{\Theta A}$ from left to right in Figure 20 using $r = -b'/2 + r'$ where r' is varied from -.3R up to 2.4R, the subscript A stands for the advancing-side vortex; (2) similarly, determine $V_{\Theta R}$ from right to left in Figure 20 starting at $y = b'/2$ and using $r = b'/2 + r'$ where r' is varied from -.3R up to 2.4R; the subscript R stands for the retreating-side vortex; and (3) sum $V_{\Theta A}$ and $V_{\Theta R}$ to obtain the results shown in Figure 20. Also shown is the swirl velocity, V_e, from results

W = 6,900 LB
R = 26.5 FT
V_T = 538 FPS

MAINROTOR
TWIST = -8 DEG
CONSTANT CHORD
NACA 0012

Figure 18. NASA Langley Test Helicopter (Ref. 37)

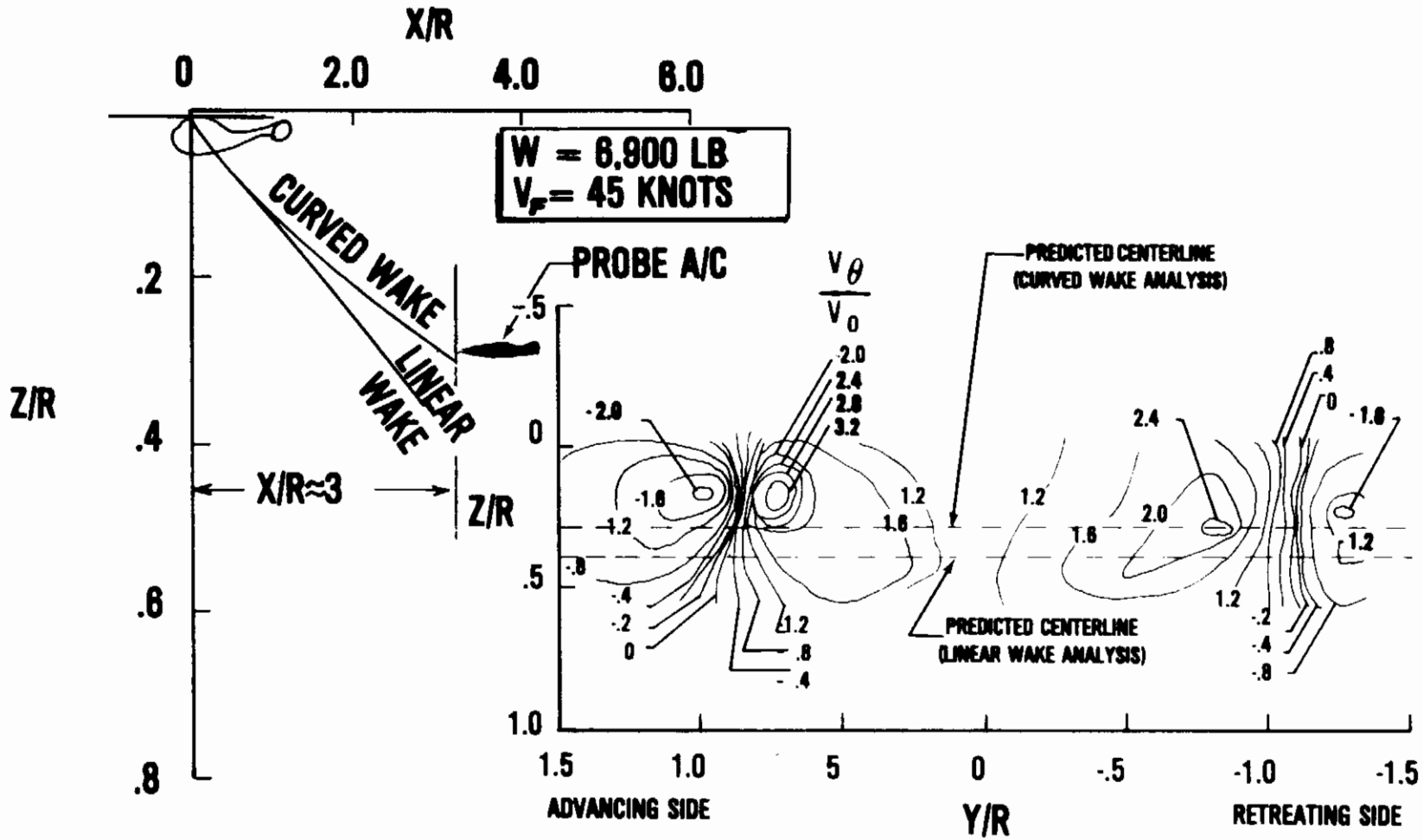

Figure 19. Wake Velocity Contour at X/R≈3 Behind Helicopter

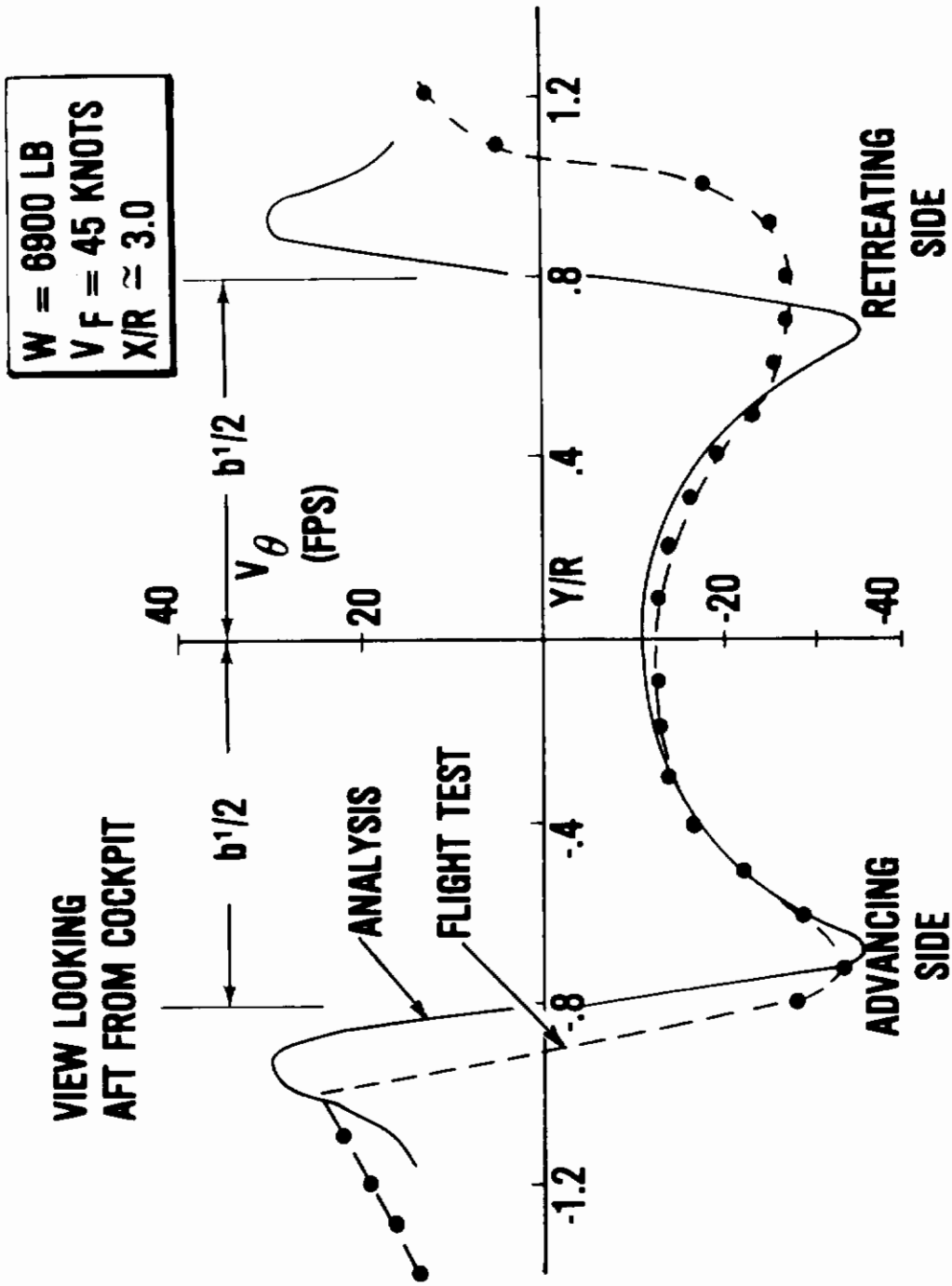

Figure 20. Correlation of Analysis with Flight Test Data (Ref. 37)

of the flight test program. The correlation between prediction and test data is very good on the advancing side but relatively poor in the vicinity of r_c on the retreating side. Nevertheless, the correlation is of sufficient merit to indicate that the method developed for predicting the location and swirling nature of the flow in the rotor wake is useful here in assessing vortical wake hazards caused by helicopters in USAF operations. Further correlations with flight test data are needed to investigate the differences between advancing and retreating side vortical-sheath rollup, and to modify the prediction technique accordingly.

The ground should have the same effect on the rollup-up sheath vortices behind a helicopter as that discussed in Section 2.1. That is, as ground is approached, the vortices slow their descent, level off at an altitude of b'/2, and travel parallel to the earth at an induced speed of $\Gamma_0/2\pi b'$. Equations (5) as developed for aircraft are also applicable here except that Γ_0 and b' are now defined by Equations (24) and (28), and H by Equation (23). Additionally, large shear changes in the atmosphere and bouyancy effects have the same impact on the helicopter vortices as those discussed in 2.1. Therefore, the error analysis, Equations (7), should also be applied to the predicted location of the helicopter vortices; that is:

$$\begin{aligned} \Delta H_v &= \pm V_o \cdot t/4 \\ \Delta Y &= \pm V_s \, t/4 \end{aligned} \qquad (29)$$

where V_o is used in defining the vertical height error band.

Aircraft vortical wake breakup by atmospheric means is discussed in Section 2.3. There, programs conducted by NASA, FAA and the Transportation System Center (TSC) of The Department of Transportation (DOT) suggest that vortices behind airplanes usually do not persist for longer than four minutes. It seems logical that this same rule also applies to the vortices behind helicopters. Of interest here are some of the comments made by the pilots of the probe aircraft in the flight test effort of Reference 37. The penetration flight tests of this study were performed by a research pilot accompanied by an observer. In the pilot's opinion, crossing through the wake center can produce lateral upsets that would be dangerous if occurring near the ground. The pilot further commented that the T-28 limits of roll control were slightly exceeded in these penetration tests. The test airplane was a military trainer which meets the demanding roll control requirements of the military handling qualities specifications.

One of the observer's tasks was to measure with a stopwatch the time interval from wake penetration until the airplane passed by the helicopter, in order to obtain distance estimates. Several attempts were made to measure the wake intensity at extended distances behind the helicopter. Comments from both the pilot and observer indicated that when the separation interval was on the order of a minute, the airplane encountered only minor turbulence. However, neither the pilot nor observer was

sure whether the low intensity encountered at this interval was due to wake dissipation or smoke dispersion, either of which would cause the wake location to be uncertain.

It can be argued that the vortices break up sooner behind helicopters than they do behind aircraft. The turbulence generated by the rotor blades immediately below the rotor disk plane should be much larger then that existing in the vorticity sheet trailed behind an aircraft wing. This additional turbulence should hasten the decay and eventual break up of the helicopter vortices. Further research in this area is needed. All that can be said at this moment is that the vortical wake behind a helicopter could break up as soon as one minute and should be all broken up at two minutes.

SECTION III

THE DEVELOPMENT OF AN ENCOUNTER MODEL

A simplified mathematical model is developed here for implementing appropriate USAF trainers and simulators with the capability of simulating an encounter. It is felt that this course is imperative because many USAF pilots are not fully aware of the dangers involved when encountering wake vortices; this is especially so if the generating aircraft is not a "heavy" transport, defined by the FAA as an aircraft weighing about 300,000 pounds or more. A hazardous example is flight in trail formation when the lead aircraft is pulling g's. Additionally, the HH-53 helicopter at 38,000 pounds is not a "heavy" configuration according to the FAA separation criteria; the strength of the vortical wake it trails while flying at 60 knots is similar to that behind a KC-135 or Boeing 707 in landing approach. Obviously an effort is necessary to impress upon all USAF pilots of the hazards associated with wake vorticity. This can be done through simulation as part of the training curriculum.

A vortex in close proximity to an aircraft influences the forces and moments exerted on all of the aerodynamic surfaces of the aircraft, causing very rapid perturbations in aircraft flight path. Therefore, unsteady aerodynamic effects may be important. A mathematical model that includes all of these effects in detail would require extensive formulation and programming for the computer system at a simulator facility. Much computer storage would be needed, and the encounter computations could not be performed in real time.

To avoid such problems, only the simplest of models representing the encounter is considered here. An isolated-vortex model is used to perturb only the roll equation of the six-degrees-of-freedom equations of motion representing the encountering aircraft.

1. The Swirl Velocity Within the Vortex

There are many analyses which include viscous and turbulent decay effects within the vortex. Many of these analyses are complex, requiring a digital computer program to yield a solution[8]. The exponential solution given by Equation (10) might impact computation time on the simulator if this calculation were performed numerous times during the encounter. Therefore, a simpler yet realistic representation for the flow in a vortex, as given by the Rankine Solid-Body solution[8], is used here:

$$V_\Theta = \frac{\Gamma_o}{2\pi r_c}\left(\frac{r}{r_c}\right), \qquad |r| \le r_c \quad \text{(within the core)}$$

$$V_\Theta = \frac{\Gamma_o}{2\pi r}, \qquad |r| > r_c \quad \text{(outside the core)} \tag{30}$$

where Γ_o is given by Equation (1), for airplanes, or Equation (24), for helicopters; the core size r_c is defined by Equation (11), for airplanes, and by Equation (26) for helicopters.

The swirl velocity V_θ is shown in Figure 21 as a function of lateral displacement. This represents, of course, the velocity distribution normal to any straight line passing through the center of the vortex at any angle. The core radius, r_c, was assumed to be 2 feet; the reason for this assumption follows. The objective of this overall effort is to use simulation to educate pilots on the dangers of a vortex encounter when flying "too close" behind a lead aircraft. On the basis of the T-38[3] and T-39[4] accidents, "too close" was defined as being within 2.5 nautical miles behind the lead airplane, where viscous decay effects have not caused a significant increase in vortical core radius. A core radius of 2 feet is considered to be representative for that location. The equations are developed in full with r_c a variable. Simplifications are then formed to represent r_c = 2 ft. Appropriate corrections will be given for this distance behind the helicopter.

With core radius equaling 2.0 ft, Equations (30) are:

$$V_\theta = \frac{\Gamma_0}{2\pi}\left(\frac{r}{4}\right), \quad |r| \leq 2.0$$

$$V_\theta = \frac{\Gamma_0}{2\pi}\left(\frac{1}{r}\right), \quad |r| > 2.0 \qquad (31)$$

Prior to formulating the effect of the vortex upon the aircraft, it is appropriate to qualitatively describe vehicle motions and pilot control actions as the vortex is encountered; reference is made to Figure 22 . At location A, the upwash field on the pilot's left wing exceeds that exerted on the right wing. Therefore, the pilot pushes his stick left of center so that the ailerons counteract the asymmetrical wing loading to maintain a wings-level attitude. As the aircraft slides from A to B, the amount of aileron required to hold wings level increases. As the aircraft enters the core (i.e., C in Figure 22), the roll moment induced on the aircraft reverses sign. The pilot moves the stick hard over to the right in an attempt to recover. His lag increases the left-rolling tendency until he reverses control. Aileron authority may be exceeded by the vortical effect. The aircraft rolls left-wing-down past 90 degrees and falls down away from the vortex (D and E in Figure 22).

When the aircraft is in between B and C the roll moment induced by the vortex changes sign. At this instant, the aircraft accelerates downward and (if stable) pitches nose-down due to the change in upwash field. Even though the pilot may use elevator and throttle to correct for this situation, it is believed that the pilot's main concern is his bank angle. Similar arguments can be presented as the aircraft passes from C, through D, and to E; the pilot's main concern is regaining wings level. Therefore, an encounter model which serves as a disturbance input only to the roll equation of motion may be adequate for the purpose.

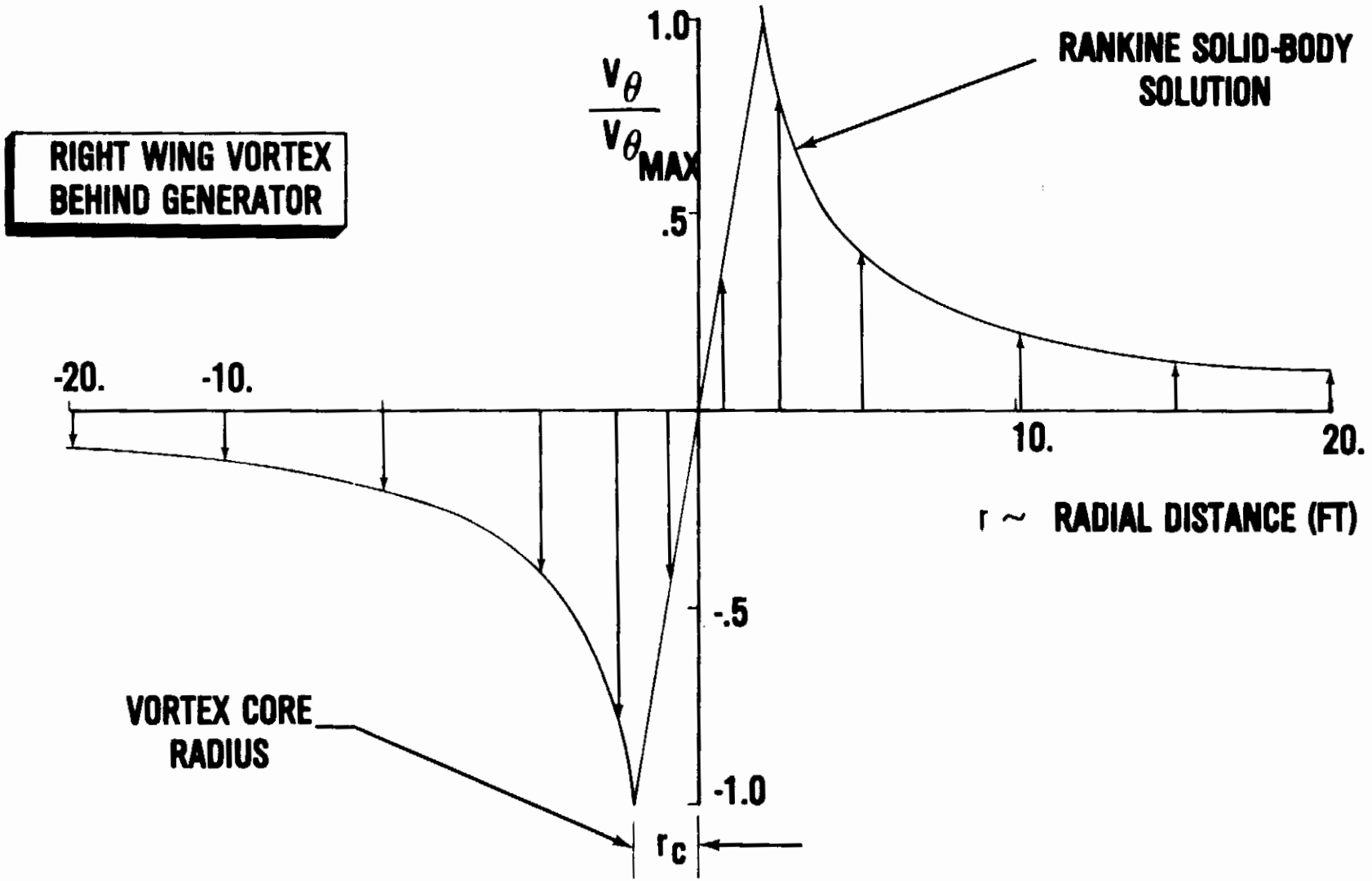

Figure 21. Normalized Swirl Velocity Used in Encounter Model

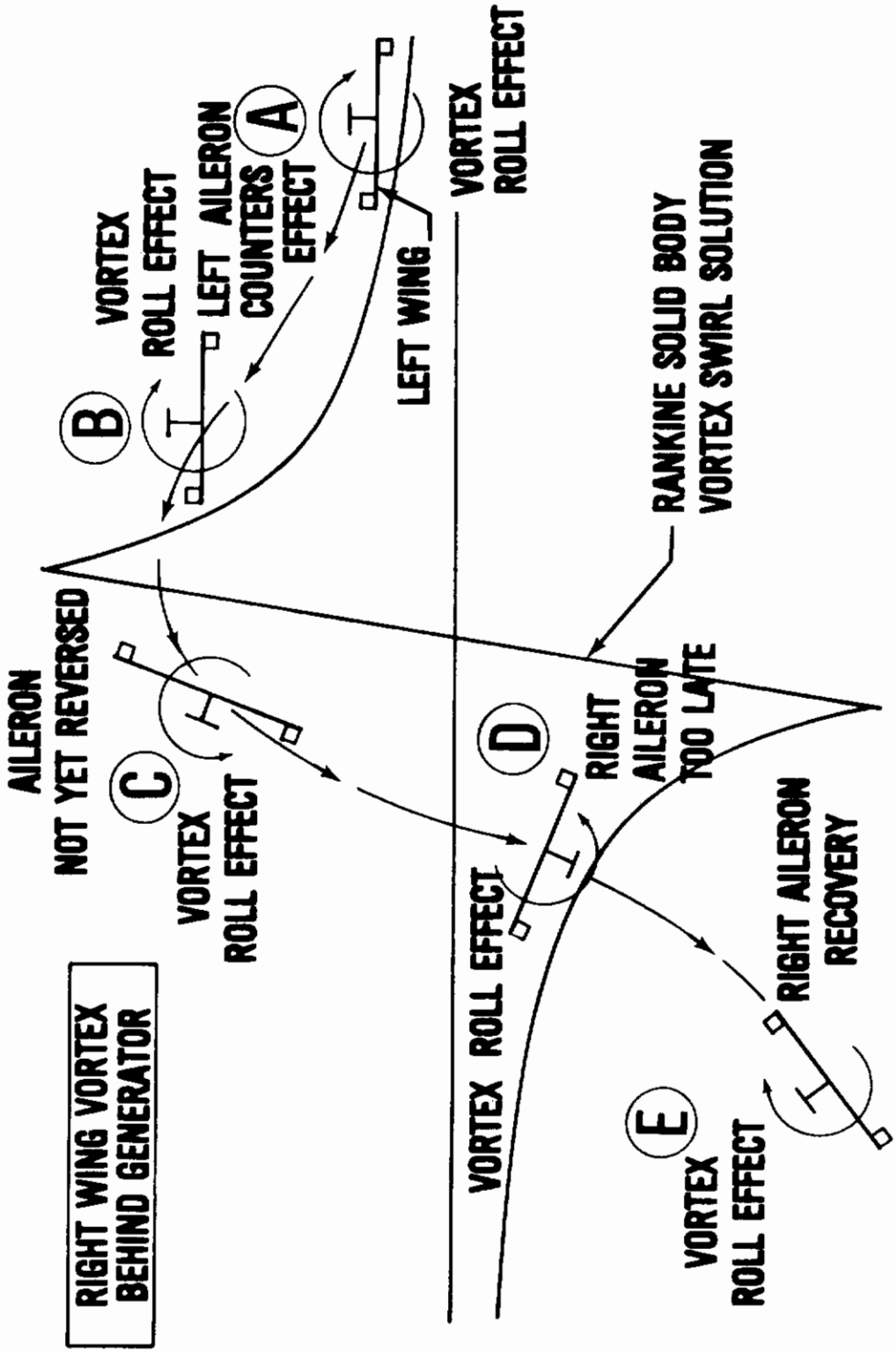

Figure 22. Pilot Action During an Encounter

2. Roll Model Formulation

The centerline of the vortex parallels the aircraft x (longitudinal) body axis and moves along the y (lateral) axis during the encounter; reference is made to Figure 23 . In addition, it is assumed that the aircraft rolls while sliding through the vortex core and falls away so quickly that the induced effect from the other wing-tip vortex behind the generating aircraft need not be considered here; the roll moment contributions from the fuselage, empennage, and landing gear are negligible in comparison to the roll moment of the wing during the encounter, and unsteady aerodynamics are neglected.

The lift on the wing element dy at spanwise station y due to a vortex located at $\bar{y}$ as shown in Figure 23 is:

$$dL = \tfrac{1}{2}\rho V^2 C_{L_{\alpha_{3\text{-}D}}} \alpha(y)c(y)dy \tag{32}$$

where $C_{L_{\alpha_{3\text{-}D}}}$ is the wing section lift curve slope, $C_{L_{\alpha_{2\text{-}D}}}$, corrected for sweepback λ and finite aspect ratio AR:

$$C_{L_{\alpha_{3\text{-}D}}} = \frac{AR\ \cos\lambda C_{L_{\alpha_{2\text{-}D}}}}{AR\sqrt{1 + \left[\frac{C_{L_{\alpha_{2\text{-}D}}}\cos\lambda}{\pi AR}\right]^2} + \frac{C_{L_{\alpha_{2\text{-}D}}}\cos\lambda}{\pi}} \tag{33}$$

Equation (33) is from Reference 38. Here, $C_{L_{\alpha_{2\text{-}D}}}$ can be taken to be 5.73 per radian. This equation for the lift curve slope provides a smooth and continuous function from $\pi AR/2$ at low aspect ratios to $C_{L_{\alpha_{2\text{-}D}}} AR/(C_{L_{\alpha_{2\text{-}D}}} + \pi AR)$ at high aspect ratios (See Reference 28).

The incremental roll moment about the X body axis of the aircraft is:

$$d\mathcal{L} = \tfrac{1}{2}\rho V^2 S b dC_l = -y dL \tag{34}$$

where the direction of positive roll moment is indicated in Figure 23.

Substituting Equation (32) into Equation (34) to obtain the roll moment coefficient yields:

$$\frac{b^2}{C_{L_{\alpha_{3\text{-}D}}}} dC_{\mathcal{L}} = -\alpha\, y dy \tag{35}$$

when it is assumed that the wing chord c(y) is a constant over the span.

Using small-angle approximations, the angle of attack induced on the wing by a vortex located at $\bar{y}$ is:

$$\alpha = V_\theta / V \tag{36}$$

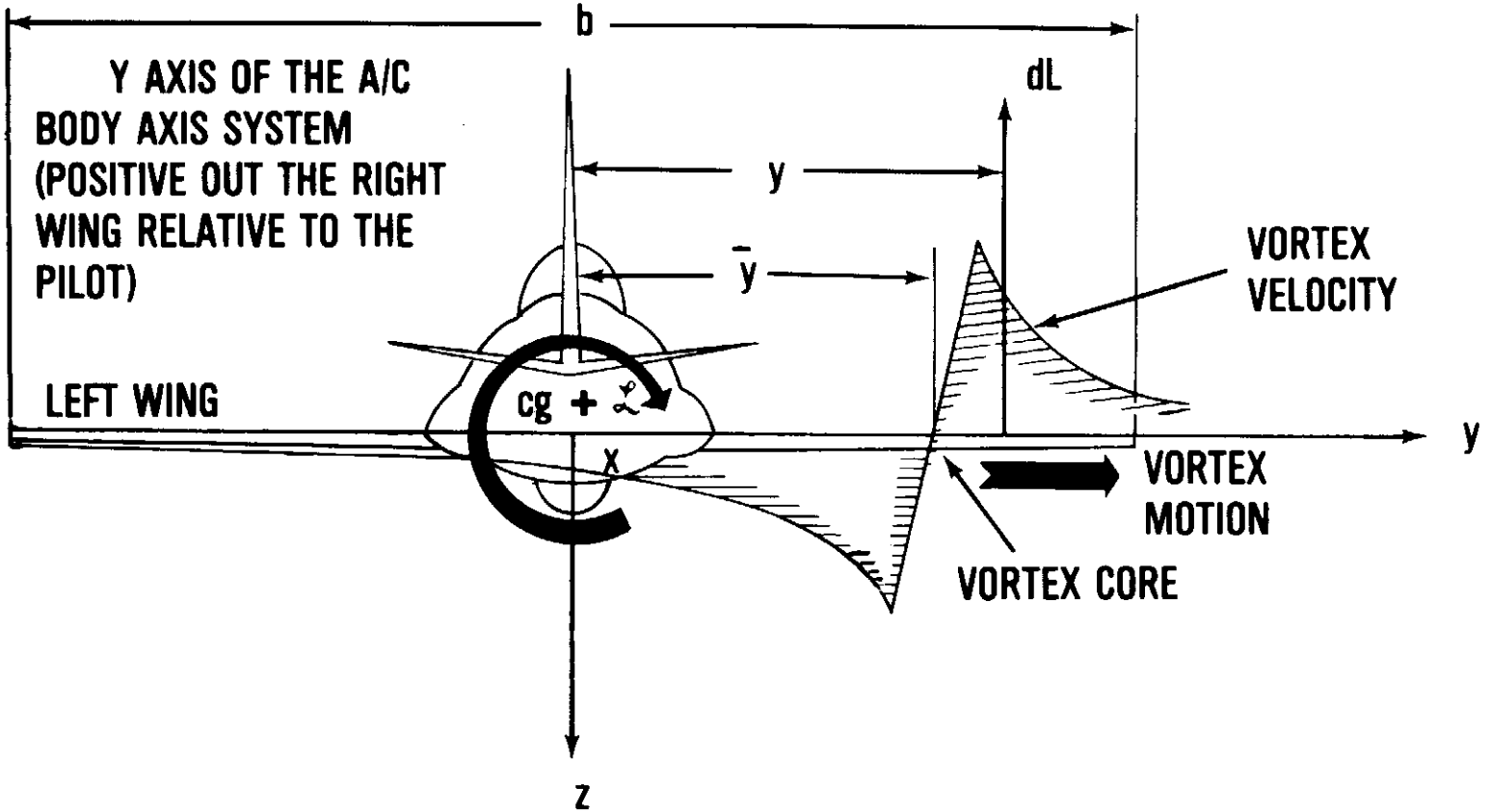

Figure 23. Schematic for Roll Model Formulation

By transforming Equation (30) so that the vortex is located at $\bar{y}$:

$$\alpha = \frac{\Gamma_o}{2\pi V r_c^2}(y - \bar{y}),\ (\bar{y} - r_c) \le y \le (\bar{y} + r_c)$$
$$\alpha = \frac{\Gamma_o}{2\pi V}\left(\frac{1}{y - \bar{y}}\right),\ y > (\bar{y} + r_c) \text{ or } y < (\bar{y} - r_c) \tag{37}$$

Substitution Equation (37) into Equation (35) and forming integrals produces:

$$\frac{2\pi V b^2 C_l}{\Gamma_o C_{L_{\alpha_{3\text{-}D}}}} = -\int_{-b/2}^{\bar{y}-r_c} \frac{y\,dy}{(y-\bar{y})} - \frac{1}{r_c^2}\int_{\bar{y}-r_c}^{\bar{y}+r_c}(y-\bar{y})y\,dy - \int_{\bar{y}+r_c}^{b/2} \frac{y\,dy}{(y-\bar{y})} \tag{38}$$

when the vortex core lies completely on the wing such that $|2\bar{y}/b| < 1 - 2r_c/b$. Additionally:

$$\frac{2\pi V b^2 C_l}{\Gamma_o C_{L_{\alpha_{3\text{-}D}}}} = -\int_{-b/2}^{\bar{y}-r_c} \frac{y\,dy}{(y-\bar{y})} - \frac{1}{r_c^2}\int_{\bar{y}-r_c}^{b/2}(y-\bar{y})y\,dy \tag{39}$$

when the vortex core is at the wing tip or when $(1 - 2r_c/b) \le |2\bar{y}/b| \le (1 + 2\,r_c/b)$. Also:

$$\frac{2\pi V b^2 C_l}{\Gamma_o C_{L_{\alpha_{3\text{-}D}}}} = -\frac{1}{r_c^2}\int_{-b/2}^{b/2}(y-\bar{y})y\,dy \tag{40}$$

when the wing is completely immersed in the vortex core or $|2\bar{y}/b| + 1 \le 2r_c/b$. Finally:

$$\frac{2\pi V b^2 C_l}{\Gamma_o C_{L_{\alpha_{3\text{-}D}}}} = -\int_{-b/2}^{b/2} \frac{y\,dy}{(y-\bar{y})} \tag{41}$$

where the core lies outside of the wing with $|2\bar{y}/b| > 1 + 2r_c/b$.

Integrating these equations in order yields:

$$\frac{2\pi V b\ C_l}{\Gamma_o C_{L_{\alpha_{3\text{-}D}}}} = -1 + \frac{1}{2}\left(\frac{2\bar{y}}{b}\right)\ln\left|\frac{(2\bar{y}/b)+1}{(2\bar{y}/b)-1}\right| + \frac{2}{3}\left(\frac{2r_c}{b}\right) \tag{42}$$

for $|2\bar{y}/b| < 1 - 2r_c/b$.

$$\frac{2\pi VbC_{l}}{\Gamma_{o}C_{L_{\alpha_{3-D}}}} = -\frac{1}{2} + \frac{1}{2}\left(\frac{2\bar{y}}{b}\right)\ln\left|\frac{1+2\bar{y}/b}{2r_{c}/b}\right| + \frac{1}{3}\left(\frac{2r_{c}}{b}\right)$$

$$- \frac{1}{6(2r_{c}/b)^{2}} - \frac{1}{12(2r_{c}/b)^{2}}\left(\frac{2\bar{y}}{b}\right)^{3} + \frac{(2\bar{y}/b)}{4}\left[\frac{1}{(2r_{c}/b)^{2}} - 1\right] \qquad (43)$$

for $(1 - 2r_{c}/b) \leq |2\bar{y}/b| \leq (1 + 2r_{c}/b)$

$$\frac{2\pi VbC_{l}}{\Gamma_{o}C_{L_{\alpha_{3-D}}}} = -\frac{1}{3(2r_{c}/b)^{2}} \qquad (44)$$

when $|2\bar{y}/b| + 1 \leq 2r_{c}/b$, and:

$$\frac{2\pi VbC_{l}}{\Gamma_{o}C_{L_{\alpha_{3-D}}}} = -1 + \frac{1}{2}\left(\frac{2\bar{y}}{b}\right)\ln\left|\frac{(2\bar{y}/b)+1}{(2\bar{y}/b)-1}\right| \qquad (45)$$

for $|2\bar{y}/b| > 1 + 2r_{c}/b$.

Taking the core radius as r_{c} = 2 ft, the last term of Equation (42) or $2/3(2r_{c}/b)$ becomes 2.6667/b. It is noted that the quantity 2.6667/b << 1 when the span of the encountering aircraft exceeds 25 feet, which is true of most of the USAF fleet of aircraft. Thus, Equation (42) or the roll moment when the core is completely on the wing span, becomes equivalent to Equation (45), the roll moment when the core lies competely outside of the wing semi span. These equations are recast to form:

$$\frac{VbC_{l}}{\Gamma_{o}K_{1}} = -1 + \frac{1}{2}\left(\frac{2\bar{y}}{b}\right)\ln\left|\frac{(2\bar{y}/b)+1}{(2\bar{y}/b)-1}\right| \qquad (46)$$

K_{1} is a "calibrated-lift-curve slope" which is discussed later in this section. This equation is seen to apply for any small vortex core located anywhere except very close to the wing tips; there, Equation (43) with r_{c} = 2 ft should be used in determining the roll moment.

Equation (46) is symmetrical about $2\bar{y}/b = 0$ and is plotted and tabulated in Figure 24. Also given in tabular form are the peak values of C_{l} at the wing tip when r_{c} = 2 was substituted in Equation (43). Also indicated is an approximate straight-line fit of this recommended function which could be used to facilitate programming of C_{l} as an input for computer facilities. The airplane is subjected to a negative roll moment when the vortex is less than 82% of the wing semispan and a positive roll moment when $\left|\frac{2\bar{y}}{b}\right| > .82$; reference is also made to the discussions regarding Figure 22.

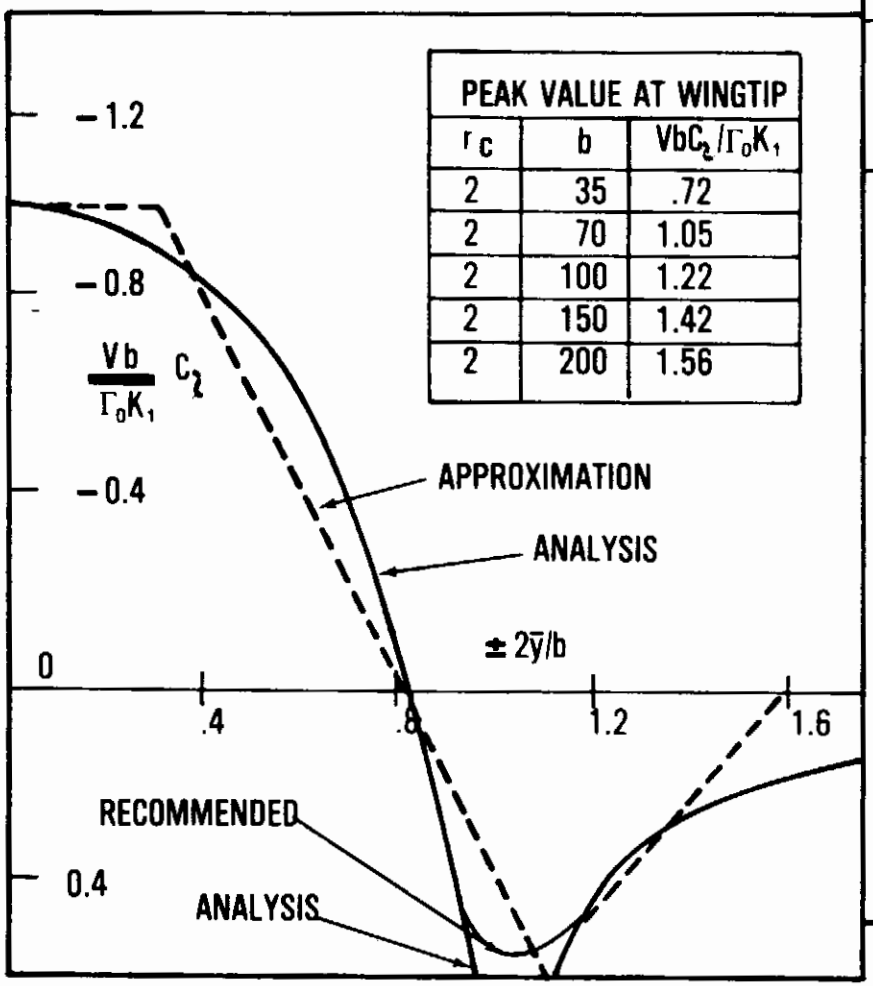

PEAK VALUE AT WINGTIP		
r_c	b	VbC_2/Γ_0K_1
2	35	.72
2	70	1.05
2	100	1.22
2	150	1.42
2	200	1.56

$K_2 = b/2V$

1	2	3	4
$2\bar{y}/b$	$\frac{Vb\,C_2}{\Gamma_0K_1}$ ANALYSIS	$\frac{Vb\,C_2}{\Gamma_0K_1}$ APPROXIMATE	t (SEC)
±1.6	.17	0	0
±1.5	.21	.14	$1K_2$
±1.4	.25	.25	$2K_2$
±1.3	.32	.37	$3K_2$
±1.2	.44	.49	$4K_2$
±1.1	.54	.60	$5K_2$
±1.0	.54	.40	$6K_2$
± .9	.33	.20	$7K_2$
± .8	− .12	0	$8K_2$
± .7	− .39	− .20	$9K_2$
± .6	− .58	− .40	$10K_2$
± .5	− .73	− .60	$11K_2$
± .4	− .83	− .80	$12K_2$
± .3	− .91	−1.00	$13K_2$
± .2	− .96	−1.00	$14K_2$
± .1	− .99	−1.00	$15K_2$
0	−1.00	−1.00	$16K_2$

FIGURE 24. Recommended Roll Function for Indoctrination Training

The function K_1 is given by:

$$K_1 = C_{L_{\alpha_{3\text{-}D}}} K_f/2\pi \qquad (47)$$

where K_f is a factor which "corrects" the analytical result to correspond to a particular observed case. The function K_1 is given in Figure 25 and discussed further following the next Equation (48).

If the aircraft approaches the vortex at a small angle Ψ to its axis, the relative lateral velocity of the vortex is $V_y \simeq V\Psi$ where we have taken a Ψ of 0.1 radian (5 or 6 degrees). Thus each increment of $2\Delta\bar{y}/b = .1$, in column 1 of the Table in Figure 24, corresponds to a time increment, Δt, of:

$$\Delta t = K_2 = \frac{b}{2V} \qquad (48)$$

where $K_2 = b/2V$. The elapsed time t can then be generated by summing these time increments as shown in column 4 in the table.

The quantity K_1 in Equation (46) still remains to be determined prior to implementing the math model for an encounter. This consists of determining K_f, since $C_{L_{\alpha_{3\text{-}D}}}$ is given in Equation (33). As noted earlier, the objective of this overall effort is to develop a simple yet realistic math model for simulating a vortex encounter when a pilot flies "too close" behind a lead aircraft. The T-38 accident described in reference 3 serves as an excellent example of such a situation. The T-38 had closed to 2-1/2 miles behind a stretched C-130 when the encounter occurred. An analysis of this accident including digital computer simulation indicated that the aileron authority of the T-38 was exceeded by more than 100%.

Since all data relevant to this accident was readily available, we decided to use it to calibrate the math model. That is, engineering judgment was used to adjust K_1 through K_f to give a realistic simulation. The result of this adjustment of C_{L_α} is given as K_1 in Figure 25, based on Equation (33). The quantities V, b, and K_1 as used in Figure 24 are now determinable. The vortex strength, Γ_o, of the generator aircraft is found from Equation (1).

As indicated earlier, the function shown in Figure 24 is the roll moment when r_c = 2 feet. This function is adequate for estimating encounters close in behind generating airplanes. However, a 2-foot radius would overestimate the roll moment caused by the wake of a helicopter flying at the same airspeed or by the wake of an airplane significantly greater than 2.5 nautical miles ahead. As shown in Equations (11) and (26), the vortex cores behind a large helciopter can be significantly larger than 2 feet, and the core size behind an aircraft increases with time. Thus, Equations (42) through (45) are recommended for use if r_c is significantly larger than 2.0.

However, a trainer may not have the computer storage to program these equations due to computer requirements for modelling the simulated

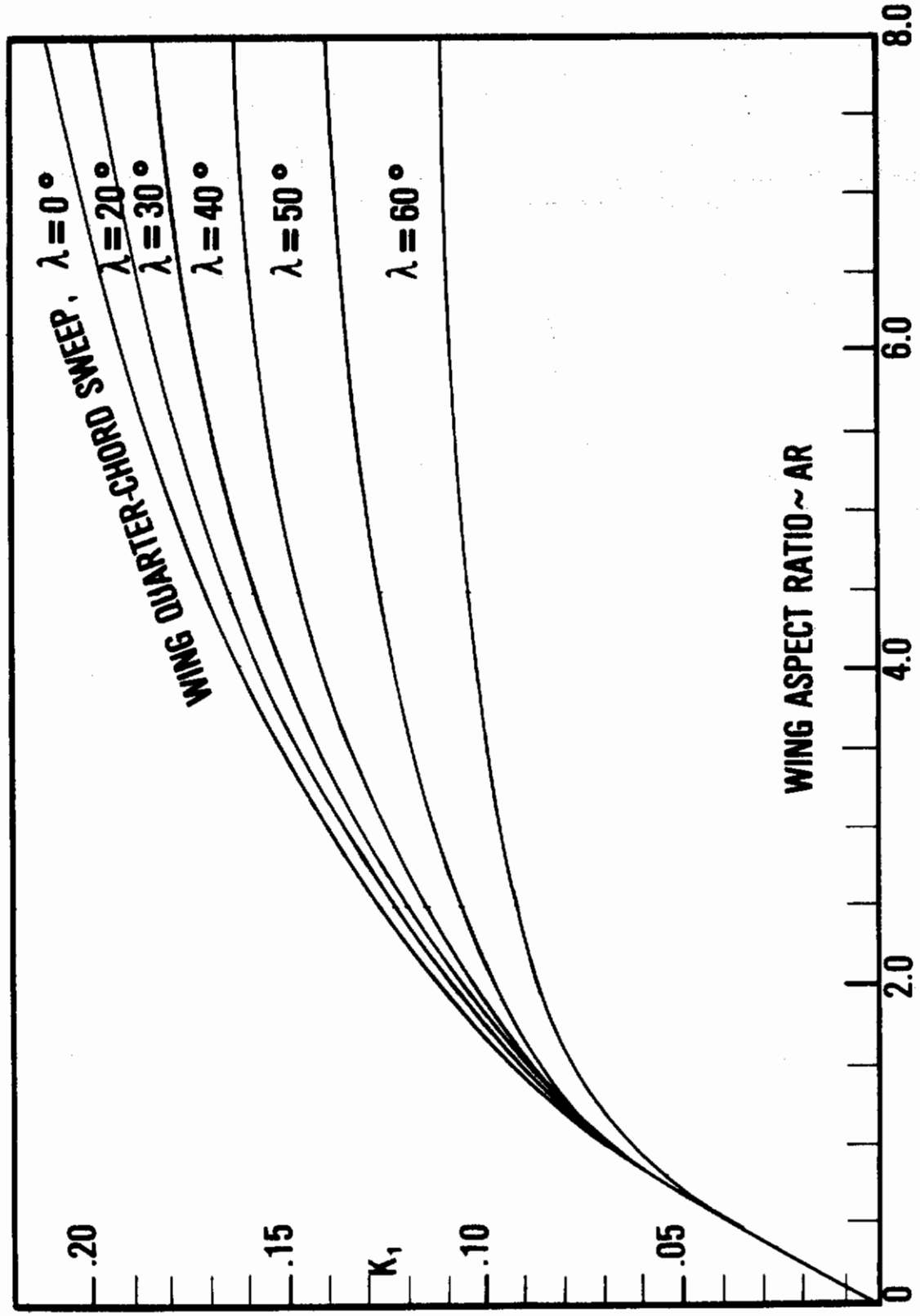

Figure 25. The Variation of K_1 with Aspect Ratio & Sweep Angle

aircraft. Here, an attenuation factor, K_3, as developed below is suggested as a "fudge factor" alternative; it is used to modify Equation (46) to allow for an increase in r_c.

Substituting $\bar{y} = 0$ into Equation (42) and using Equation (44) yields:

$$\frac{2VbC_l}{\Gamma_o C_{L_\alpha 3\text{-}D}} = \begin{cases} -1 + \frac{2}{3}\left(\frac{2r_c}{b}\right), & r_c \leq \frac{b}{2} \\ -\frac{1}{3}\frac{1}{(2r_c/b)^2}, & r_c > \frac{b}{2} \end{cases} \tag{49a}$$

For a small-core vortex on the airplane centerline, Figure 24 shows that $2\,VbC_l/\Gamma_o C_{L_{\alpha 3\text{-}D}}$ is -1. Then we can define an attenuation factor, K_3, as the ratio of large-core rolling moment to small-core rolling moment. This leads to expressions which can be used as a crude engineering approximation for the attenuation in roll moment or:

$$\begin{aligned} K_3 &= 1 - \frac{2}{3}\left(\frac{2r_c}{b}\right) && r_c \leq \frac{b}{2} \\ K_3 &= \frac{1}{3}\left(\frac{b}{2r_c}\right)^2 && r_c > \frac{b}{2} \end{aligned} \tag{49b}$$

The attenuation factor K_3 is shown as a function of $2r_c/b$ in Figure 26. Equation (46) is multiplied by this factor to account for roll moment attentuation as a result of an increase in vortical core size.

Let us summarize the above results. The equations to be used in simulating an encounter where the core size, r_c, is a variable are:

$$\frac{Vb}{\Gamma_o K_1} C_l = -1 + \frac{1}{2}\left(\frac{2\bar{y}}{b}\right) \ln\left|\frac{(2\bar{y}/b) + 1}{(2\bar{y}/b) - 1}\right| + \frac{2}{3}\left(\frac{2r_c}{b}\right) \tag{50a}$$

for $|2\bar{y}/b| < 1 - 2r_c/b$,

$$\frac{VbC_l}{\Gamma_o K_1} = -\frac{1}{2} + \frac{1}{2}\left(\frac{2\bar{y}}{b}\right) \ln\left|\frac{1+2\bar{y}/b}{2r_c/b}\right| + \frac{1}{3}(2r_c/b) - \frac{1}{6(2r_c/b)^2} - \frac{1}{12}\frac{(2\bar{y}/b)^3}{(2r_c/b)^2} + \frac{(2\bar{y}/b)}{4}\left[\frac{1}{(2r_c/b)^2} - 1\right] \tag{50b}$$

for $(1 - 2r_c/b) \leq |2\bar{y}/b| \leq (1 + 2r_c/b)$,

$$\frac{VbC_l}{\Gamma_o K_1} = -\frac{1}{3(2r_c/b)^2} \tag{50c}$$

when $|2\bar{y}/b| + 1 \leq 2r_c/b$,

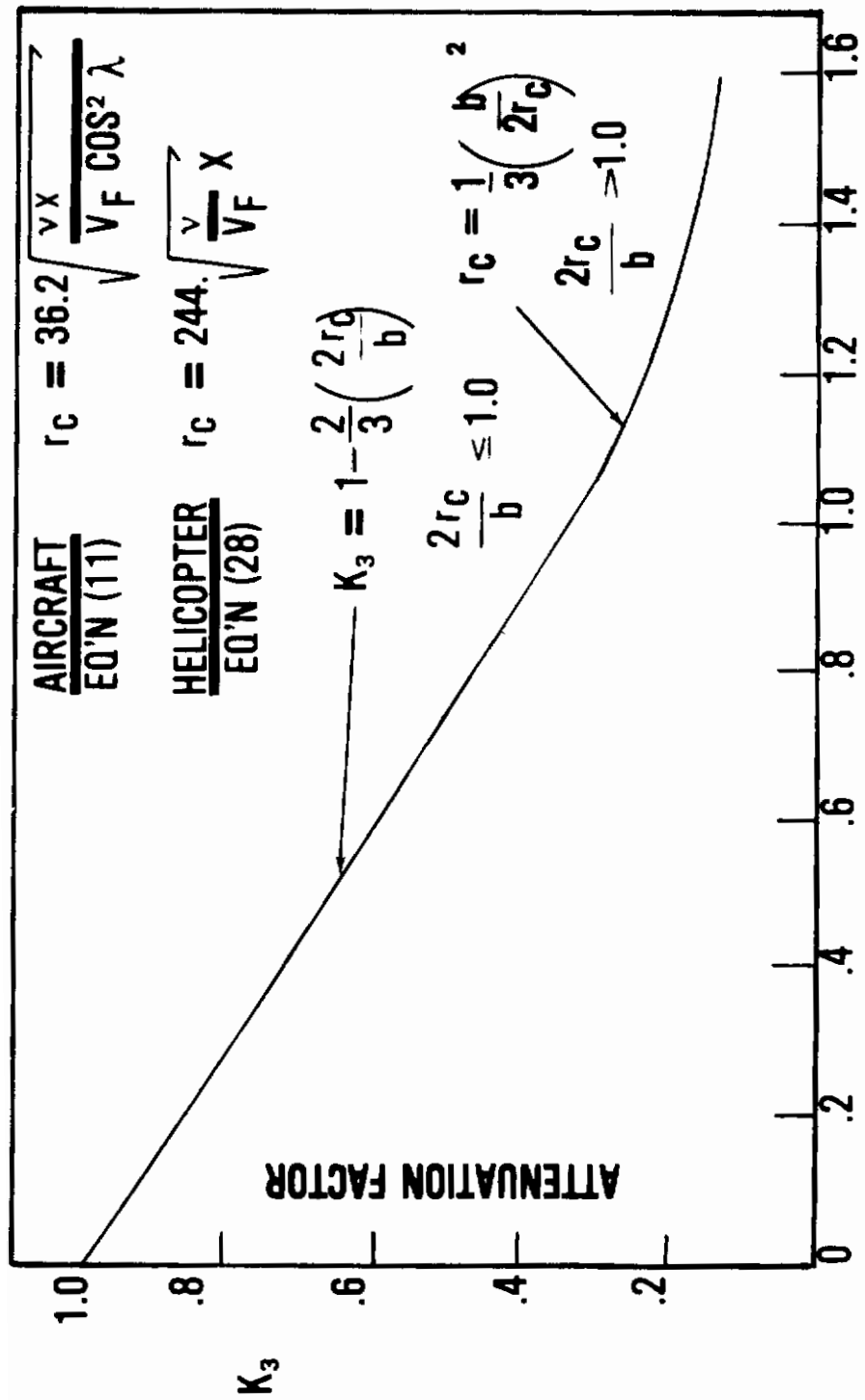

Figure 26. The Variation of Attenuation Factor K_3 with Core Size

$$\frac{VbC_1}{\Gamma_o K_1} = -1 + \frac{1}{2}\left(\frac{2\bar{y}}{b}\right) \ln \left|\frac{(2\bar{y}/b)+1}{(2\bar{y}/b)-1}\right| \qquad (50d)$$

when $|2\bar{y}/b| > 1 + 2r_c/b$. The quantity K_1 is given in Figure 25 and Γ_o by Equation (1).

The equations recommended for indoctrinational use on USAF trainers for simulating trail formation and terminal area operations where one aircraft follows another is obtained by letting r_c = 2 ft. The result is:

$$\frac{VbC_1}{\Gamma_o K_1} = -1 + \frac{1}{2}\left(\frac{2\bar{y}}{b}\right) \ln \left|\frac{(2\bar{y}/b)+1}{(2\bar{y}/b)-1}\right| \qquad (51)$$

where this function is shown in Figure 24. Again V, b, Γ_o, and K_1 are known quantities.

Equation (51) can be modified to allow for an increase in core size, r_c, by using the attenuation factor K_3; that is:

$$\frac{VbC_1}{\Gamma_o K_1 K_3} = -1 + \frac{1}{2}\left(\frac{2\bar{y}}{b}\right) \ln \left|\frac{(2\bar{y}/b)+1}{(2\bar{y}/b)-1}\right| \qquad (52)$$

where extensive use is made of the function given in Figure 24. However, it is recommended that Equations (50) be used if there is a need for a variable r_c as an input to the simulation.

3. Parameters of USAF Aircraft

An effort to categorize airplanes in terms of vortex generating aircraft and encountering aircraft is summarized in Tables 1 and 2. The geometrical parameters needed for tracking the vortices behind these aircraft and for determining core size are presented in Table 1. The stall velocity, V_S, is the minimum obtainable speed while flying at maximum landing weight. Table 2 presents these aircraft as categorized from 3 to 10 as generators. Category 10 contains the heaviest of USAF transports or air carriers, which are most dangerous to other following aircraft; while category 3 contains the smallest airplanes within the USAF fleet. Excluded are the Remotely Piloted Vehicles (RPV's) or unmanned aircraft, since these vehicles generally are small and do not operate in the terminal environment near an airfield. The circulation, Γ_o, for each airplane was determined by considering its landing speed to be 1.2 V_{STALL}, while the weight was taken as 85 percent of the landing gear placard weight. A mean average Γ_o was then formed for aircraft in each category. It is assumed that this Γ_o is applicable for normal ascent and descent at sea level standard during terminal area operation.

Army helicopters that may operate from the same field as USAF airplanes are categorized in Table 3; also listed are some commercial helicopters that could operate in joint FAA-USAF airspace such as Kirtland AFB or in adjacent FAA-USAF airspace such as Wright-Patterson AFB. These helicopters are categorized from 5 to 9 as generators.

TABLE 1 USAF AIRPLANE CONFIGURATIONS

AIRPLANE	W (lb)	b(ft)	V_s(fps)	CARGO $S(ft^2)$	AR	λ(deg)
C-5A	769,000	219.0	201.0	6,200	7.75	25.0
C-7A	28,500	95.6	78.3	912.4	10.00	-3.0
C-9A	99,000	93.3	175.5	1,000.7	8.65	24.5
C-10A	14,500	52.0	142.0	270.0	10.00	0.0
C-47D	33,000	95.0	109.8	987.0	9.00	12.0
C-54G	82,500	117.5	148.5	1,462.0	9.44	0.0
C-97G	159,000	141.2	178.0	1,768.7	11.50	5.5
C-118A	108,000	117.5	153.2	1,463.0	9.44	0.0
C-119G	72,700	109.3	158.5	1,447.2	8.25	4.0
C-121G	122,000	123.0	162.7	1,650.0	9.17	6.5
C-123B	58,800	110.0	136.7	1,223.2	9.89	1.0
C-123K	60,000	110.0	138.4	1,223.2	9.89	1.0
C-124C	194,500	174.1	175.6	2,506.0	11.96	2.5
C-130B	135,000	132.6	165.4	1,745.5	10.09	0.0
C-130P	130,000	132.6	172.7	1,745.0	10.09	0.0
C-131E	50,670	105.3	141.8	920.0	12.00	6.5
C-133B	284,760	179.7	190.7	2,673.0	12.10	0.0
C-135B	230,000	130.0	228.0	2,433.0	7.10	35.0
VC-137C	207,000	145.9	222.9	2,892.0	7.30	35.0
C-140A	30,000	53.7	193.4	542.5	5.30	30.0
C-141A	323,100	160.7	194.2	2,338.1	7.90	24.0
			BOMBER			
B-47E	180,000	116.0	288.3	1,428.0	9.43	35.0
B-52H	450,000	185.0	258.3	4,000.0	8.55	35.0
B-57E	41,000	64.0	184.1	960.0	4.27	5.0
B-58A	95,000	56.8	250.0	1,542.5	2.10	51.5
B-70A	296,300	105.0	184.0	6,300.0	2.00	58.0

TABLE 1 USAF AIRPLANE CONFIGURATIONS (CONT'D)

A/C Airplane	W (lb.)	b(ft)	V_s(fps)	S(ft^2)	AR	Λ(deg)
				ATTACK		
A-1H/J	21,000	50.0	174.0	400.3	6.25	3.5
A-7D	28,850	38.7	254.5	375.0	4.00	35.0
A-26A	36,380	71.5	168.0	541.0	9.00	0.0
A-37B	14,000	38.4	178.0	183.9	8.02	0.0
A-10	30,000	57.6	202.0	506.0	6.54	0.0
				TANKER		
KC-135A	230,000	130.8	228.0	2433.0	7.10	35.0
				FIGHTER		
F-4E	46,000	38.4	268.0	530.0	2.82	25.0
F-5E	21,818	28.0	266.9	186.0	3.82	24.0
F-86H	24,296	39.1	222.0	313.4	4.88	35.7
F-100F	34,950	38.8	266.5	400.2	3.72	45.0
F-101C	44,000	39.7	301.0	368.0	4.28	36.5
F-102A	38,230	38.1	238.0	695.1	2.20	49.5
F-104G	17,200	21.94	327.5	196.1	2.45	18.1
F-105G	51,727	34.9	321.8	385.0	3.18	45.0
F-106B	36,834	38.3	253.7	697.8	2.20	49.5
F-111A	72,000	63.0	248.0	525.0	7.56	12.0
F-16	20,000	29.2	210.0	283	3.0	40.0
				TRAINER		
T-28A	7,812	40.6	119.9	271.1	6.1	0.0
T-29A	41,500	91.7	138.6	817.0	10.3	5.0
T-33A	12,500	38.9	177.3	234.8	6.0	3.5
T-34A	2,900	32.8	79.3	177.6	6.1	0.0
T-37C	8,180	35.9	131.5	183.9	6.2	0.0
T-38A	11,761	25.3	253.5	170.0	3.8	24.0
T-39A	18,650	44.5	165.2	342.1	5.8	28.6
TF-102A	29,530	38.1	241.5	695.1	2.2	51.0
TF-104G	16,000	21.9	300.3	196.1	2.5	18.1

TABLE 1 USAF AIRCRAFT CONFIGURATIONS (CONCLUDED)

A/C	W (lb)	b(ft)	V_s(fps)	S(ft^2)	AR	λ (deg)
			UTILITY			
U-1A	8,000	58.0	84.5	375.0	9.0	0.0
U-3A	4,600	35.7	113.0	962.1	13.3	0.0
U-6A	5,100	48.0	87.7	250.0	9.2	0.0
U-7A	1,581	35.3	48.9	178.5	7.0	0.0
U-17	3,350	35.8	77.1	174.0	7.5	0.0
U-10	3,400	39.0	34.5	231.0	6.6	0.0
			OBSERVATION			
O-2A	4,850	38.0	103.0	201.0	7.2	0.0
OV-10A	14,444	40.0	129.9	291.0	5.5	0.0
			RECON.			
EC-121D	122,000	126.2	177.5	1,653.6	9.17	4.50
RB-66B	83,000	72.5	224.3	780.0	6.75	36.5
			MISC.			
HU-16A	32,000	80.0	128.2	833.0	7.7	2.5
HU-16B	36,000	96.7	126.7	1035.0	9.2	0.0

TABLE 2 AIRPLANES CATEGORIZED AS GENERATORS

CATEGORY	AIRPLANE	W/bV_F	W/bV_F AVERAGE	Γ_o * AVERAGE	CATEGORY	AIRPLANE	W/bV_F	W/bV_F AVERAGE	Γ_o * AVERAGE
10	BOE/747	18.10	14.7	7852	5	A-7	2.26	2.4	
10	C-5A	11.23	14.7			C-131	2.22		
						F-100	2.21		
9	C-141	6.77	6.5	3480		T-29	2.14		1285
9	B-52	6.16	6.5			TF-102	2.10		
						C-47	2.07		
8	BOE/747	5.61	5.4		5	F-102	2.01	2.4	
8	C-133	5.43	5.4	2897					
8	KC-135	5.04	5.4		4	F-5	1.91	1.5	
						C-140	1.89		
7	B-58	4.37	4.2			A-1	1.85		
	C-124	4.16		2250		OV-10	1.82		
	C-97	4.14				T-39	1.66		
7	C-130	4.03	4.2			U-10	1.65		
						TF-104	1.59		
6	C-121	3.99	3.5			A-37	1.58		803
	C-9	3.95				F-104	1.57		
	C-118	3.92				C-10	1.28		
	B-47	3.52				O-2	1.24		
	RB-66	3.34		1874		T-38	1.20		
	C-54	3.09				T-33	1.19		
	F-16	3.08				T-37	1.13		
	F-111	3.01				U-1	1.07		
6	F-105	3.01	3.5		4	T-28	1.05	1.5	
5	F-4	2.92	2.4		3	U-17	.79	.73	
	C-119	2.75				U-6	.79		
	C-123	2.58				U-3	.75		391
	C-7	2.49		1285		T-34	.73		
	F-106	2.48			3	U-7	.60	.73	
	F-101	2.41							
	A-26	2.33							
5	B-57	2.28	2.4						

* in 1-g flight at sea level, at the given weight and $V_F = 1.2\ V_S$ (See Table 1)

TABLE 3 USA SINGLE-ROTOR HELICOPTERS AS GENERATORS

CAT.	COMPANY	DESIGNATION	W (LB.)	ROTOR DIA 2R (FT)	Γ_o (FT^2/SEC)	CATEGORY AVERAGE FOR Γ_o & 2R
9	SIKORSKY	CH53E	60,000	79	4013	Γ_o = 3396
9	SIKORSKY	HH-53B/C	38,000	72.25	2779	2R = 75.6
6	SIKORSKY	S-61A,B,C S-61L,N,R	20,000	62	1704	
6	SIKORSKY	YUH-60A	20,000	53.67	1969	
6	SIKORSKY	S-72	20,000	62	1704	Γ_o = 1649
6	SIKORSKY	YUH-60A UTTAS	15,000	53	1495	2R = 54.9
6	HILLER	YAH-64	14,000	48	1541	
6	BELL	214A,B,C	14,000	50	1479	
5	SIKORSKY	S-58T	10,000	56	943	
5	KAMAN	UH-2,HH-2 SH-2	10,000	44	1200	
5	SIKORSKY	S-76	9,000	44	1081	Γ_o = 1076
5	BELL	UH-1D	9,040	48	995	2R = 47.4
5	BELL	AH1G,Q, S & J	9,500	44	1141	
5	BELL	UH-1N	10,000	48.2	1096	

HELICOPTER V_F = 60 KNOTS, SEA LEVEL, 1-G FLIGHT

Category 9 reflects the heaviest helicopters, which are most dangerous, while category 5 contains the 10,000 lb variety. Helicopters lighter than 10,000 lbs were not included in this list. The circulation strength, Γ_0, for each helicopter was determined by considering straight and level flight V_F of 60 knots. A mean average for Γ_0 and 2R was then formed to represent the helicopters in a particular category.

The category number assigned to the helicopters parallels those assigned to the aircraft categories given in Table 2; that is, the mean average Γ_0 of the category 9 helicopter (Γ_0 = 3396) is approximately equal to the mean average Γ_0 of the category 9 aircraft (Γ_0 = 3480) and so on. It can be seen that the wake behind the CH53E and HH-53 can be as hazardous to other aircraft as the C-141 and B-52 when Γ_0 averages alone are being considered. The Boeing Vertol helicopters such as the CH-47 and CH-47A/B have not been included in this list. The Boeing products are tandem helicopters; the analysis developed in Section 2 is only applicable to single-rotor configurations. An analysis applicable to tandem or co-axial twin rotors was beyond the scope of this study.

Additionally, V/STOL configurations such as the tilt-rotor under development by the Army at Moffett Field are not listed; these vehicles are not a part of the inventory and would not be a part of joint Army/USAF operations in the immediate future. Navy V/STOL configurations have not been included as these are designed primarily for ship-board use, and so would not impact USAF operations.

4. Encounter Model Implementation (T-38 Simulator)

The encounter model as developed for a T-38 simulator is discussed here to illustrate the step-by-step computations involved. The formulations as developed in this section are valid for simulating encounters from 2-1/2 miles behind the generating aircraft up to the vortical roll-up region just behind the generator; that is, the function K_3 was taken to be 1.0.

The aspect ratio, AR, and span, b, for the T-38 are given in Table 1; these parameters and V are also shown in Figure 27. The time increment K_2 of Equation (51) is then:

$$K_2 = b/2V$$

$$K_2 = .04208 \text{ sec.} \qquad (53)$$

The T-38 accident[3] discussed previously was selected for simulation on the T-38 flight simulator; the generating aircraft was the C-130 transport. From Table 2, the C-130 is a category 7 configuration with a circulation of:

$$\Gamma_0 = 2250 \text{ ft}^2/\text{sec} \qquad (54)$$

$K_2 = b/2V = .04208$ $\quad\quad$ $\Gamma_o K_1/Vb = .0413$

5 $2\bar{y}/b$	6 C_{ℓ} Analysis	7 C_{ℓ} Approximate	8 t Sec	9 $2\bar{y}/b$	10 C_{ℓ} Analysis	11 C_{ℓ} Approximate	12 t sec
-1.6	.0070	0	.0	0	∓.0413	∓.0413	.673
-1.5	.0086	.0057	.042	.1	∓.0408	∓.0413	.715
-1.4	.0103	.0103	.084	.2	∓.0396	∓.0413	.757
-1.3	.0132	.0152	.126	.3	∓.0375	∓.0413	.799
-1.2	.0181	.0202	.168	.4	∓.0342	∓.0330	.842
-1.1	.0223	.0247	.210	.5	∓.0301	∓.0247	.844
-1.0	.0223	.0165	.353	.6	∓.0239	∓.0165	.926
- .9	.0136	.0082	.295	.7	∓.0161	∓.0082	.968
- .8	∓.0049	0	.337	.8	∓.0049	0	1.010
- .7	∓.0161	∓.0082	.379	.9	.0136	.0082	1.052
- .6	∓.0239	∓.0165	.421	1.0	.0223	.0165	1.094
- .5	∓.0301	∓.0247	.463	1.1	.0223	.0247	1.136
- .4	∓.0342	∓.0330	.505	1.2	.0181	.0202	1.178
- .3	∓.0375	∓.0413	.547	1.3	.0132	.0152	1.220
- .2	∓.0396	∓.0413	.589	1.4	.0103	.0103	1.262
- .1	∓.0408	∓.0413	.631	1.5	.0086	.0057	1.304
0	∓.0413	∓.0413	.673	1.6	.0070	0	1.347

T-38

W = 10,500 LB
V = 300 FPS

$I_x = 1428$ SL-FT^2
$I_y = 25{,}874$ SL-FT^2
$I_z = 26{,}779$ SL-FT^2

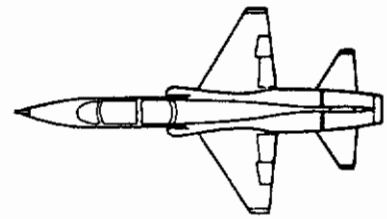

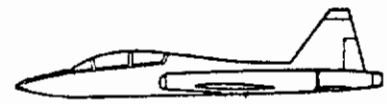

Figure 27. T-38 Encounter Model

The function K_1 for the T-38 is now determined; with the wing sweep angle λ and aspect ratio given in Table 1, Figure 25 is used to obtain:

$$K_1 = .139 \tag{55}$$

The function $\Gamma_o K_1/Vb$ is then formed:

$$\frac{\Gamma_o K_1}{Vb} = .0413 \tag{56}$$

Reference is now made to the tables given in Figure 24 and in Figure 27. It is noted that the columns of the table in Figure 24 are numbered from 1 through 4. The table in Figure 27 serves as a continuation of that table. The T-38 encounter model is now developed; that is: (1) form columns 6, 7, 10 and 11 by multiplying columns 2 & 3 by $\Gamma_o K_1/Vb$, (2) form columns 8 and 10 by summing the Δt time increments as indicated in column 4.

The T-38 encounter model developed in tabular form in Figure 27 is shown in Figure 28. For implementation on a simulator, it is recommended to use that the straight-line approximation for C_ℓ. That is, the part of the C_ℓ function between t = 0 and t = .21 could be generated by an integrator with a negative gain constant. A switch to a positive gain constant could then be used to generate C_ℓ between t = .21 and t = .54 seconds. The "plateau" portion of C_ℓ could be generated by "clipping" the generated signal function, and so on. For that matter, the C_ℓ function could be generated by means of a short digital computer subroutine if a digital computer is available as part of the T-38 facility.

In the equations of motion on the simulator, the roll equation of motion is:

$$\frac{1}{2}\rho V^2 Sb C_{\ell_{AERO}} = I_{XX}\dot{P} - I_{XZ}\dot{R} + QR(I_{ZZ} - I_{YY}) - I_{XZ}PQ \tag{57}$$

where $C_{\ell\ AERO}$ includes the aerodynamic roll contributions of control deflection, roll and yaw rates, etc. Adding the rolling moment from the vortex gives:

$$\frac{1}{2}\rho V^2 Sb(C_{\ell\ AERO} + C_{\ell}) = I_{XX}\dot{P} - I_{XZ}\dot{R} + QR(I_{ZZ} - I_{YY}) - I_{XZ}PQ \tag{58}$$

where C_ℓ is the function shown in Figure 28, which is switched on by the operator at the controls of the simulator.

The C_ℓ function given in Figure 28 reflects a T-38 encounter from the right with the right wing vortex behind a C-130. By just reversing

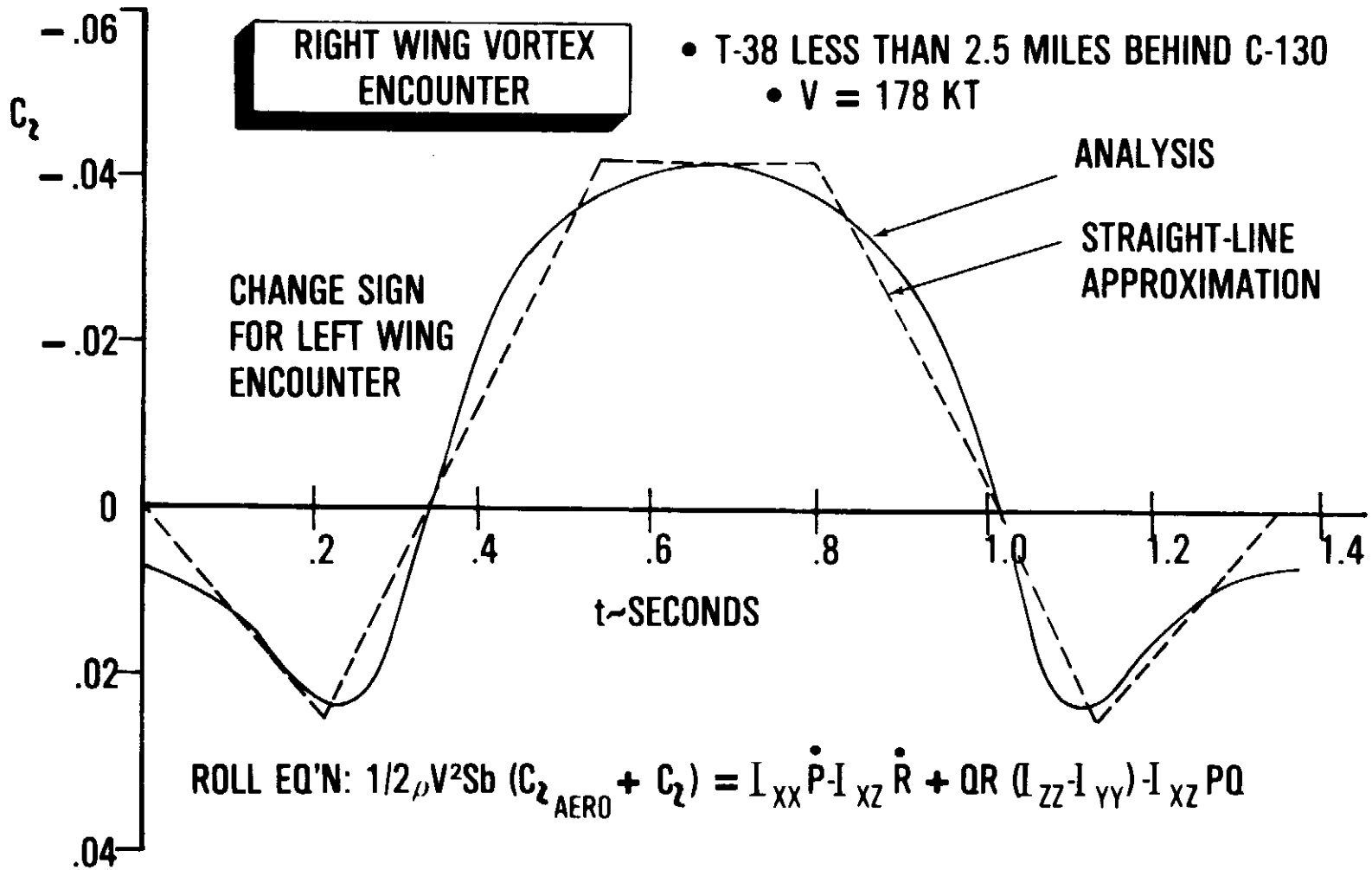

Figure 28. Recommended Encounter Model for T-38 Simulators

the sign of the encounter math model, the opposite direction or C-130 vortex can be presented.

Now, it is recommended that a T-38 simulator, or a category 4 aircraft, be equipped with at least three constant vortex intensities (Γ_0) reflecting aircraft in categories 9, 7, and 4 (see Table 2) and at least one variable Γ_0 to reflect air combat. The category 9 and 7 encounter models would educate the pilot on the vortex hazard behind "heavy" and "less-than-heavy" transports during normal landings and take-off, while the category 4 encounter model would familiarize the pilot with the hazard during formation flight. For air combat, variations in speed, ρ, and normal load factor, n, should be provided, to reflect the maneuvers of the two aircraft. A fifth encounter model could be that for a typical helicopter wake as given in Table 3.

Separate subroutines need not be prepared and programmed in detail for the first three encounter models. These can be a part of one subroutine; the T-38 is used again to indicate how this can be accomplished.

Detailed programming is required for one encounter; say the aircraft of the same type are in formation flight. In the case of the T-38 this means that the encounter model should reflect a generator aircraft of the type found in category 4 of Table 2 where:

$$\Gamma_0 = 803 \tag{59}$$

The steps given in the previous section are then followed to produce:

$$C_\ell = C_\ell \Big|_{\text{CATEGORY 4}} \tag{60}$$

The other models for landing approach are then ratioed by the circulation strengths of category 7 and 9 type aircraft. That is, the circulation strength of category 7 aircraft is from Table 2.

$$\Gamma_0 = 2250 \tag{61}$$

The encounter model reflecting category 7 as generators is then:

$$C_\ell = \frac{2250}{803} C_\ell \Big|_{\text{CATEGORY 4}} \tag{62}$$

Similarly, the encounter model reflecting category 9 type generators is:

$$C_\ell = \frac{3480}{803} C_\ell \Big|_{\text{CATEGORY 4}} \tag{63}$$

The latter two models are achieved by a change in a multiplying constant.

5. Examples of Simulation Use

A T-38 incident occurred in late April 1975 during formation flight. The wing man encountered the right wing vortex from the lead aircraft. As a result, the affected aircraft rolled left-wing-down to a near wings-level inverted attitude; contact was made between the wing man's pitot static tube and the right stabilizer of the lead aircraft. In light of this incident and the T-38 accident presented in Reference 3, an analysis was made to assess the roll power capability of the T-38 when encountering the vortices generated behind all aircraft given in Table 2; the results are shown in Figure 29. The vertical axis is the calculated maximum roll moment induced by the vortex, divided by the aileron authority available. When this ratio is unity, the aircraft would be capable of maintaining wings level if the pilot and control system could respond instantaneously. The horizontal axis is the category of aircraft, from the "heavy" or category 10 containing the C-5 to our lightest aircraft in category 3.

It is seen that the aileron authority of the T-38 is exceeded by a factor of 7 when encountering the wake turbulence behind the C-5. It is also seen that approximately 70 percent of the aileron authority is required to counteract the vorticity field behind another T-38. Now, an actual encounter is a dynamic situation wherein the aircraft is perturbed quickly from its flight path; the pilot lags the motion, and the control system has maximum deflection and rate limitations in addition to time lags. With almost 70 percent of the aileron authority required, it is very conceivable that a T-38 could be inverted before a pilot regained control of his aircraft upon encountering the wake of another T-38 in 1-g flight.

Clearly, the David and Goliath syndrome as described in Section 1.2 must be dispelled. A means of doing this is through pilot education during training sessions on the simulators. That is, pilots would be trained on the simulator and then briefed on past incidents and accidents that have occurred during formation flight.

It is recommended that Table 4 be consulted when selecting encounter models for a simulator. The column titled SIMULATOR A/C CATEGORY reflects the aircraft simulated at a facility; the aircraft listed in each category are given in Table 2. The column titled GENERATOR A/C CATEGORY reflects the aircraft generating the vorticity field during the encounter where the aircraft and their circulation strength are listed in Table 2. The final column indicates tha type of USAF operation where the encounter might take place.

It is noted that Table 4 does not include air combat. The lead aircraft is maneuvering so its Γ_o becomes variable through variations in n, V_F, and ρ through altitude changes (Equation (1a)). Additionally, K_2 in Equation (48) is varying through changes in V of the trail aircraft (see Table in Figure 24).

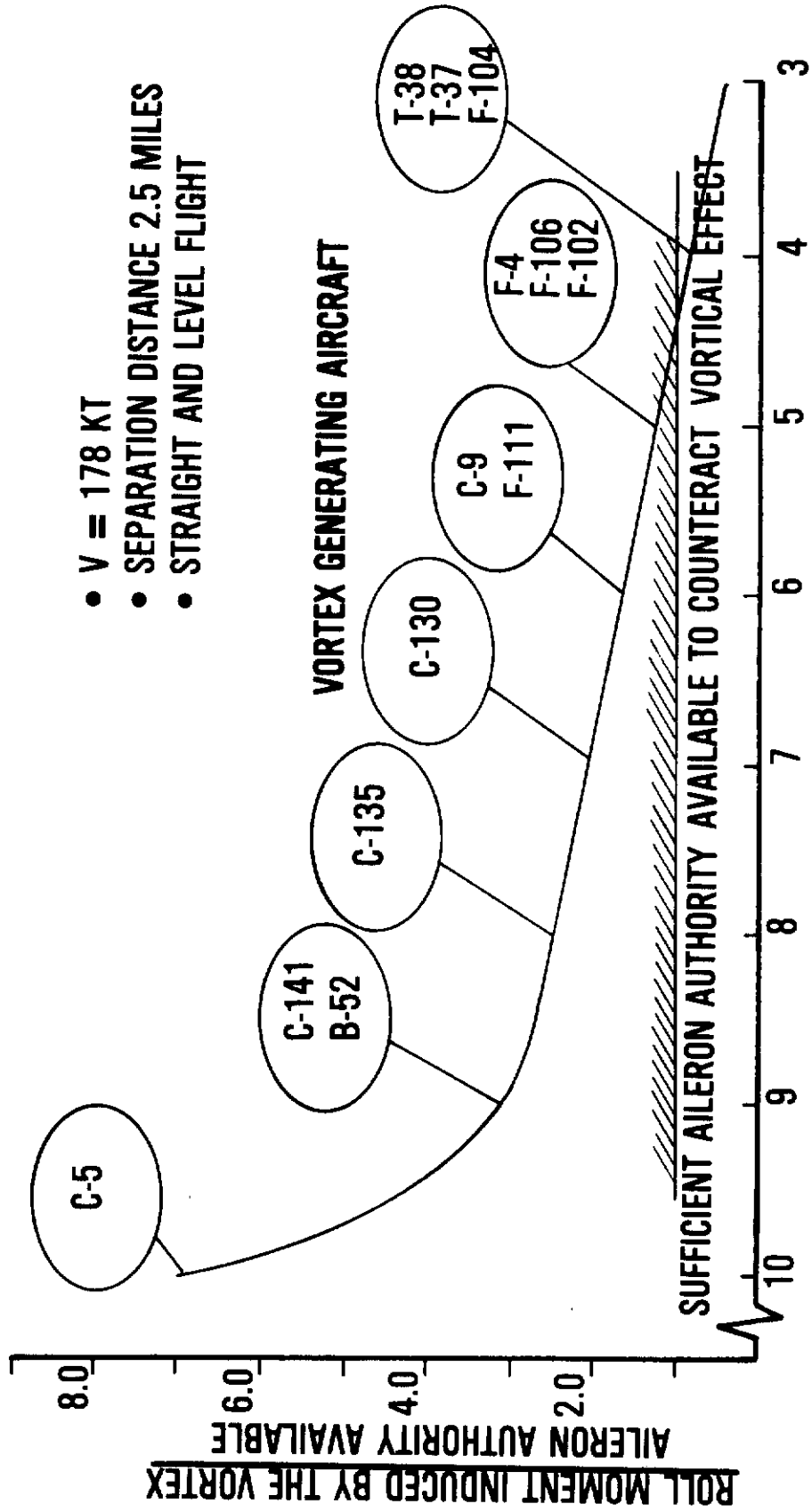

Figure 29. The Effect of Wake Vorticity on the T-38

TABLE 4 GENERATOR AIRCRAFT ENCOUNTER MODEL

SIMULATOR A/C CATEGORY	GENERATOR A/C CATEGORY	USAF OPERATION
10	10	NOR. APP. MITO
9	10 9	NOR. APP. MITO
8	10 8	NOR. APP. MITO
7	9 7	NOR. APP. MITO
6	10, 8 6	NOR. APP. FORMATION
5	9, 7 5	NOR. APP. FORMATION
4	9, 7 4	NOR. APP. FORMATION
3	7, 5, 4	NOR. APP.

NOR. APP. = NORMAL APPROACH & TAKE-OFF

MITO = MINIMUM INTERVAL TAKE-OFF

SECTION IV

WAKE ENCOUNTERS ANALYZED

The T-38 incident discussed previously, wherein a wing man encountered the right wing vortex of a lead T-38, is also of interest from another aspect. That is, some pilots may not realize that a T-38 during pullup can trail a wake that is as hazardous as that behind an F-4, F-111, or C-130 during landing; the effects of these wakes upon the T-38 can be substantial even at speeds much higher than the approach speed. Further discussion is warranted.

Figure 30 illustrates this example. It is assumed that the lead T-38 initiates a steady pullup or turn as shown. The lift coefficient necessary in this maneuver is given by:

$$C_L = \frac{nW}{\frac{1}{2}\rho V_F^2 S} \tag{64}$$

Let the trail T-38 encounter the vortical wake of the lead T-38 after the vorticity rollup is complete, as shown in Figure 30. Both aircraft are flying at the same speed; the circulation strength, Γ_o, of the vortex encountered can be determined from Equation (1a).

The circulation strength Γ_o behind the lead T-38 at sea level in a pullup or turn of n g's is shown in Figure 31; the stall limit is based on landing approach data given in Reference 9 and on Equation (64). The horizontal axis in Figure 31 reflects the g's sustained by the lead T-38. The results suggest that a T-38 in a 7'g pullup at 400 knots trails a wake equivalent to that of a category 7 generator in landing approach as described in Table 2; the category 7 generator airplanes include the C-124, C-130, B-58, and C-97 cargo and bomber type USAF configurations. The situation becomes even worse at altitude. It is seen from Equation (1a) that Γ_o is inversely proportional to density so that:

$$\Gamma_{o_{ALTITUDE}} = \frac{\rho_{SEA\ LEVEL}}{\rho_{ALTITUDE}} \Gamma_{o_{SEA\ LEVEL}} \tag{65}$$

The circulation strength, Γ_o, shown in Figure 31 increases as the density ratio increases with altitude.

This wake can have a significant impact upon the roll of the following T-38 as shown in Figure 32. The analysis presented in section 3.2 determines the maximum roll moment exerted on the following T-38 when it is located at the center of the vortex behind the lead T-38. The results are presented as a function of speed in knots of both aircraft and as a function of the g's initiated and maintained by the lead T-38.

Now, the aileron authority available on an aircraft increases with dynamic pressure, $1/2\rho V^2$. Additionally, the circulation strength, Γ_o, trailed behind an aircraft decreases with forward speed as seen in Equation (1a). These factors may lead to the belief on the part of some pilots that a formation flight or air combat encounter at high speeds may not be too severe.

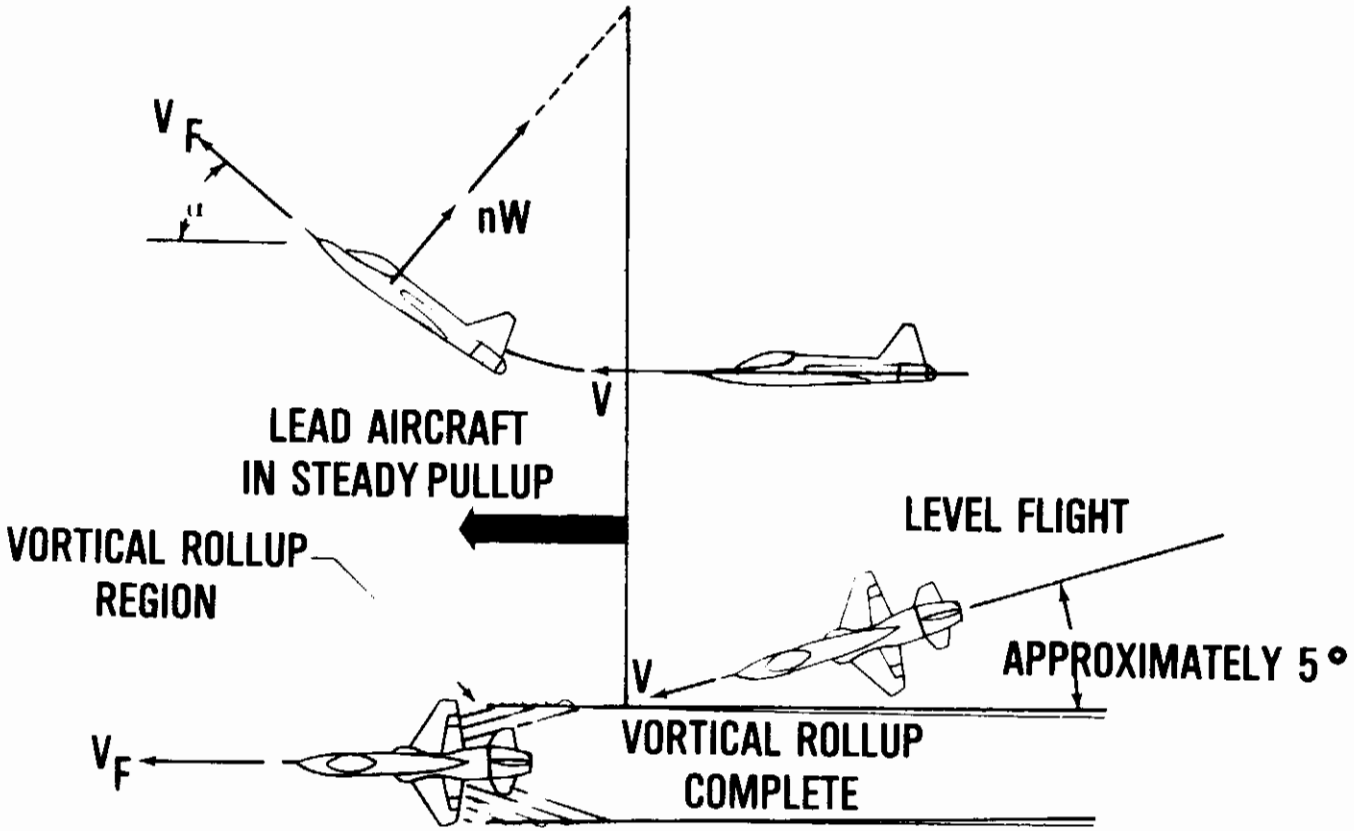

Figure 30. Schematic for Two T-38's in Trail Formation

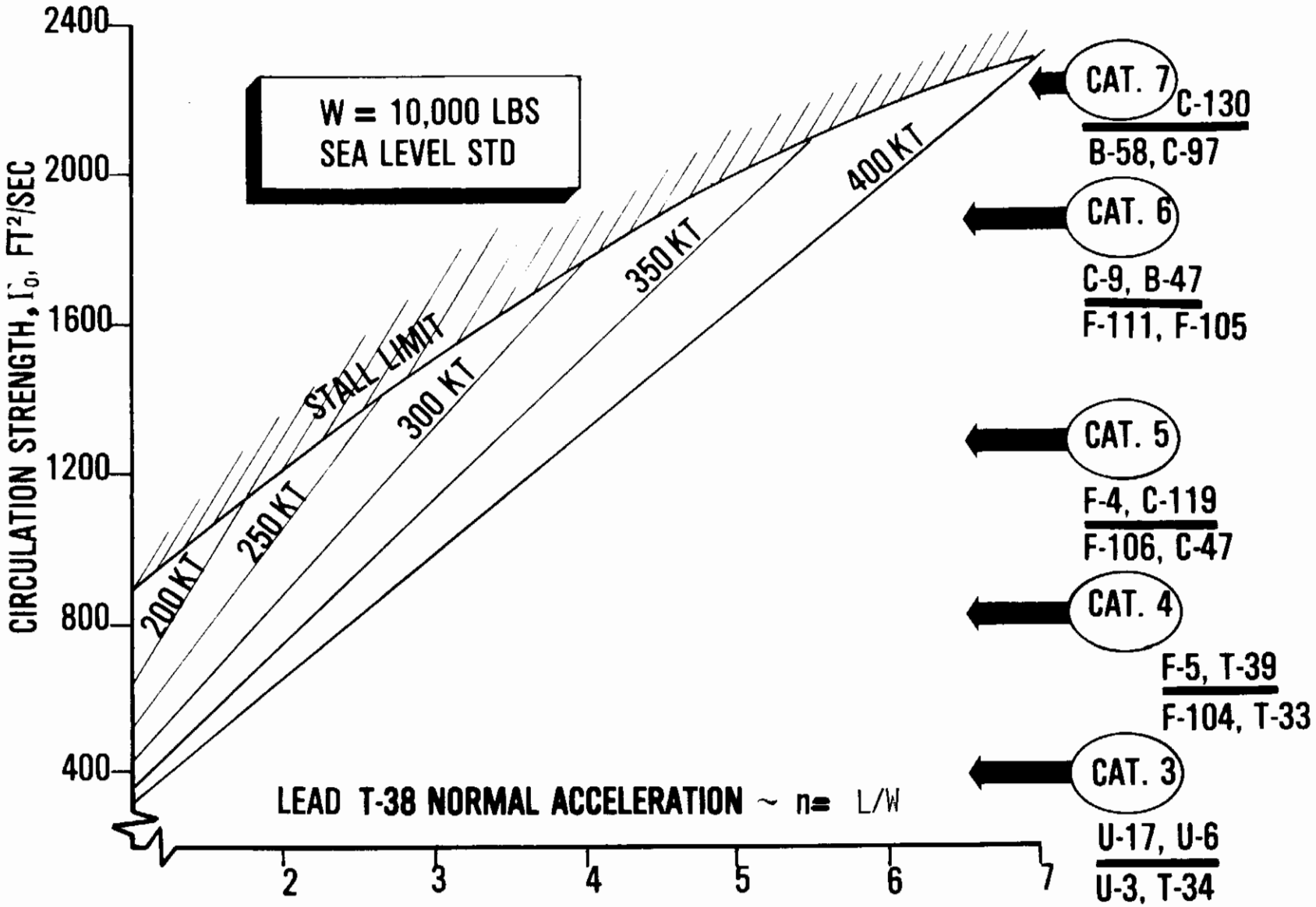

Figure 31. Vortical Wake Strength Behind Lead T-38

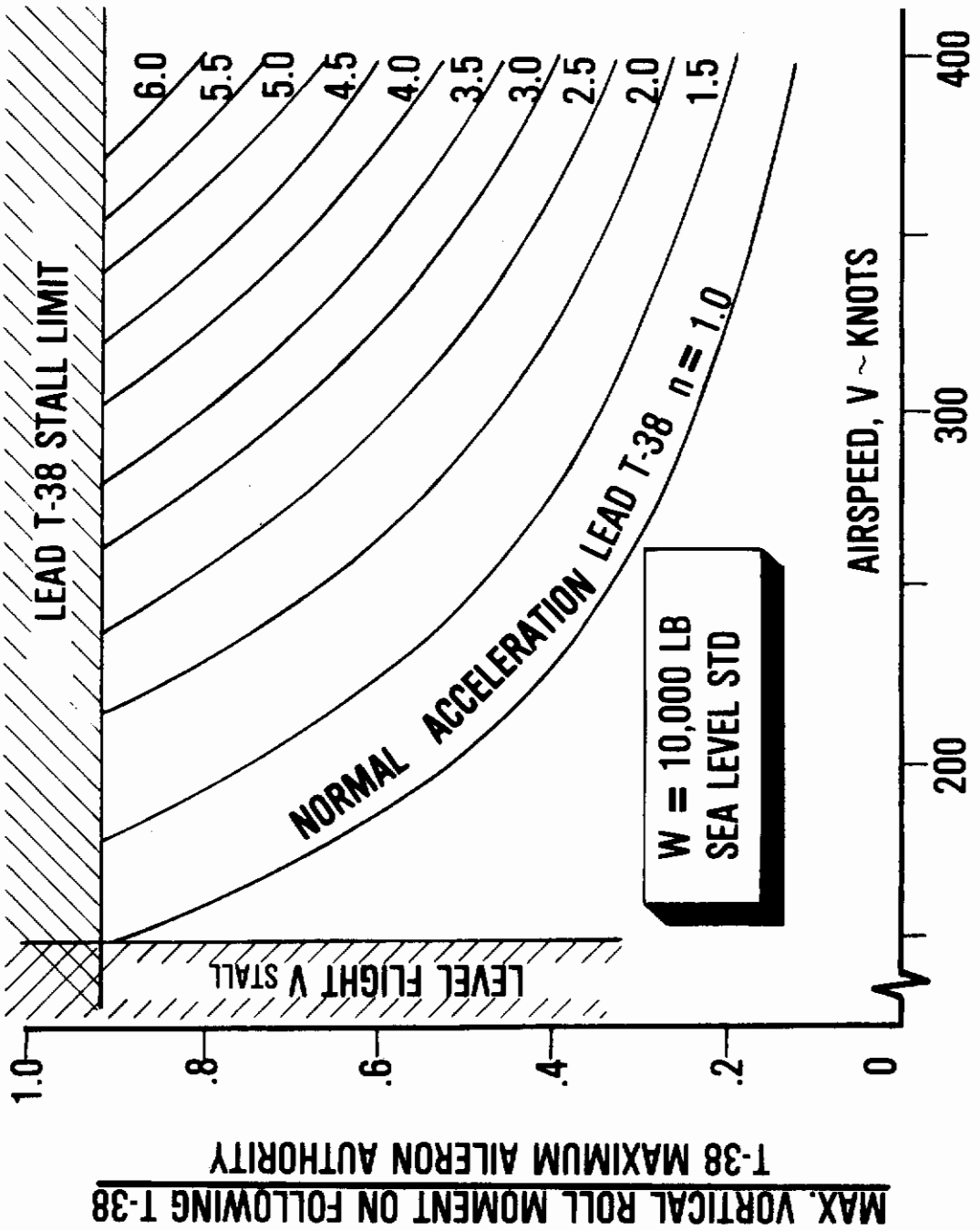

Figure 32. Roll Moment Induced on Trailing T-38 by Lead T-38

That is not necessarily so, from the results given in Figure 32 because the capability of the lead T-38 has a significant impact upon the results. For example, a lead T-38 at 6g's at 375 knots can create vorticies that would require the pilot of the encountering T-38 to use 90% of his aileron authority to maintain wings level. It is no wonder that one T-38 can invert another T-38 during formation flight. An actual encounter is a dynamic situation in which the pilot must act very quickly to maintain wings level. The inevitable time lags on the part of the pilot and in the response of the control system can cause a break in formation, roll while falling out of the vortex, and loss of altitude before regaining control. It is important, then, that formation-flight maneuvers, especially where air combat is involved, be performed with sufficient altitude so that safe recovery can always be made. The situation is even worse at altitude since the roll moment ratio increases as the density ratio is increased.

USAF operations require that some formation maneuvers be practiced at unsafe altitudes for wake encounters; an example of this is tactical weapon delivery. Here the formation approaches the target at low level at approximately 400 knots. A steep climb is then initiated to approximately 8000 feet followed by a steep descent of approximately 30 degrees towards the target. The bombs are released at approximately 3500 feet above ground level, and all aircraft pullup to level flight at approximately 1500 feet altitude.

Consider the F-104 with the characteristics shown in Figure 33; Equations (64) and (1a) produced the results shown in Figure 34. It is seen that the impact of the wake behind a lead F-104 pulling 4.5 g's at 400 knots is equivalent to that behind a category 8 generator given in Table 2; this category includes the C-135 weighing over 200,000 lbs, according to the data given in Table 1.

The aileron authority needed to control the wing man's aircraft while encountering the vortical wake behind the lead F-104 is shown in Figure 35. At 400 knots with a pullup of 4 g's, the aileron authority is exceeded if the trailing F-104 passes through the center of the vortex behind the lead. Now, the amount of roll energy affecting the perturbed aircraft is a function of the length of time that the aircraft remains within the vortex and the angle of intersection between the vortical-core axis and the X axis of the aircraft. The amount of time spent within the core dictates the severity of the encounter.

Reference is now made to the results shown in Figure 24. Maximum roll moment is induced when the affected aircraft is at the center of the trailed vortex (i.e., $\frac{Vb\ C_l}{\Gamma_o K_1} = -1.0$ when $2\overline{y}/b = 0$). This induced roll moment reduces rapidly with separation between aircraft and vortex core; for example the quantity $\frac{Vb\ C_l}{\Gamma_o K_1}$ becomes .19 when $2\overline{y}/b$ equals 1.6.

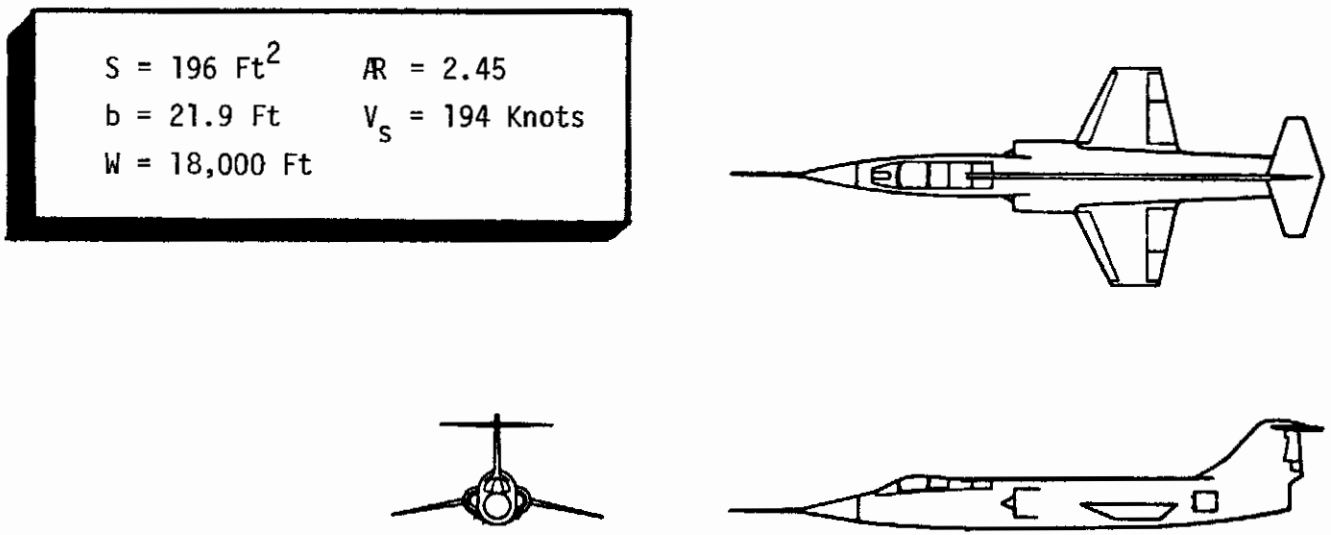

Figure 33. F-104 Fighter Geometrical Characteristics

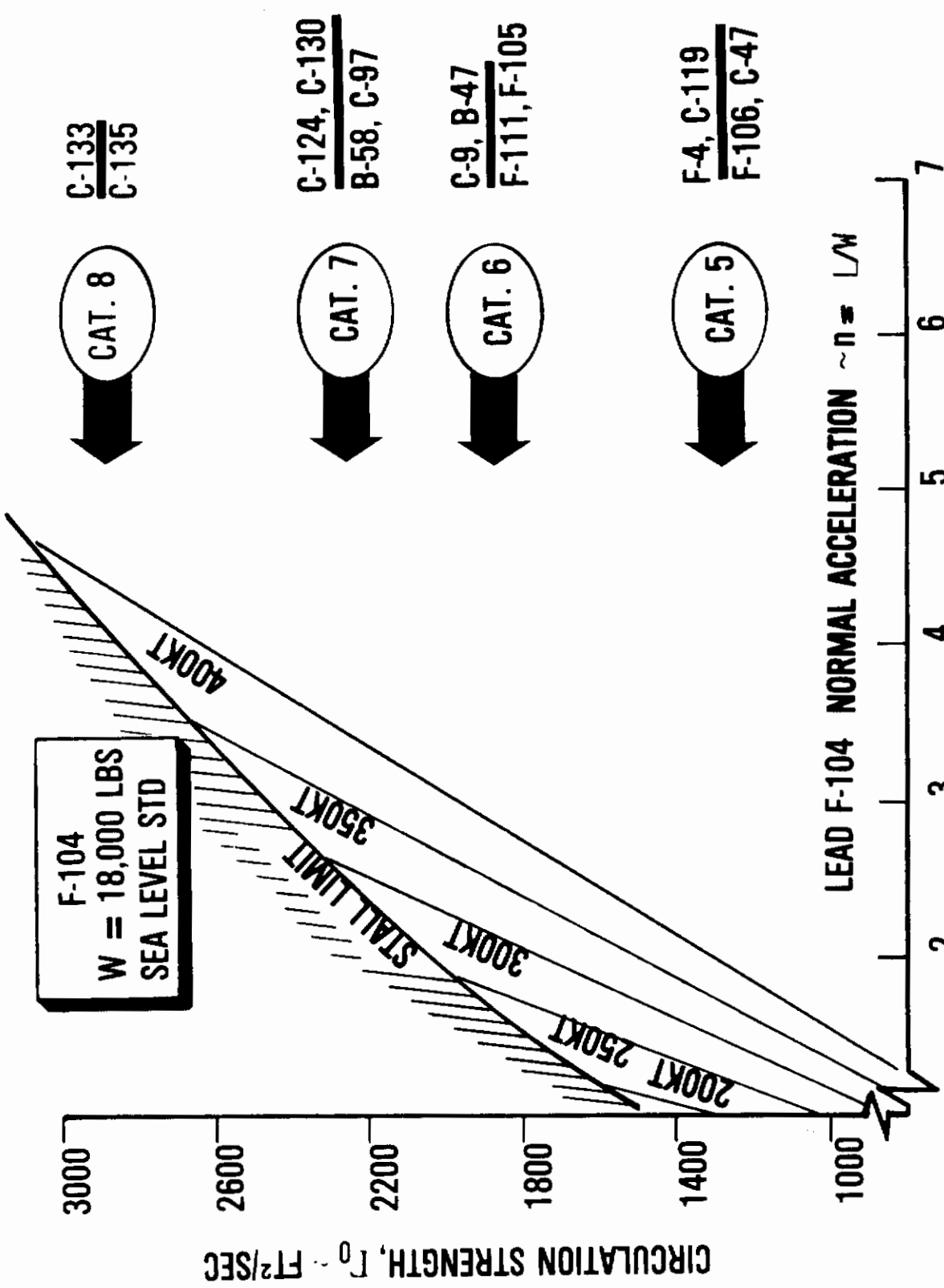

Figure 34. Vortical Wake Strength Behind Lead F-104

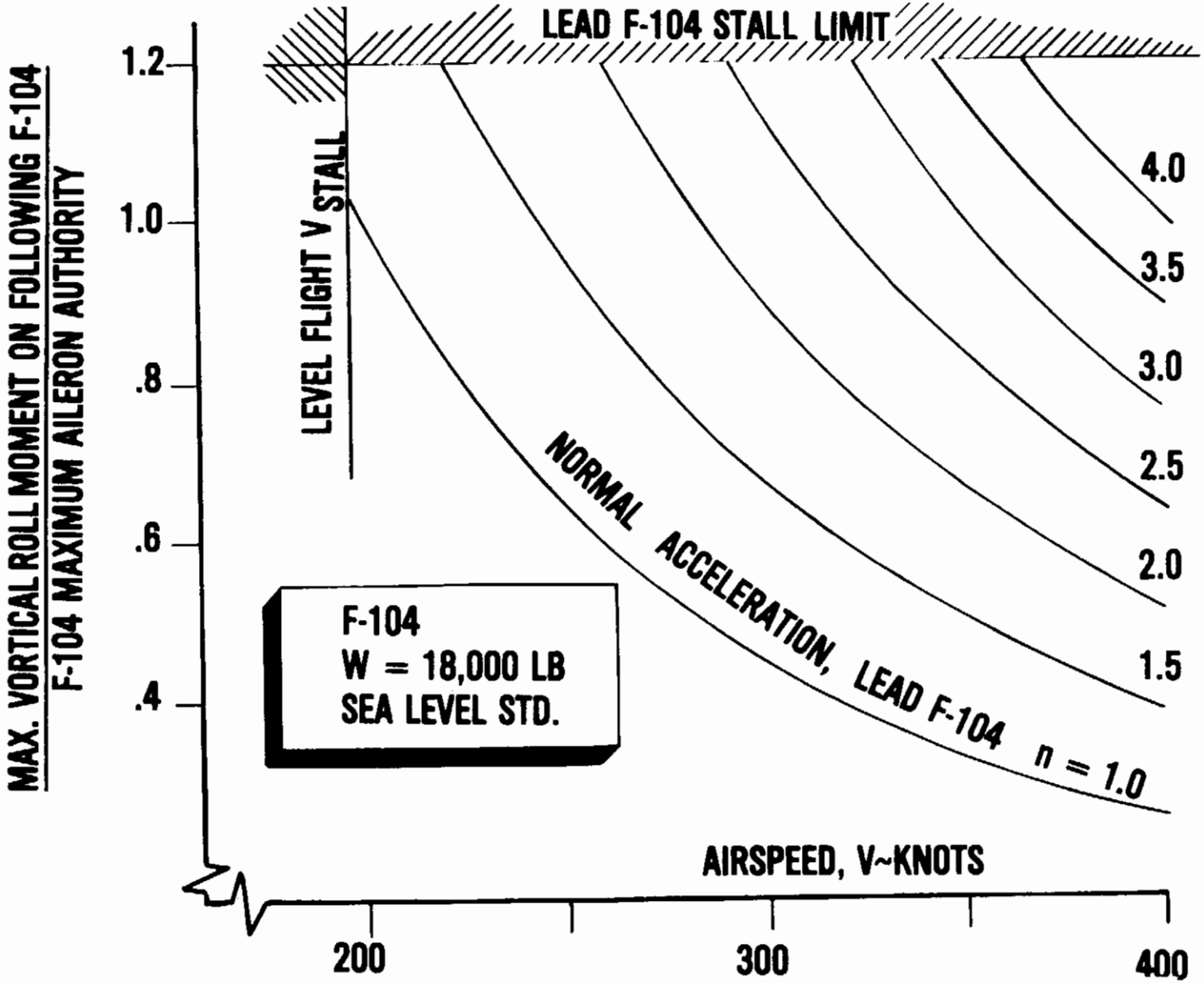

Figure 35. Roll Moment Induced on Trailing F-104 by Lead F-104

Of importance to any formation maneuver, then, is that sufficient spacing between the aircraft must be maintained throughout the maneuver. A break in the formation due to a vortical wake encounter is most likely if the wing man becomes careless and slips through the vortical core of the wake behind the lead aircraft.

The whole wake-vortex problem (Reference 29) received dramatic emphasis from the crash of a T-38 which ended in two fatalities and the loss of the aircraft (see Figure 36). This accident should serve as an example to all USAF pilots of the deadly swiftness of events possible when a trainer or fighter-type aircraft encounters this hazard during landing approach. A reconstruction of the accident is given in Figure 36; it is emphasized that the T-38 crashed approximately 5 seconds after the encounter with the vortical-wake hazard.

The sequence of events leading to this crash was as follows, according to the findings of investigators and the results from a digital computer simulation[3] of the fateful flight. The T-38 was performing an approach prior to landing behind a stretched C-130 transport. Although the T-38 pilot and air traffic control personnel were operating within all applicable directives, the T-38 closed to approximately one minute behind the transport. Then (t = 0 in Figure 36), the T-38 was approximately 2-1/2 miles from touchdown when it penetrated the right-wing vortex trailed behind the C-130.

One second later (t = 1.0), the T-38 was banked left-wing-down to an angle greater than 90 degrees, despite the efforts of the pilot. This was followed by a rapid decrease in altitude as the pilot attempted to regain a wings-level attitude; the aircraft crashed.

Analysis[3] indicated that the roll moment exerted by the vorticity field of the C-130 exceeded the aileron authority of the T-38 by at least 100%; reference is also made to Figure 29. There was no way to keep the T-38 wings-level following this encounter. Neither the pilot(s) nor control tower personnel were aware of the severity of the situation. Present air traffic control directives provide increased separation to certain fighter and trainer aircraft when an approach is made behind a "heavy" aircraft; by definition, a "heavy" aircraft is one that weighs over 300,000 pounds. Some pilots may harbor the incorrect belief that an approach made behind a stretched C-130 (130,000 lbs.) is relatively "safe".

Now, this accident is illustrative of a definite problem in landing procedures. The separation distance between the T-38 (V = 180 knts) and the stretched C-130 (V = 110 knts) was approximately 5 nautical miles when the T-38 entered the landing pattern. The T-38 closed to approximately 2 nautical miles behind the C-130 where the wake encounter occurred. The closing rate between fast fighters behind slow transports must be considered with care during landing approach.

As indicated earlier, USAF operations do involve mixed operations in terminal areas where Army helicopters and USAF attack aircraft

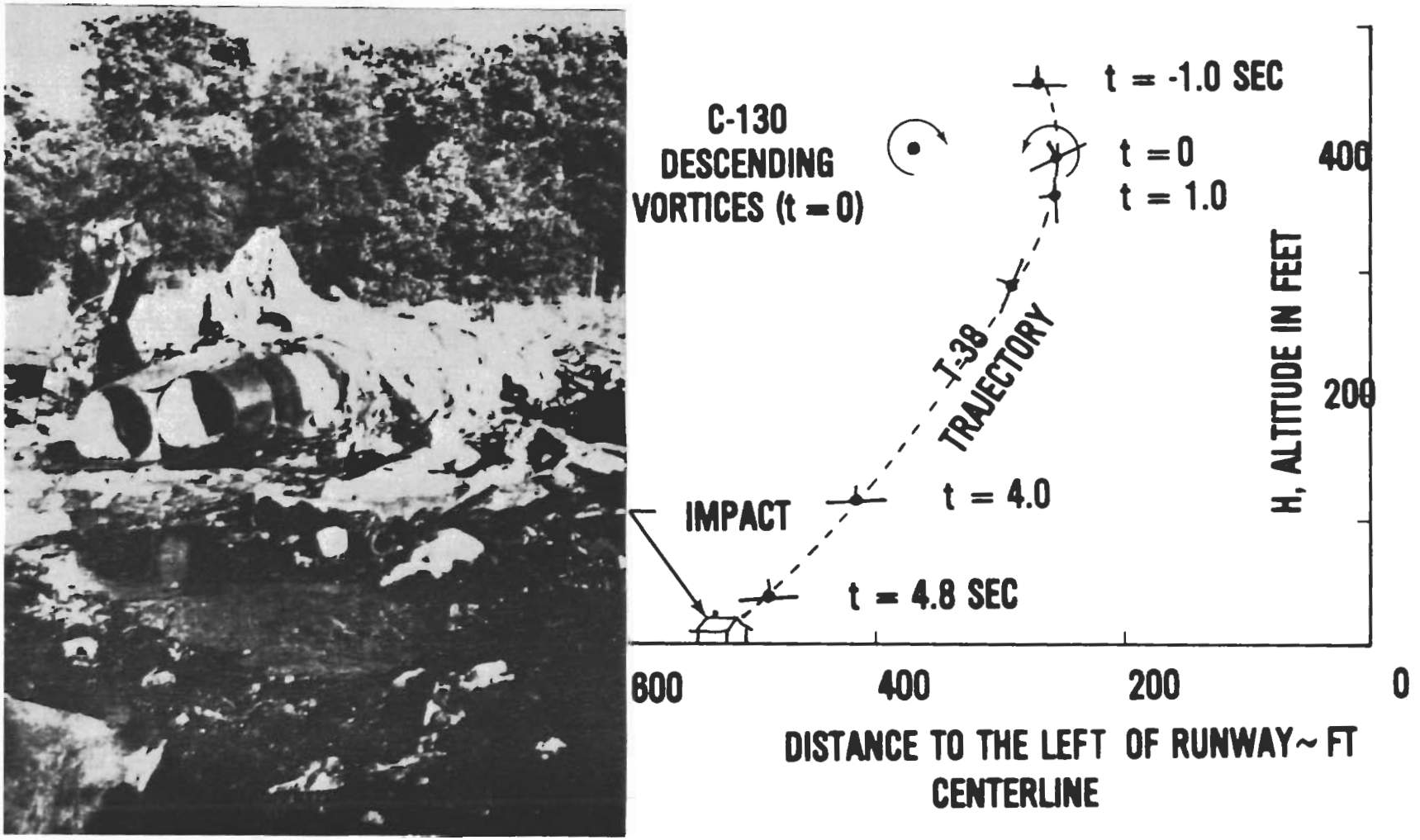

Figure 36 T-38 Vortical Wake Accident (Ref. 3)

operate in close proximity from the same field. An example of such operations is Nellis AFB, where one mix consists of A-10 aircraft and HH-53 helicopters; reference is made to Tables 2 and 3 for airplane and helicopter characteristics as a vortical-wake generator.

The analysis presented in Section 2.5, for tracking the wake location behind the HH-53 helicopter, was used in defining the wake contaminated airspace shown in Figure 37. The NASA, FAA, and DOT Transportation system Center (TSC) programs indicated that the vortices behind aircraft usually do not persist for more than 4.0 minutes. It can be argued that the vortices break up sooner behind helicopters than they do behind airplanes since: (1) their core sizes are larger, and (2) the turbulence generated immediately below the rotor disk plane by the rotor blades should hasten vortical decay. Therefore it is felt that the HH-53 vortical wake to the right of the 2.0-minute boundary shown in Figure 37 has probably been broken up by atmospheric means. The uncertain airspace region is in between the 1.5 and 2.0-minute boundary lines. It is possible that the vortical wake is broken up here, based upon the comments of the pilots that participated in the flight test documented in Reference 37. It is felt, however, that a thorough analysis of helicopter flight tests more recent than that of Reference 37 should be made before commenting about this any further.

The results in Figure 37 suggests that the A-10 should operate no closer than 2 minutes behind a HH-53, and no closer than 6 radii or approximately 220 feet below the helicopter, for V_F in excess of 45 knots. It is also recommended that the A-10 never pass below a HH-53 when it is between hovering flight and a forward speed of 45 knots. The possibility exists that the operations at Nellis, if affected by helicopter wakes could be so arranged so that the contaminated airspace shown in Figure 37 never impacts the glide path of an A-10 in landing approach or take-off. This would mean conducting the helicopter operations either below the glide path of the A-10 or downwind from the runway so as not to impact the A-10 sortie rate.

A further example regarding the HH-53 and the A-10 assumes that the HH-53 flies at an altitude of 100 feet directly above a runway prior to slowing down and descending off to the side of the runway. The flight speed of the HH-53 is taken to be V_F = 60 knots while over the runway and while generating a wake that could be potentially dangerous to a following A-10.

Again, the equations given in Section 2 were used to track the vortices trailed behind the HH-53; the results are shown in Figure 38 for sidewind, V_S, of 0. It is seen that the vortices descend and level off parallel to the runway at an altitude of .8R, at a distance 85R aft of the HH-53 helicopter. At this point above the runway, the vortices spread apart with the vortex cores travelling sideways at the rate of 7.7 fps parallel to the ground.

One minute behind the helicopter, the vortices are at least 10.8R apart. An A-10 performing a landing at this time between the vortices

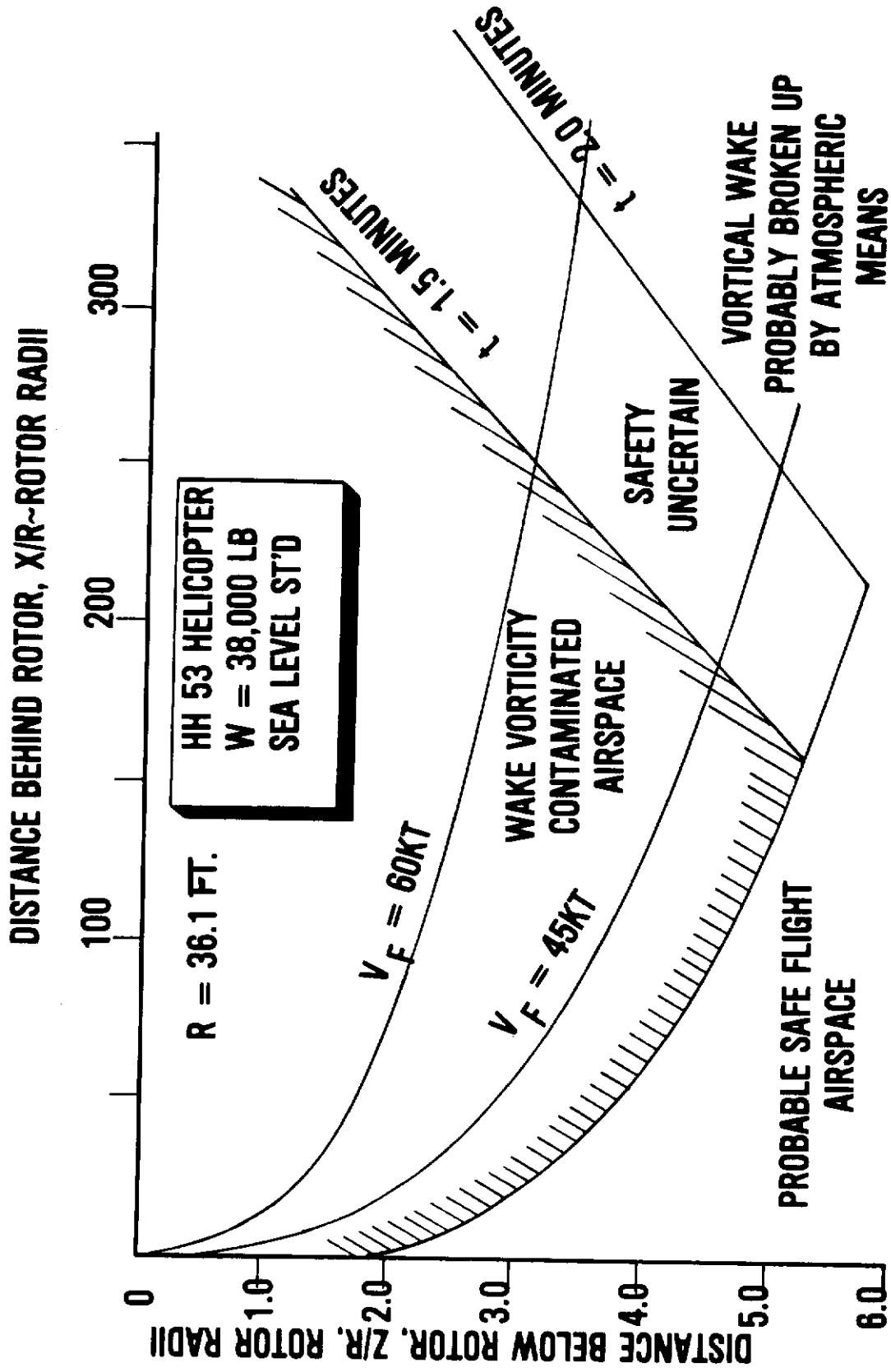

Figure 37. Contaminated Airspace Below an HH-53 Helicopter

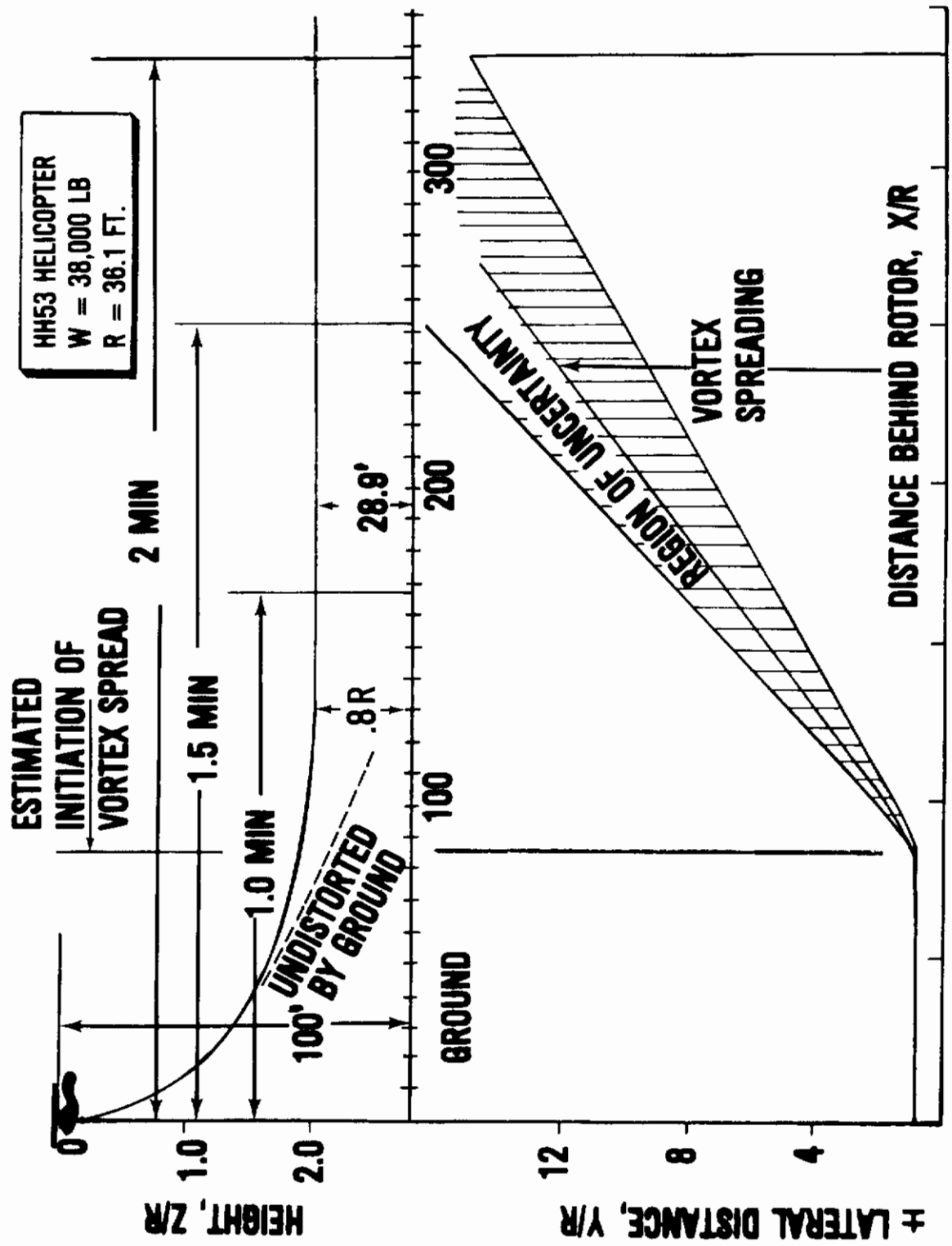

Figure 38. HH-53 Vortical Wake Tracking (V_F = 60 KNOTS, H = 100FT)

would be subjected to a down gust, V_d, of from 3.5 to 4.5 fps as shown in Figure 39. It is felt that this down gust would not perturb the A-10 significantly from its glidepath. Furthermore, this downgust decays rapidly, roughly 1 fps at 2 minutes behind the helicopter. Also shown in this figure is the growth of the vortex core behind the helicopter as a function of time. At 1-1/2 minutes, the diameter of the core is approximately equal to the span of the A-10. At 2 minutes, the estimate for the core diameter is approximately 1.2 times the wing span.

It is seen that an A-10 can land approximately 1 minute behind an HH-53 if the landing is performed between these vortices as they spread out. The real problem occurs if there is a slight side wind, V_s, such that one of these vortices becomes stalled over the runway. For example, the vortices shown spreading apart in Figure 38 travel at the rate of 7.7 fps parallel to the ground. A side wind, Vs, of 7.7 fps would cause one vortex to stall over the runway while the other vortex would travel at a rate of 15.4 fps away from the runway. An A-10 performing a landing then could penetrate the core of a vortex trailed behind the helicopter.

The hazard involved in this situation is illustrated in Figure 40. The vertical axis is the roll moment induced on an A-10 located at the center of a helicopter vortex, divided by the total A-10 aileron control available. The horizontal axis displays the various categories of helicopters given in Table 3. The solid lines shown in this figure reflect the roll moment induced on the A-10 when the mean Γ_o of each category in Table 3 was considered; the curves reflect a vortex age $t = X/V_F$, or 1/2 minute and 2 minutes. Also shown are the results of the CH-53E, HH-53A/B, YUH-60A, and UH-1D where the separation distance behind these helicopters is 1 minute.

It is seen that the roll control authority of the A-10 is exceeded if it lands 1 minute behind the CH-53E. Also 80% of the A-10 aileron authority is needed to maintain wings level when landing 1 minute behind an HH-53A/B. Of interest as well is the result for the UH-1D. This helicopter weighs only 9000 lbs according to the data given in Table 3. It certainly cannot be categorized as a "heavy" configuration, and some pilots may harbor the incorrect belief that an A-10 approach behind this helicopter can be made at any time. Yet it is seen in Figure 40 that an A-10 pilot would require the use of 30% of his aileron authority to maintain wings level while landing through the vortex core of the UH-1D 1 minute behind the helicopter.

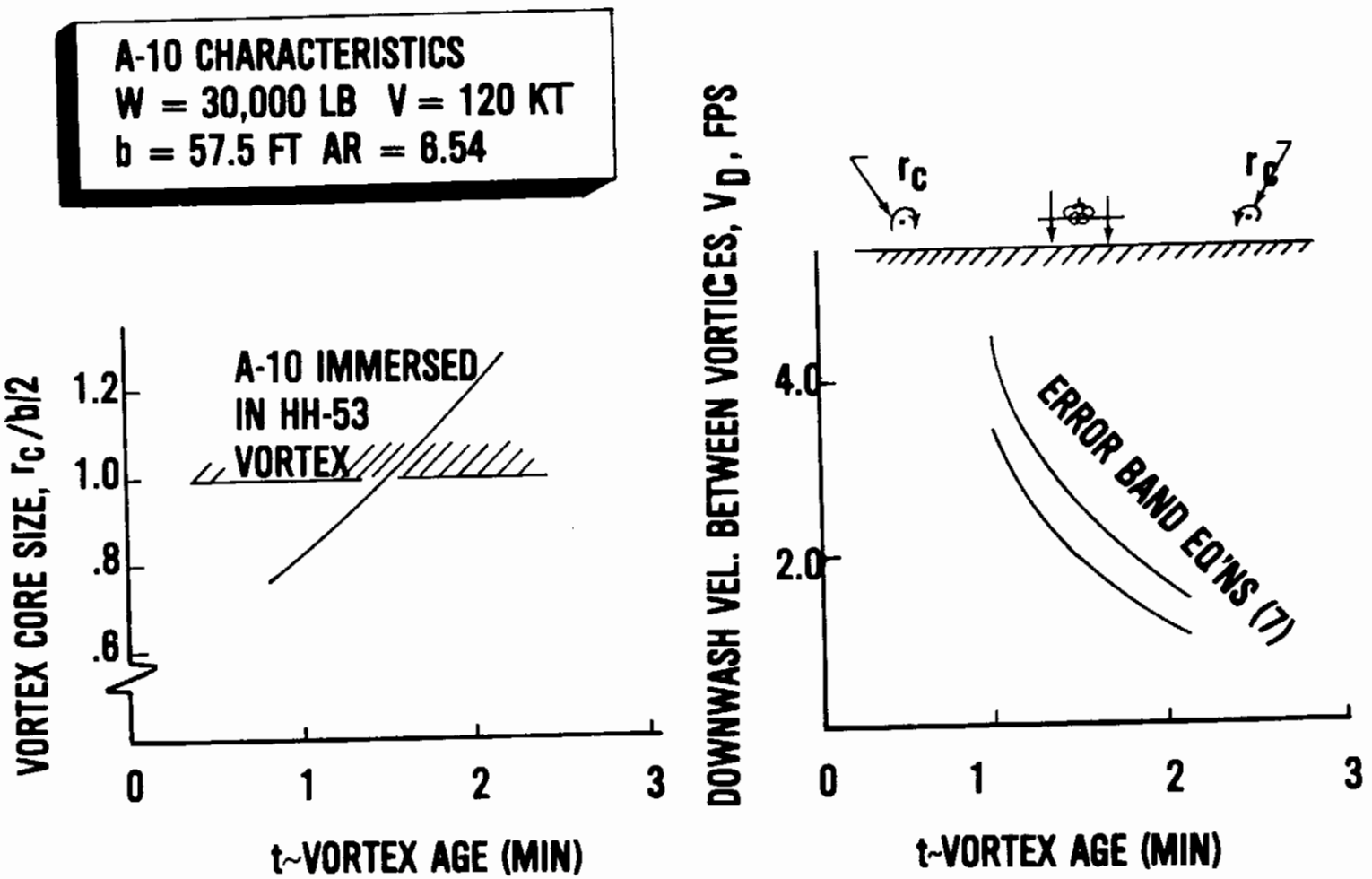

Figure 39. The Effect of Helicopter Downwash on the A-10

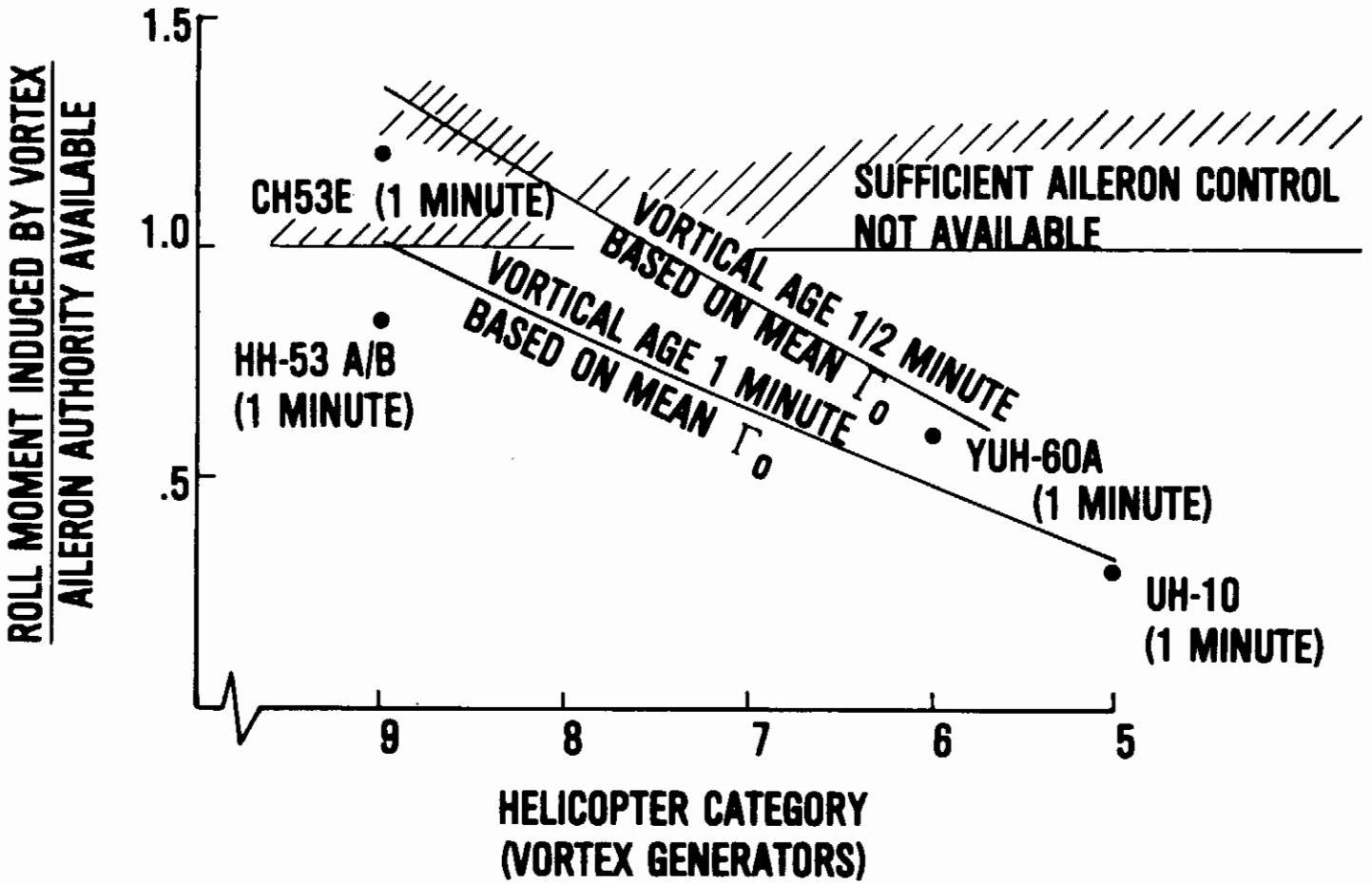

Figure 40. The Effect of Helicopter Vortical Core on the A-10

SECTION V

VORTICAL WAKE EQUATIONS SUMMARIZED

An assessment of when wake vorticity is a hazard in USAF operations consists of three steps which are: (1) determine the location, strength, and persistance of the vortices behind a generating airplane or helicopter, (2) determine whether another aircraft could fly into these vortices as part of an operation being assessed, and (3) determine the influence of the vortical wake on the flight path of the encountering aircraft. An assessment so formed should indicate whether an operation is safe or not. If the potential for wake-related accidents exists, the recourse is either to accept the losses as part of normal operating procedures, or to modify the operation so that the chances for an encounter are avoided.

Now, it is not the purpose of this section to address USAF operation. Our purpose is to synopsize the relevant equations presented earlier so that an engineer can perform the necessary assessments. Reference can be made to section 2 through 4 when further details are needed.

1. Strength and Location of Airplane Vortical Wakes

The vortical wake structure behind an airplane is shown in Figures 1 and 3, and is described in Section 2.1.

The vortical wake strength, Γ_o, for an airplane in level flight, or in steady pullup or turn is given by Equations (1) which are:

$$\Gamma_o = \frac{4nW}{\pi\rho V_F b} \tag{66}$$

when flaps and landing gear are retracted and:

$$\Gamma_o = \frac{4nW}{\pi\rho V_F b}, \quad \frac{XC_L}{b\bar{A}R} \leq 9.58$$

$$\Gamma_o = 9.58\left(\frac{4nW}{\pi\rho V_F b}\right)\left(\frac{XC_L}{b\bar{A}R}\right)^{-1}, \quad \frac{XC_L}{b\bar{A}R} > 9.58 \tag{67}$$

when flaps and landing gear are fully extended. Equation (66) is applied to aircraft in the cruise configuration and to fighters in formation flight, trail formation, or in air combat. Equation (67) applies to all airplanes in landing approach. Reference can be made to Table 1 if the airplane weight, W, or the wing span, b, for an aircraft are not readily at hand. Terminal area operations can be evaluated by using the data given in Table 2; here, airplanes of the USAF fleet have been categorized from 3 to 10 as generators in straight level flight at low speeds. Category 10 contains the heaviest of USAF transports or air carriers, which are most dangerous to other following aircraft, while category 3 contains the smallest airplanes within the USAF fleet. Reference is made to Section 3.3.

The location of the trailing wake behind an airplane is given by Equations (2), (3), (4), (5), (7), (8) and (9), (also see Figure 3). These equations are recast to give the wake location as:

$$
\begin{aligned}
X_v &= (V_F + V_w)t \\
H_v &= H - H_{INV} - \Gamma_o t/(2\pi b') \pm \Gamma_o t/(8\pi b') \\
Y_L &= -b'/2 + V_s t \pm \Gamma_o t/(8\pi b') \\
Y_R &= b'/2 + V_{st} \pm \Gamma_o t/(8\pi b')
\end{aligned}
\qquad (68)
$$

ANALYTICAL ERROR BAND

for the effect " out of ground" or well above a temperature inversion layer located at altitude H_{INV} and:

$$
\begin{aligned}
X_v &= (V_F + V_w)t \\
H_v &= H_{INV} + b'/2 \pm \Gamma_o t/(8\pi b') \\
&\quad\ 0.0 \\
Y_L &= Y_{G_L} + \left(V_s - \frac{\Gamma_o}{2\pi b'}\right)(t - t_G) \pm \Gamma_o t/(8\pi b') \\
Y_R &= Y_{G_R} + \left(V_s - \frac{\Gamma_o}{2\pi b'}\right)(t - t_G) \pm \Gamma_o t/(8\pi b')
\end{aligned}
\qquad (69)
$$

A N A L Y T I C A L ERROR BAND

where

$$
\begin{aligned}
Y_{G_L} &= -\frac{b'}{2} + V_s t_G \\
Y_{G_R} &= \frac{b'}{2} + V_s t_G \\
t_G &= \frac{2\pi b'}{\Gamma_o}(H - H_{INV} - b'/2)
\end{aligned}
\qquad (70)
$$

in the vicinity of the ground or an inversion layer where the subscript G refers to reaching a height of b'/2 above the ground or inversion layer. The quantity b' in Equations (68) through (70) is given by:

$$
b' = \frac{\pi b}{4} \qquad (71)
$$

Equations (68) provide the "out of ground effect" location of the vortices which are trailed from the wing tips at t = 0. These vortices slow their descent as they approach ground until they level-off at an altitude of b'/2 above ground or a temperature inversion layer.

Equations (68) through (70) consist of an analytical expression and an error band reflecting vagaries caused by the atmosphere; these are discussed in detail in Section 2.1. The above equations can be used in

determining the strength and location of the vortical wake behind airplanes.

2. Strength and Location of Helicopter Vortical Wakes

The vortical wake structure behind a helicopter is shown in Figures 2 and 10. The manner in which the vortex sheath distorts below the rotor disk plane and forms the two vortices starting at and trailing from approximately 1.5 radii aft of the rotor is discussed in Section 2.4.

The vortical wake strength, Γ_o, and the downwash velocity normal to the rotor, V_o, through the rotor disk plane are found from Equations (24) and (15),

$$\Gamma_o = \frac{2W}{\pi\rho V_F R}, \quad \frac{XW}{4\rho V_F^2 R^3} \leq 9.58$$

$$\Gamma_o = 9.56\left(\frac{2W}{\pi\rho V_F R}\right)\left(\frac{XW}{4\rho V_F^2 R_3}\right)^{-1}, \quad \frac{XW}{4\rho V_F^2 R^3} > 9.58 \qquad (72)$$

$$V_o = \frac{W}{2\rho\pi R^2 V_F}$$

where these equations only apply to helicopters in level flight at advance ratios of V_F/V_T greater than 0.1. Reference can be made to Table 3 if the helicopter weight, W, or the rotor radius, R, are not readily at hand. Table 3 gives the characteristics of those Army helicopters that may operate from the same field as USAF airplanes. Also listed are some commercial helicopters that could operate in joint FAA-USAF airspace such as Kirtland AFB or in adjacent FAA/USAF airspace such as Wright-Patterson AFB. Reference is made to Section 3.3.

The location of the trailing wake behind a helicopter are described by Equations (28), (28), and (29); details are given in Sections 2.4 and 2.5. In keeping with the format used in Equations (68) and (67), these equations become:

$$X_v = .11R\left(\frac{V_F}{V_o}\right)^{2.6}\left(\frac{Z}{R}v\right)^3 + R\left(\frac{Z}{R}v\right)\cot\Theta_w$$

$$Y_L = -b'/2 + V_s t \quad \pm V_o t/4 \qquad (73)$$

$$Y_R = \underbrace{b'/2 + V_s t}_{\text{ANALYTICAL}} \quad \underbrace{\pm V_o t/4}_{\text{ERROR BAND}}$$

$$t = X_v/(V_F + V_w)$$

for "out of ground" or temperature inversion layer effects. The vortices are separated by:

$$b' = 1.6R \qquad (74)$$

Equation (73) reflects the "out of ground effect" location of the vortices which are formed from the distorted vortex sheath below the rotor disk plane following t = 0. These vortices slow down their descent as they do behind an airplane, and level-off at an altitude of b'/2 above the ground or a temperature inversion layer. While in ground effect, the lateral displacement of these vortices is given by:

$$
\begin{aligned}
X_v &= (V_F + V_w)t \\
H_v &= H_{INV} + b'/2 \qquad\qquad + V_o t/4 \\
Y_L &= Y_{G_L} + (V_s - \frac{\Gamma_o}{2\pi b'})(t - t_G) \pm \frac{V_o t}{4} \\
Y_R &= \underbrace{Y_{G_R} + (V_s - \frac{\Gamma_o}{2\pi b'})(t - t_G)}_{\text{ANALYTICAL}} \underbrace{\pm \frac{V_o t}{4}}_{\text{ERROR BAND}}
\end{aligned}
\qquad (75)
$$

where Y_{G_L} and Y_{G_R} are defined by Equation (70).

The expression for X_v in Equation (73) is used as follows: (1) the wake efflux angle θ_w is determined from Figure 11 where W, R, ρ, and V_F are known parameters, and (2) X_v is determined for a range of Z_v/R values as the input parameter into the equation. The expression X_v in Equation (73) is then used three times in locating the vortices as they descend below a helicopter; that is, once to determine the most probable location of the vortices, once to determine the error band, and once to find t_G needed to locate the vortices laterally.

Now, the quantity t_G in Equation (75) is the time needed for the trailed vortices to reach the altitude b'/2 above the ground or above a temperature inversion layer. The value for t_G is obtained by substituting X_v into the t equation of Equation (73):

$$
t_G = \frac{.11R}{(V_F + V_w)}\left(\frac{V_F}{V_o}\right)^{2.6}\left[\frac{H-H_{INV}-b'/2}{R}\right]^3 + \left[\frac{H-H_{INV}-b'/2}{V_F + V_w}\right]\cot\theta_w \qquad (76)
$$

The error bands given in the above equations reflect atmospheric anomolies that impact the location of the vortices; these are discussed in detail in Section 2.1 and 2.6.

3. The Persistence of the Vortical Wake

The trailing vortices from an airplane or helicopter are generated into an environment that is rarely quiescent. Thermals, temperature inversions, and winds which include updrafts and downdrafts cause decay and eventual transition into a form of clear-air turbulence. In many instances the atmosphere has caused these vortices to burst. Bursting produces some combination of a marked increase in the size of the vortex core, an increase in turbulence level, and/or an instability and significant restructuring of the wake vorticity behind an airplane[17]

or helicopter. By hastening the interplay between the vortical wake and the atmosphere, bursting may significantly reduce the wake hazard as discussed in Section 2.3. Statistical studies helped determine when separation distance should be based upon the wake hazard. Details are provided in Sections 2.3 and 2.6.

It is recommended that the results shown in Figures 8 and 9 be used in determining the life time of a vortex when evaluating USAF operations. The data reflects measurements that were made of over 50,000 landings involving commercial airliners.

The probability that a vortex persists longer than any given time in the approach alley is given in Figure 8 as a function of side wind. The data suggests that the vortices probably breakup or drift out of the approach alley in less than 2 minutes. The approach alley is from the middle marker on in to touchdown, 150 feet on either side of the runway centerline, and up to an altitude of 300 feet. Strong vortices may still persist longer than 2 minutes outside the approach alley, posing a menace to aircraft that are landing or taking off on a parallel runway.

Of particular interest is Figure 9a taken from Reference 25. If the wind vector at the point of touchdown lies inside the inner ellipse then current FAA 3-nautical-mile criteria does not assume against a vortex encounter in the approach alley. In these circumstances the aircraft must spread out since the criteria poses a menace to following aircraft. On the other hand, a wind vector that lies outside the outer ellipse of Figure 9a indicates that a vortex encounter does not pose a menace to following aircraft separated by 3 nautical miles regardless of size. The vortical wake from the lead aircraft has been dissipated or has been blown out of the approach alley by the prevailing winds. Figure 9b gives the life time of the vortex as a function of the total wind. The results suggest that the vortical wake behind an airplane can persist for 4 minutes if the total wind is less than 6 knots and the atmospheric conditions are just right.

It can be argued that the vortices break up sooner behind helicopters than they do behind airplanes. The turbulence generated by the rotor blades immediately below the rotor disk plane should be much larger than that existing in the vorticity sheet trailed behind an aircraft wing. This additional turbulence should hasten the decay and eventual break up of the helicopter vortices. Further research in this area is needed. All that can be said at this moment is that the vortical wake behind a helicopter could break up as soon as one minute behind the helicopter and should be all broken up at two minutes behind the helicopter.

4. Vortical Wake Effects Upon Encountering Airplanes

A simplified mathematical model was developed for analysis of the way (1) penetration (Figure 1) and for equipping appropriate USAF trainers and simulators with the capability of simulating a vortex encounter. It is felt that this simulation capability is imperative

because many USAF pilots are not fully aware of the dangers involved with encountering wake vortices; this is especially so if the generating aircraft is not a "heavy" transport, defined by the FAA as an aircraft weighing about 300,000 pounds or more. A hazardous example is flight in trail formation when the lead aircraft is pulling g's. Additionally, the HH-53 helicopter at 38,000 pounds is not a "heavy" configuration according to the FAA separation criteria; the strength of the vortical wake it trails while flying at 60 knots is similar to that behind a KC-135 or Boeing 707 in landing approach.

Details of the analysis are found in Section 3 of this report. The roll moment exerted on an aircraft due to a way (1) encounter as shown in Figure 1 is given by (Equation 50):

$$\frac{VbC_l}{\Gamma_o K_l} = -1 + \frac{1}{2}\left(\frac{2\bar{y}}{b}\right) \ln \left|\frac{(2\bar{y}/b)+1}{(2\bar{y}/b)-1}\right| + \frac{2}{3}\left(\frac{2r_c}{b}\right) \tag{77}$$

for $|2\bar{y}/b| < 1 - 2r_c/b$ when the vortex is located on the wing.

$$\frac{VbC_l}{\Gamma_o K_l} = -\frac{1}{2} + \frac{1}{2}\left(\frac{2\bar{y}}{b}\right) \ln \left|\frac{1+2\bar{y}/b}{2r_c/b}\right| + \frac{1}{3}\left(\frac{2r_c}{b}\right) - \frac{1}{6(2r_c/b)^2} - \frac{1}{12}\frac{(2\bar{y}/b)^3}{(2r_c/b)^2} + \frac{(2\bar{y}/b)}{4}\left[\frac{1}{(2r_c/b)^2} - 1\right] \tag{78}$$

for $(1 - 2r_c/b) \leq |2\bar{y}/b| \leq (1 + 2r_c/b)$ when the vortex is at the wing tip,

$$\frac{VbC_l}{\Gamma_o K_l} = -\frac{1}{3(2r_c/b)^2} \tag{79}$$

$|2\bar{y}/b| + 1 \leq 2r_c/b$ when the wing is totally immersed in the vortex core,

$$\frac{VbC_l}{\Gamma_o K_l} = -1 + \frac{1}{2}\left(\frac{2\bar{y}}{b}\right) \ln \left|\frac{(2\bar{y}/b)+1}{(2\bar{y}/b)-1}\right| \tag{80}$$

for $|2\bar{y}/b| > 1 + 2r_c/b$ when the vortex core lies outside of the wing. The vortex core size is defined by (Equation (11)):

$$r_c = 36.2 \sqrt{\frac{\nu x}{V_F \cos^2 \lambda}} \tag{81}$$

for airplanes and (Equation (26)):

$$r_c = 244 \sqrt{\frac{\nu x}{V_F}} \tag{82}$$

for helicopters. The circulation strength, Γ_o, is determined from Equations (66) and (67) for airplanes or Equations (72) for helicopters. Tables 1 through 3 present data that can be used for the circulation strength, Γ_o, of airplanes (landing approach) and helicopters. The geometrical details for USAF airplanes are given in Table 1 while mean

averages for Γ_o where the aircraft have been categorized as generators are found in Table 2. Helicopter circulation strengths, Γ_o, are found in Table 3; reference is made to Section 3.3.

The function K_1 is shown in Figure 25. The wing aspect ratio, AR, and quarter-chord sweep angle, λ, are given in Table 1; these parameters are used in obtaining the function K_1 from Figure 25. Reference is made to Section 3.2.

A simplier version of Equations (77) through (79) is recommended for simulator use in indoctrinating pilots. It was assumed that r_c = 2 ft and the result is (Equation (51)):

$$\frac{VbC_l}{\Gamma_o K_1} = -1 + \frac{1}{2}\left(\frac{2\bar{y}}{b}\right) \ln \left|\frac{(2\bar{y}/b)+1}{(2\bar{y}/b)-1}\right| \tag{83}$$

This approximation is shown in Figure 24 and can be used for analytical purposes in evaluating USAF operations involving landing approach, formation flight, trail formation, and air combat where one airplane follows another. It is noted however that this equation is an approximation with r_c = 2 ft. Equations (77) through (79) is preferred if the core size of the vortex is significantly different than 2 ft.

A further approximation is (Equation 52):

$$C_l = \Gamma_o\left(\frac{VbC_l}{\Gamma_o K_1}\right) \frac{K_1}{bV} K_3 \tag{84}$$

where $\frac{VbC_l}{\Gamma_o K_1}$ is obtained from Figure 24 and K_3 is given in Figure 26. The attenuation factor K_3 is assumed to be K_3=1 when an encountering airplane is less than 2-1/2 miles behind the generating airplane, and is as shown in Figure 26 when the separation distance between the airplanes exceeds 2-1/2 miles. The attenuation factor for generating helicopters is as shown in Figure 26 for all separation distances between the aircraft. Equation (84) was used in obtaining the results shown in Figures 32, 35, and 40. Reference is made to Section 4.

The way (2) encounter shown in Figure 1 results in a sudden loss in lift upon entering the more-or-less symmetric downwash field between the vortex cores of the airplane or helicopter. The parameters necessary for analytically constructing this downwash field are the vortex core separation, b', and the swirl velocity, V_θ. Reference is made to the discussion concerning Figure 20 (Section 2.6). The core separation, b', is given by Equations (71) or (74) while the swirl velocity, V_θ, is given by Equation (10) and its approximation for large radii:

$$V_\theta = \frac{\Gamma_o}{2\pi r}\left(1 - e^{-1.26\left(\frac{r}{r_c}\right)^2}\right), \quad \frac{r}{r_c} \leq 2.0$$

$$V_\theta = \frac{\Gamma_o}{2\pi r}, \quad \frac{r}{r_c} > 2.0 \tag{85}$$

where r_c is given by either Equation (81) or Equation (82). The downwash field is then constructed as shown in Figure 41. The centers of the vortices are separated by b' and located at the left and right vortex origins. The induced velocity V_{Θ_L} is constructed by using Equation (85) starting at the left vortex origin while varying r as shown in this Figure. Similarly, the induced velocity V_{Θ_R} is constructed by using Equation (85) now at the right vortex origin while varying r as shown. The downwash velocity induced on the aircraft then becomes $V_{\Theta_L} + V_{\Theta_R}$. The angle of attack distribution along the wing is then approximated by Equation (36) or

$$\alpha = V_{\Theta_L} + V_{\Theta_R}/V \tag{86}$$

We believe that the equations presented in this section can be used in assessing the extent of the vortical wake hazard in USAF operations. This includes terminal area operations, formation flight maneuvering during combat or tactical weapon delivery, and mid-air refueling. Further details regarding these equations are given in Sections 2 through 4 of this report.

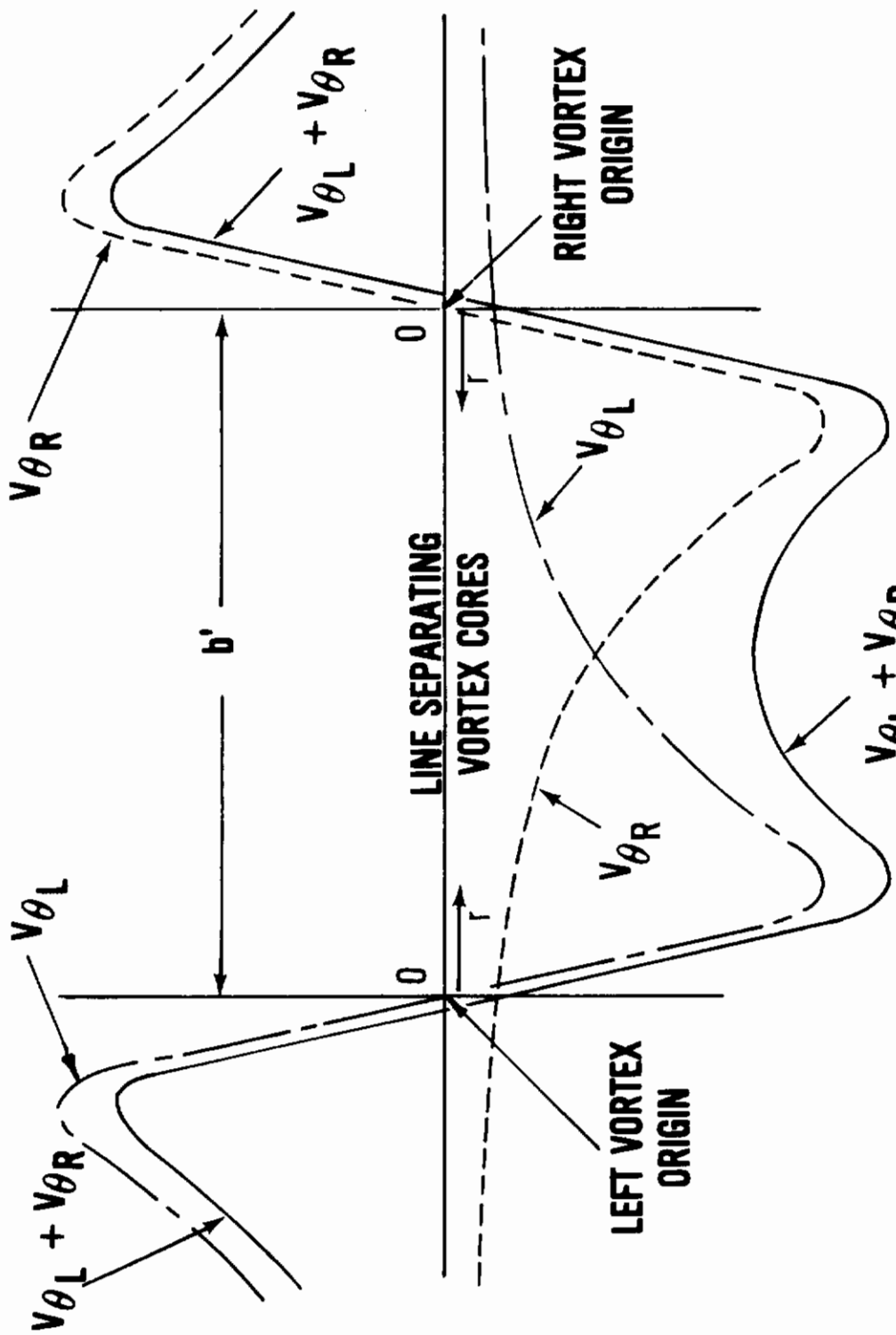

Figure 41. Downwash Field During Way (2) Encounters

SECTION VI

CONCLUDING REMARKS

During 1972 through 1976, an effort was conducted formulating an analysis for assessing the impact of wake vorticity on USAF aircraft operations. Extensive use of experimental results and NASA/FAA flight test data resulted in empiricisms that simplified the formulations and that represented the effects of atmospheric disturbances upon the vortical wake flow field. Examples of the latter are turbulent mixing and decay, buoyancy, and the eventual restructuring of this vortical wake into a form of clear-air turbulence far down stream behind the generating aircraft. The resulting formulations provide: (1) an analytical description of the flow field in the wake and its location relative to the generating airplane, (2) the length of time that the vortical wake may persist in the atmosphere , and (3) a means for determining the effect of this wake upon the flight path of an encountering aircraft. An engineer can use these formulations to assess whether an operation is safe or not. If the potential for wake-related accidents exist, the recourse is either to accept the losses as part of normal operating procedures, or to modify the operation so that the chances for an encounter are avoided. The formulations for performing the assessments are given in detail in the report; a detailed assessment of USAF operations was beyond the scope of this effort.

Initially, the program was primarily concerned with airplane vortical flow fields. Recent experience indicates, however, that attack aircraft such as the A-10 operate in close proximity with Army helicopters from the same field. The analyses presented here have been expanded in late 1978 and early 1979 to include the vortical wake field behind helicopters. Thus, the engineering methods compiled can be used not only in evaluating airplane type operations but also airplane encounters with helicopter wakes.

The equations are synopsized in Section 5 and permit quick hand computations for the wake vorticity field behind an aircraft. An engineer investigating an accident or evaluating operations can use these equations to assess whether a following aircraft encountered a vortical flow field or not. Also given are results from flight tests and the monitoring of wake vorticity behind civil aviation as conducted by the FAA during the 1971 through 1978 time period. These results can be used in assessing whether the vortical flow field could have been broken up for the separation distance involved in any incident/accident or operation under analysis.

An example of a definite problem in landing procedures is a T-38 that crashed in 1974. The T-38 was performing an approach prior to landing behind a stretched C-130 transport. Although the T-38 pilot and air traffic control personnel were operating within all applicable directives, the T-38 ($V = 180$ kt) closed to approximately one minute

behind the transport (V = 110 kt) when the crash occurred. The separation distance between the T-38 and the stretched C-130 was the required 5 nautical miles when the T-38 entered the landing pattern; but, the closing rate between these airplanes was too high. The closing rate between fast fighters, or trainers, behind slow relatively heavy transports must be monitored with care during landing approach; reference is made to Section 4.

There is emphasis within the Air Force and FAA that appropriate separation be maintained only behind large or heavy jets. As a result, pilots may not be aware that the wake behind a small light aircraft may also form a hazard. For example, a fighter is a potential hazard to another fighter where both aircraft are of the same weight; additionally, helicopters can trail a vorticity field as strong as the wake behind heavy USAF cargo aircraft. Several examples in the text indicate: (1) a T-38 pilot that can initiate and sustain a 7-g pullup at 400 knots trails a wake similar to that behind a C-130 in landing approach; (2) an F-104 performing the same maneuver at 400 knots and 4 g's trails a wake as strong as a C-135 in landing approach; and (3) an HH-53A/B helicopter in straight level flight at 60 knots trails a wake as strong as a KC-135 tanker in approach. The ramifications of these vortical wakes upon a following T-38, F-104, and A-10 are given; reference is made to Section 4.

In terms of pilot education, a simplified mathematical model is presented so that appropriate USAF simulators can be given the capability of simulating encounters behind USAF aircraft and Army helicopters. Thus, pilots could be made well aware of what a vortex can do to their aircraft as part of their training curriculum; also presented are the step-by-step computations necessary in implementing the model(s) for any simulator. The model only provides an input function to the roll equation of motion that is used in the simulator. However, it could be extended if desired (see Section 3).

The detailed formulations of this analysis are given in Section 2. Also given is the impact of atmospheric disturbances upon the vortical wake structure. Described are some qualitative experiments where it was observed that the downwind vortex of the vortical wake often rises while the upwind vortex sinks below the altitude predicted by the analysis. Additionally, buoyancy effects and temperature inversion layers can significantly influence the motion of the vortical wake. Even though the analysis gives an error band to account for some of the above, it is felt that much more work is needed in this area before the impact of atmosphere disturbances on the structure and motion of the vortical wake can be clearly understood.

Another area where more effort is needed is in understanding the fluid phenomena that causes vortex bursting. Bursting produces some combination of a marked increase in the size of the vortex core, an increase in turbulence level, and/or an instability and significant restructuring of the wake vorticity behind an aircraft. In our opinion the state of knowledge in this area needs improvement.

The analysis for the vortical wake structure behind a helicopter was correlated with the results of a NASA flight test program document as a report in 1962. Even though the agreement between analysis and test data was good, it is felt that other correlations should be performed to validate and to develop the mathematical model further. Additional work is needed in defining the core size of the vortices trailed behind helicopters, how these vortices are impacted by atmospheric conditions (buoyancy, bursting, etc.), and when these vortices cease to be a hazard to following aircraft. It is also felt that a test effort similar to but not nearly as extensive in scope as, the one conducted by the FAA for airplanes in landing approach should also be considered for helicopters; that is, if the assessment of USAF operations indicates that the helicopter has, and will pose a significant problem. The FAA monitored the vortical wakes of over 50,000 landing approaches at Kennedy, Denver, Heathrow, and Toronto Airports between 1971 and 1978. The helicopter test program could be much more modest than the FAA effort and could consist of monitoring the wake of helicopters at Nellis AFB where helicopters and A-10's operate jointly, as an example.

As indicated earlier, a simplified mathematical model is presented so that appropriate USAF simulators can be given the capability of simulating encounters behind USAF aircraft for pilot training. The model only provides an input function to the roll equation of motion that is used in the simulator; thus, it may be over simplified. An effort should be made to validate the model with existing flight test data of encounters conducted by NASA. The flight test conditions could be duplicated on a moving base simulator using the model. Comparisons of flight test trajectories and pilot comment of both actual encounters and simulated results would then indicate whether the simplified model of the encounter is adequate for training purposes or not.

The engineering tools presented represent the state of the art in 1978. Additionally, an assessment of current USAF operations should be made with the formulations presented for vortical wake hazards in regard to both aircraft and mix helicopter/aircraft operations to determine whether wake vorticity is a significant hazard or not. The results of these analyses should be used to assess the need and direction of further work in this area, and where the effort should be conducted -- USAF, NASA, or FAA.

REFERENCES

1. Williams, G. M., Trailing Vortex Wake Systems - A Preview of the Wake Turbulence Problem , Lockheed-California Co. Report LR 24275, Part III, Jan 1971.

2. McCormick, B. W., Aircraft Wakes: A survey of the Problem , presented at FAA Symposium on Turbulence, Washington, D.C., Mar 1971.

3. Kurylowich, G. and Nelson, R. C., Analysis of a Wake Turbulence Hazard in USAF Operations , AFFDL-TM-74-132-FGC, Jun 1974.

4. Gee, D. R., Kurylowich, G. and Paillet, F. L. , Analysis of a Wake Turbulence Hazard in USAF Operations (T-39 Accident) , AFFDL-TM-75-19-FGC, Jan 1975.

5. Bleviss, Z. O., Theoretical Analysis of Light Plane Landing and Take-off Accidents Due to Encountering the Wakes of Large Aircraft , Douglas Report No. SM-18674, Dec 1954.

6. Flinn, E. H., Helicopter Rotor Wash Effects , FDCC TM 67-2, Oct 1967.

7. Kurylowich, G. and Paillet, F. L., AFFDL Wake Turbulence Program (Phases 1, 2, and 3) , AFFDL/FGC-TM-74-205, Oct 1974.

8. Kurylowich, G., Analyses Relating to Aircraft Vortical Wakes , AFFDL/FGC-TM-73-23, Feb 1973.

9. Gee, D. R., Lt, Kurylowich, G., Banta, A. J., Capt, and Bise, M. E., Preliminary Assessment of Aircraft Separation Distances in USAF Operatings (Vol 1 and 2), AFFDL/FGC-TM-75-118, Aug 1975.

10. Jenkins, M. W. M. and Meyer, R. T., Vortical Wake Hazard Advisory , AFFDL-TR-76-146, Feb 1977.

11. Kurylowich, G., A Study of Air Force Wake Turbulence Accidents , AFFDL-FGC-TM-72-3, Mar 1972.

12. Brashears, M. R., et al., Analysis of Predicted Aircraft Wake Vortex Transport and Comparisons with Experiment , Report LMSC-HREC TR D306747, Department of Transport, Transportation Systems Center, Cambridge, MA, Dec 1973.

13. Kuethe, A. M. and Schetzer, J. D., Foundations of Aerodynamics , John Wiley & Sons, Inc., 1959.

14. Rauscher, M., Introduction to Aeronautical Dynamics , John Wiley & Sons, Inc., 1953.

15. Tombach, I. H., Transport of a Vortex Wake in A Stably Stratified

Atmosphere , Aircraft Wake Turbulence and Its Detection, (Ed. J. H. Olsen), Plenum Press, pp. 41-56, 1971.

16. Scorer, R. S. and Davenport, L. J., Contrails and Aircraft Downwash , J. Fluid Mech,. Vol. 43, pp. 451 - 464, 1970.

17. Kurylowich, G., Wake Turbulence Abatement by Blowing and Other Means , AGARD Fluid Dynamics Panel, Brussels, Belgium, Sep 1973.

18. Crow, S. C., Stability Theory for a Pair of Trailing Vortices , Boeing Scientific Research Laboratory Document DI-82-0918, 1970.

19. MacCready, P. B., Jr., An Assessment of Dominant Mechanisms in Vortex-Wake Decay , Proceedings of a symposium on Wake Turbulence held in Seattle, WA, Sep 1970.

20. Garodz, J. L., Miller, N. J. and Lawrence, D., The Measurement of DC-7 Trailing Vortex System Using the Tower Fly-By Technique , Report No. FAA-RD-73-141, Nov 1973.

21. Garodz, L. J., Lawrence, D. and Miller, N., The Measurement of the Boeing 727 Trailing Vortex System Using the Tower Fly-By Technique , Report No. FAA-RD-74-90, Aug 1974.

22. Garodz, L. J., Lawrence, D. and Miller, N., The Measurement of the Boeing 707 Trailing Vortex System Using the Tower Fly-By Technique , Report No. FAA-RD-75-15, Mar 1975.

23. Barber, M. R., et al., Flight Test Investigation of the Vortex Wake Characteristics Behind a Boeing 727 During Two-Segment and Normal ILS Approaches (A Joint NASA/FAA Report) , NASA TM X-62398 (FAA-NA-75-151), Jan 1975.

24. Hallock, J. N., et al, Joint US/UK Vortex Tracking Program at Heathrow International Airport, Report No. FAA-RD-76-58, Nov 77.

25. Hallock, J. N., Vortex Advisory System Safety Analysis: Analytical Model, Report No. FAA-RD-78-68, I, Sep 78.

26. Anon, Analysis of a Jet in a Subsonic Crosswind , NASA-Langley NASA SP-218, Sep 1969.

27. Gessow, A. and Myers, G. C., Jr., Aerodynamics of the Helicopter , the MacMillan Company, 1952.

28. Heyson, H. H. and Katzoff, S., Induced Velocities Near a Lifting Rotor with Nonuniform Disk Loading , NACA Report 1319, 1957.

29. Heyson, H. H., Nomographic Solution of the Momentum Equation for VTOL-STOL Aircraft , NASA TN D-814, 1961.

30. Margason, R. J. and Fearn, R., Jet-Wake Characteristics and their Induced Aerodynamic Effects on V/STOL Aircraft in Transition Flight , NASA-Langley Symposium Analysis of a Jet in a Subsonic Crosswind , Sep 1969, NASA SP-218, Sep 1969.

31. Heyson, H. H., Wind Tunnel Wall Effects at Extreme Force Coefficients , International Congress of Subsonic Aerodynamics, New York, Apr 3-6, 1967.

32. Abramovitch, G. N., The Theory of Turbulent Jets , Cambridge: Massachusetts Institute of Technology, 1963.

33. Keffer, J. F. and Baines, W. D., The Round Jet in a Cross-Wind , Journal of Fluid Mechanics, Vol 15, 1963.

34. Jordinson, R., Flow in a Jet directed Normal to the Wind , Aeronautical Research Council R & M 3074, 1958.

35. Braun, G. W. and McAllister, J. D., Cross Wind Effects on Trajectory and Cross Sections of Turbulent Jets , NASA-Langley Symposium Analysis of a Jet in a Subsonic Crosswind , Sep 1969, NASA SP-218, Sep 1969.

36. Davenport, F. J., Analysis of Propeller and Rotor Performance in Static and Axial Flight by an Explicit Vortex Influence Technique , Vertol Division, The Boeing Co., Report F-372, Morton, PA, Feb 1965.

37. Connor, A. B. and O'Bryan, T. C., A Brief Evaluation of Helicopter Wake as a Potential Operational Hazard to Aircraft , NASA TN D-1227, Mar 1962.

38. Diederich, F. W., A Planform Parameter for Correlating Certain Aerodynamic Characteristics of Swept Wings , NASA TN 2355, Apr 1951.

39. Kurylowich, G., The Hidden Killer of the Airways , Aerospace Safety Magazine, May 1975.

☆U.S.Government Printing Office: 1979 — 657-002/38